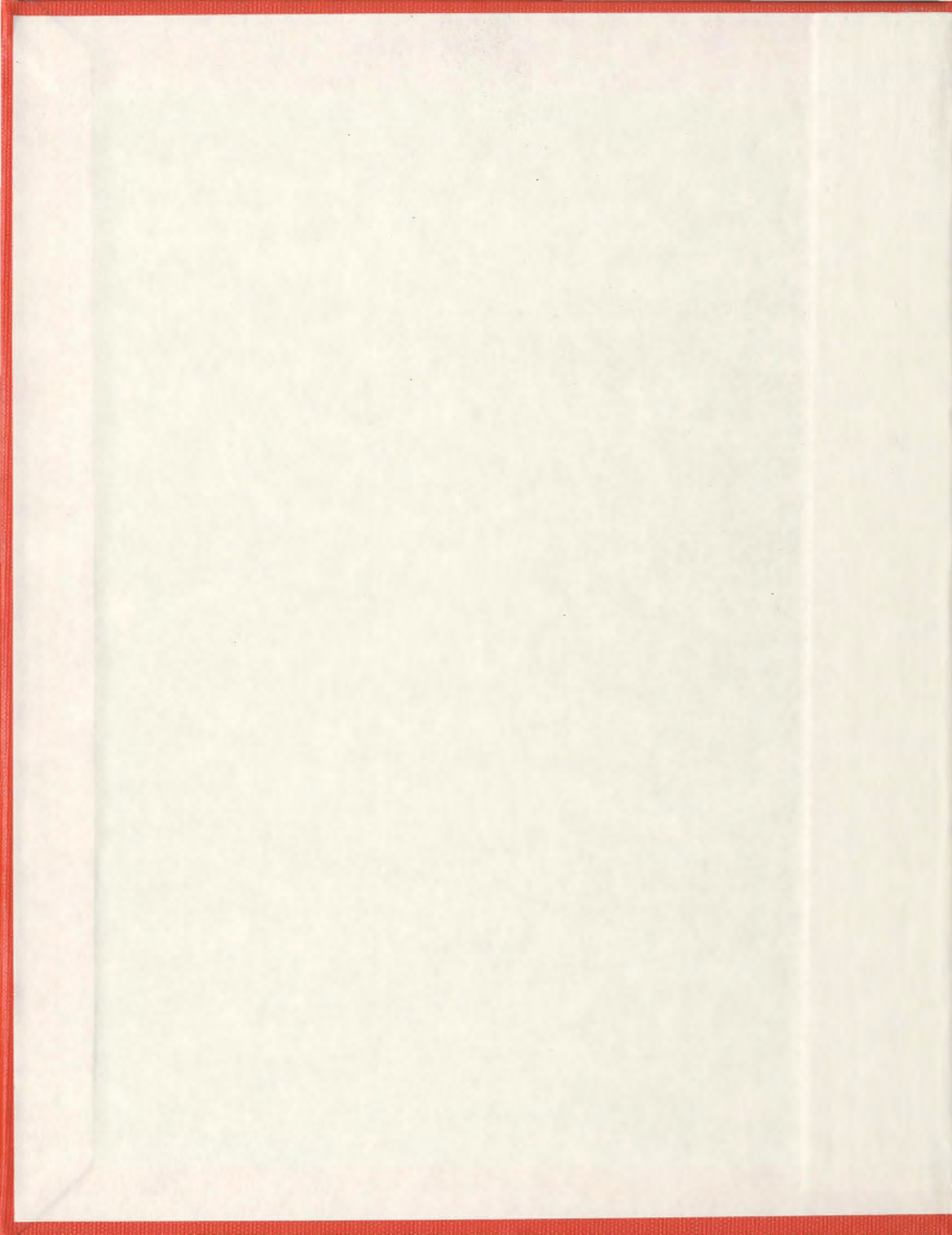


**SHEAR BEHAVIOUR OF MACRO-SYNTHETIC
FIBRE-REINFORCED CONCRETE BEAMS WITH
GFRP REINFORCEMENT**

YAHIA EBRAHIM



Shear Behaviour of Macro-Synthetic Fibre-Reinforced Concrete

Beams with GFRP Reinforcement

by

© Yahia Ebrahim, B.Sc. (Eng.)

A thesis submitted to the School of Graduate

Studies in partial fulfillment of the

requirements for the degree of

Degree of Master of Engineering

Faculty of Engineering and Applied Science

Memorial University of Newfoundland

May 2013

St. John's

Newfoundland

Canada

Abstract

The purpose of this study was to investigate the influence of macro synthetic fibre on the shear behaviour of Glass Fibre Reinforced Polymers (GFRP) reinforced concrete beams. The experimental program was carried out in two phases: material tests and structural investigation.

In the material investigation, thirty two prisms ($100\text{ mm} \times 100\text{ mm} \times 400\text{ mm}$) and thirty six cylinders ($100\text{ mm} \times 200\text{ mm}$ and $150\text{ mm} \times 300\text{ mm}$) were cast to determine the mechanical properties of concrete containing macro-synthetic fibres. The samples were tested to investigate and to develop a clear understanding of the effect of the amount of macro synthetic fibre on the concrete properties. For the prisms, the investigation focused on the modulus of rupture, flexural toughness, toughness indices, while for the cylinders, the compressive strength and splitting tensile strength were investigated.

In the structural investigation, sixteen reinforced concrete beams were tested up to failure at the structural laboratory of Memorial University (MUN) to study the behaviour of the beams in terms of deflection characteristics, shear and flexural behaviour, concrete and GFRP strains and ultimate load capacity. The dimensions of the simply supported beams were $250 \times 350 \times 2840$, $250 \times 350 \times 2840$, $250 \times 500 \times 3540$ and $250 \times 350 \times 3540$, measured in millimetres. The main variables in the structural investigation were the amount of synthetic fibre by volume, reinforcement ratio, effective depth, and shear span to depth ratio.

The test results revealed that the inclusion of different volumes of macro synthetic fibre enhanced the shear failure behaviour of GFRP reinforced concrete beams, and increased the normalized shear strength of the reinforced concrete beams by an average

of 35% for beams reinforced with $1.3 \rho_b$ and $1.5 \rho_b$ respectively. The increase in the normalized shear strength for the deeper beams with a depth of 441 mm was approximately 39 %. Furthermore, GFRP reinforced concrete beams an increase in the post cracked stiffness of the beams. As it was expected, the addition of fibre increased the increased the beams' maximum deformation by 35%, when it was compared to the control beams that had 0% of macro synthetic fibre.

The capacity of the beams was compared to the predictions of the different models proposed in the literature for steel fibre reinforced beams. The model proposed by Greenough and Nehdi (2008) which gave the best predictions of the test results.

Finally, a finite element analysis was carried out using ANSYS and a finite element model was developed. The FEA model was calibrated using the experimental results. All the necessary steps to create and calibrate the model are presented and explained. A comparison of the test results with the finite element model predictions was carried out in terms of the ultimate load capacity, the maximum deflection and the cracks pattern of the test specimens. The load-deflection characteristics obtained from the finite element solution at the center of the beam were in close agreement with the experimental test results at first cracking stage and at failure stage. In terms of, the initial crack, progressive cracking or the failure mechanism, the finite element model compared well to the experimental data obtained and the predicted failure load was very close to the measured load during experimental testing.

Acknowledgements

The author would like to express his gratitude to his supervisor Dr. A. Hussein, Associate Professor of Civil Engineering, Memorial University of Newfoundland, for his financial support, keen supervision and guidance throughout my program of studies.

I also express my appreciation to my colleague and friend Shah Alam, for his friendship and help during the experimental program. Special and sincere thanks are extended to Emad Rizk for his help with preparing this manuscript.

I also express my appreciation to the technical staff of the structural engineering laboratory at Memorial University of Newfoundland, especially Shawn Organ and Mathew Curtis.

Sincere thanks are due to the Concrete Products for donating the concrete, Grace Canada for donating the fibres and the chemicals and Holcim cement for donating the cement.

Finally, my warmest appreciation goes to my family and friends for their support.

Table of Contents

Abstract.....	i
Acknowledgements	iii
Table of Contents	iv
List of Figures.....	viii
List of Tables	xi
List of Symbols	xii
List of Symbols	xii
Chapter 1	1
Introduction.....	1
1.1. General.....	1
1.2. Problem Definition.....	3
1.3. Scope and Objectives.....	4
1.4. Thesis Outline	5
Chapter 2	7
Literature Review	7
2.1. Introduction.....	7
2.2. Historical Background	8
2.3. Composition of Fibres.....	10
2.3.1. Steel Fibre Reinforced Concrete (SFRC)	10
2.3.2. Synthetic Fibre Reinforced Concrete (SNFRC)	10
2.3.2.1. Polypropylene Fibres	11

2.3.2.2.	Polyethylene Fibres.....	12
2.3.2.3.	Macro-Synthetic Fibres.....	13
2.4.	Fibre Reinforced Polymers (FRP)	14
2.5.	Shear Strength of GFRP Reinforced Concrete Beams	15
2.6.	Shear Strength of FRC Beams	17
2.6.1.	Direct Shear Tests	18
2.6.2.	Shear in FRC Beams.....	19
2.6.3.	Shear in FRC beams with Synthetic Fibres	22
2.7.	Existing Shear Strength Models for FRC	23
2.8.	Design Codes Equations for FRP Reinforced Concrete Members	24
2.8.1.	American Concrete Institute (ACI 440.1R-06).....	25
2.8.2.	Canadian Standard Association (CSA S806-10)	25
2.9.	Finite Element Analysis.....	27
Chapter 3	41
Material Properties	41
3.1.	Introduction.....	41
3.2.	Materials	41
3.2.1.	Concrete	41
3.2.2.	Synthetic Fibres	43
3.2.3.	GFRP Bars	43
3.3	Properties of Hardened Concrete	44
3.3.1.	Compressive Strength	44
3.3.2.	Splitting Tensile Strength	45

3.3.3. Modulus of Rupture	46
Chapter 4	52
Experimental Program	52
4.1. Introduction.....	52
4.2. Test Specimens	52
4.3. Formwork and Fabrication.....	54
4.4. Casting and Curing of the Specimens.....	54
4.5. Test Setup.....	55
4.6. Instrumentation	56
4.7. Data Acquisition System.....	57
4.8. Test Procedure	58
Chapter 5	65
Test Results and Discussion	65
5.1. Introduction.....	65
5.2. Load-Deflection Characteristics	65
5.3. Strain Behaviour	69
5.3.1. Concrete Strains.....	69
5.3.2. GFRP Strains	70
5.4. Crack Patterns	71
5.5. Failure Modes	72
5.6. Shear Capacity	73
5.6.1. Effect of Reinforcement Ratio	74
5.6.2. Effect of Shear Span to Depth Ratio.....	75

5.6.3.	Effect of Effective Depth	75
5.6.4.	Effect of Fibre Volume	75
5.7.	Test Results versus Design Models Predictions	77
Chapter 6	94
Finite Element Analysis	94
6.1.	Introduction.....	94
6.2.	Constitutive Models.....	94
6.2.1.	Concrete Model.....	94
6.2.2.	Reinforcement.....	96
6.3.	Finite Element Model	96
6.2.3.	Finite Element Mesh.....	96
6.2.4.	Material Properties.....	97
6.2.5.	Analysis Type	99
6.4.	Finite Element Model Predictions	100
6.4.1.	Load-Deformation Response	100
6.4.2.	Behaviour at First Cracking.....	100
6.4.3.	Behaviour beyond First Cracking	101
6.4.4.	Ultimate Capacity	102
Chapter 7	112
Summary and Conclusions	112
References	116

List of Figures

Figure 2.1: Steel, glass, synthetic and natural fibres with different length and shape.....	35
Figure 2.2: Polypropylene fibres are produced either as (left) fine fibrils with rectangular cross section or (right) cylindrical monofilament.....	35
Figure 2.3: Available shapes of FRP products (ISIS, 2003).....	36
Figure 2.4: Stress vs. strain relationships for FRP reinforcement and matrix (ISIS, 2003)	36
Figure 2.5: Internal forces in a cracked beam without stirrups.....	36
Figure 2.6: Variations of normal and shear stresses according to flexural deformation at cross section (Choi et al., 2007).....	37
Figure 2.7: FEM discretization for a quarter of the beam (Kachlakev et al., 2001).....	38
Figure 2.8: Load vs. deflection plot (Kachlakev et al., 2001)	38
Figure 2.9: Typical cracking signs in finite element models: (a) Flexural cracks; (b) Compressive cracks; (c) Diagonal tensile cracks (Kachlakev et al., 2001).....	38
Figure 2.10: Models for reinforcement in reinforced concrete: (a) Discrete; (b) Embedded; (c) Smeared (Tavarez, 2001)	39
Figure 2.11: Tensile load vs. deformation for plain and fibre reinforced concrete	40
Figure 3.1: GFRP bars used in the test	48
Figure 3.2: Compressive strength test setup	48
Figure 3.3: Splitting tensile test setup.....	49
Figure 3.4: Relative increases in splitting tensile strength due to fibre addition.....	49
Figure 3.5: Fibres holding the concrete on test cylinder: (a) Splitting tensile failure; (b) Compression failure	50

Figure 3.6: Modulus of rupture test setup.....	50
Figure 3.7: Relative increases in flexural tensile strength due to fibre addition.....	51
Figure 3.8: Flexural strength and energy absorption capacity due to fibre addition	51
Figure 4.1: Definition of variables.....	60
Figure 4.2: Experimental details and objectives	60
Figure 4.3: The equivalent stress block	61
Figure 4.4: Typical formwork and reinforcement layout (Top view of typical formwork and reinforcement layout (before placing the top cross bracing for the formwork).)	61
Figure 4.5: Test setup.....	62
Figure 4.6: Instrumentation used during a test(Note: CS refers concrete strain gauges and RS refers reinforcement strain gauges).....	63
Figure 4.7: Test setup and data acquisition system.....	64
Figure 4.8: Cracks mapping.....	64
Figure 5.1: Load vs. deflection curves for the different fibre volumes and the same variables (reinforcement ratio, effective depth and shear span to depth ratio).....	81
Figure 5.2: Load vs. deflection curves for the different reinforcement ratios and the same variables (fibre volume, effective depth and shear span to depth ratio).....	82
Figure 5.3: Load vs. deflection curves for the different effective depths and the same variables (fibre volume, reinforcement ratio and shear span to depth ratio)	83
Figure 5.4: Load vs. concrete strains	84
Figure 5.5: Load vs. mid-span GFRP strain for all beams.....	85
Figure 5.6: Load vs. mid-shear span GFRP strain for all beams	86
Figure 5.7: Crack patterns for beams of Group 1 ($a/d = 2.5$)	87

Figure 5.8: Crack patterns for beams of Group 2 ($a/d = 2.6$)	88
Figure 5.9: Crack patterns for beams of Group 3 ($a/d = 2.5$)	89
Figure 5.10: Crack patterns for beams of Group 4 ($a/d = 3.5$)	90
Figure 5.11: Typical cracks: (a) Flexural and diagonal shear cracks; (b) shear flexural crack, and (c) bond/anchorage crack	91
Figure 5.12: Influence of fibre volume on the normalized shear strength (shear strength is normalized with respect to $\sqrt{f'_c}$)	92
Figure 5.13: Values of normalized shear strength (w.r.t. $\sqrt{f'_c}$) for all test beams	93
Figure 5.14: Values of predicted shear capacity for the beams tested in this study using design models proposed in the literature	93
Figure 6.1: Solid 65 element (ANSYS, 2005)	105
Figure 6.2: Failure surface in principal stress space (ANSYS, 2005)	105
Figure 6.3: Concrete cracking model	106
Figure 6.4: Used mesh; concrete elements and the GFRP reinforcement	106
Figure 6.5: Applied displacement and boundary conditions	107
Figure 6.6: Uniaxial stress-strain curve for concrete	107
Figure 6.7: Predicted and experimental load versus deflections	108
Figure 6.8: First crack: model prediction and experimental observation	109
Figure 6.9: Significant flexural and diagonal shear cracks	110
Figure 6.10: Severe cracking near failure (model prediction)	111

List of Tables

Table 2.1: Properties comparison of macro-synthetic, Polypropylene and Polyethylene fibres	33
Table 2.2: Existing shear strength models for FRC beams without web reinforcement ..	34
Table 3.1: Mix proportions of one cubic meter of concrete	47
Table 3.2: ISOROD Glass-Vinyl ester properties provided by the manufacturer	47
Table 3.3: Properties of hardened concrete.....	47
Table 3.4: Concrete compressive strength of mix no. 2 for different cylinder sizes	47
Table 4.1: Details of test specimens	59
Table 5.1: Load, deflection and stiffness values at first crack and at failure.....	79
Table 5.2: Shear Capacity of beams ($V_{c, test}$)	79
Table 5.3: Nominal shear strength of beams ($v_n = V_{c, test} / bd$)	79
Table 5.4: Normalized shear strength w. r. t. $\sqrt{f'_c}$ ($v_n / \sqrt{f'_c}$)	80
Table 5.5: Strength predictions by existing models.....	80
Table 6.1: Typical material parameters used in the model	103
Table 6.2: Load-deflection comparison at first cracking	104
Table 6.3: Comparison between experimental and FE model at failure.....	104

List of Symbols

a	Shear span, mm
A_f	Reinforcement area, mm ²
a/d	Shear span to depth ratio
b_w	Minimum effective web width, mm
d	Effective depth, mm
D	Diameter of the fibre, mm
E_c	Modulus of elasticity of concrete, MPa
E_f	Modulus of elasticity of longitudinal FRP reinforcement
f	Stress at any strain ϵ
f'_c	Concrete compressive strength, MPa
f_r	Modulus of rupture, MPa
f_{sp}	Splitting tensile strength, MPa
f_t	Direct tensile strength, MPa
f_u	Ultimate strength of FRP reinforcement, MPa
F	Fibre factor suggested by Narayanan and Darwish (1987) equal to $F = V(L/D)\beta$
I	Cross sectional moment of inertia
I_5, I_{10}, I_{20}	Toughness indices
k_m	Coefficient taking into account the effect of moment at section on shear strength
k_r	Coefficient taking into account the effect of reinforcement rigidity on its shear strength

k_s	Coefficient taking into account the effect of member size on its shear strength
L	Span length; length of fibre
L/D	Aspect ratio of fibre
M_f	Factored moment
P	Maximum applied load indicated by the testing machine
V	Volume ratio of fibre
V_c	Factored shear resistance provided by concrete
V_f	Factored shear resistance
α_1	Ratio of average stress in rectangular compression block to the specified concrete strength
β_1	Ratio of depth of rectangular compression block to depth of the neutral axis
β	Factor for fibre shape and concrete type
λ	Factor to account for concrete density
ϕ_c	Resistance factor for concrete
μ	Poisson's ratio
ρ_f	Longitudinal FRP reinforcement ratio, $\rho_f = A_f / b d$
ρ_b	Balanced reinforcement ratio
ε	Strain at stress f
ε_o	Strain at the ultimate compressive strength
η_o	The orientation factor that was theoretically derived by Romualdi and Mandel (1964) and can be taken as 0.41

τ	Average interfacial bond stress of fibre matrix = 4.15 MPa as suggested by Narayanan and Darwish (1987)
ACI	American Concrete Institute
CSA	Canadian Standard Association
FRC	Fibre Reinforced Concrete
FRP	Fibre Reinforced Polymer
GFRP	Glass Fibre Reinforced Polymers
ISIS	Intelligent Sensing for Innovative Structures
LVDT	Linear Variable Differential Transformer
SNFRC	Synthetic Fibre Reinforced Concrete

Chapter 1

Introduction

1.1. General

The use of fibres in building materials to improve their behaviour is an old and intuitive concept. For example, adding straw fibres to sun-dried mud bricks and asbestos fibres to pottery to create a composite with a better performance. Moreover, the use of strong and discrete fibres as concrete reinforcement has been a challenge to many material engineers. Adding the reinforcement to the mixer in the form of fibres, like adding the aggregates, to create a homogeneous, isotropic and mouldable material is a task that started more than a century ago and nowadays can be considered a reality. The successful employment of fibre reinforced concrete started in early sixties, and, since then, many researchers have been trying to evaluate the potential properties of this material for a broader use.

Because of the brittle behaviour of plain concrete in tension, shear failure in reinforced concrete (RC) beams is generally catastrophic. However, this type of failure can be avoided with proper shear reinforcement. Despite every effort, therefore, shear failure remains a distinct possibility in RC elements and one of the primary reasons for building collapse. There is another issue with reinforcement congestion and lack of concrete quality itself. Shear reinforcement, such as stirrups, which are placed too closely in an element, interfere with concrete compaction, resulting in poor quality concrete. Therefore, if the shear strength and shear toughness of concrete as a material could be improved, shear failure in RC beams could be avoided, and the mode of failure in reinforced concrete beams could be changed from brittle to ductile. It is now well known

that fibre reinforcement is one of the most effective means of enhancing fracture toughness in all failure modes.

Most of the civil structures made of steel reinforced concrete normally suffer from corrosion of the steel, which results in the failure of those structures. Constant maintenance and repairing is needed to enhance the life cycle of those civil structures. Canada's adverse climate and extensive use of de-icing salts have very significant effects on traditional concrete structures in an exposed environment such as bridges and airport pavement. Besides that, underground structures all over the world are always affected by environmental effects. Maintaining, repairing and rebuilding the concrete structures are expensive, and a more effective and affordable solution is needed.

Minimizing the failure and enhancing the life cycle of the concrete structures made of steel reinforced concrete by replacing the steel bars with fibres to produce a fibre reinforced concrete and this is termed as FRC. Adding small quantities of fibres by weight or by volume to fibre reinforcing concrete can basically alter the properties of the cement-based matrix, which is brittle in nature and possesses little tensile strength. The principal reason for incorporating fibres into a cement matrix is to increase the toughness, tensile strength and to improve the cracking deformation characteristics of the resultant composite.

Randomly oriented fibres are an effective way of improving the concrete properties. Fibre reinforced concrete has a wide range of applications, particularly for airport, highway pavements, structures exposed to severe environment, bridge decks, bridge piers, erosion resistant structures, explosion resistant structures and sewer pipes. In order

for fibre reinforced concrete to be available as a construction material, it must be able to compete economically with existing reinforcing systems.

In recent years, there has been considerable interest in fibre reinforced polymer (FRP) as non metallic reinforcement for concrete structures. FRP reinforcement has high tensile strength, low density, and is non susceptible to classical type of corrosion. Hence, they are ideal for concrete structures in the aggressive Canadian environment such as structures in marine environment, and bridges and parking garages exposed to de-icing salts.

Synthetic fibres, typically made of polypropylene, have primarily been used in concrete materials to control shrinkage cracking and, to a limited extent, to improve toughness and impact resistance. In recent years, increasing efforts have been devoted toward the development of new generation of macro-synthetic fibres that impart significant toughness and ductility to concrete comparable to commonly used steel fibres. Accordingly, the application of synthetic fibres in the concrete industry has extended beyond shrinkage and thermal cracking control to structural applications.

1.2. Problem Definition

Generally, the shear failure of a reinforced concrete beam is directly related to the diagonal tensile cracking that develops in a direction perpendicular to the principal tensile stress. Once the tensile cracking occurs, the tensile stress at the crack surfaces softens, which significantly reduces the shear strength of the beam.

Most of the published work on shear of FRC has focused exclusively on steel fibres. A large data bank of test results for shear strength of steel fibre reinforced concrete

beams was reported by several investigators. However, most of the research on steel-fibre reinforced concrete reported in literature has been concerned on small size beams and slabs on grade.

On the other hand, there is little data on macro-synthetic fibres and their applications in reinforced concrete members. The few available studies were conducted on steel-reinforced concrete elements. No data are available on the use of macro-synthetic fibres in structural elements reinforced with Fibre reinforced polymer (FRP) bars. Hence, the current study focuses on large scale beams to investigate the effect of macro synthetic fibre on the shear behaviour of GFRP reinforced concrete beams without shear reinforcement.

1.3. Scope and Objectives

This investigation deals specifically with the behaviour of GFRP fibre-reinforced concrete beams in shear. The main variables in this investigation are the amount of macro synthetic fibre by volume (V), reinforcement ratio (ρ), effective depth (d), and shear span to depth ratio (a/d). The primary objective of this investigation is to develop a better understanding of the effect of the amount of non-metallic fibres in volume percentage with respect to other variables included in this investigation on the:

- The properties of fresh concrete (workability and balling at higher quantities of fibres) and the mechanical properties of hardened concrete (tensile strength, compressive strength and flexural toughness).
- Load capacity and failure modes of reinforced concrete beams.

- Flexural behaviour (up to the occurrence of the shear failure) with a special focus on deflection and load carrying capacity.
- Shear behaviour of longitudinally reinforced concrete beams without shear reinforcement.

1.4. Thesis Outline

Chapter 2 contains the literature review that is relevant to this investigation. In this chapter, some of the previous work is discussed concerning the effectiveness of adding fibres to the reinforced concrete in terms of shear strength, ductility, workability, compressive strength, flexural strength, and cracking mechanism.

Chapter 3 presents a material investigation that covers the properties of hardened concrete that was used to cast the beams (compressive strength, splitting tensile strength, flexural toughness and toughness indices).

In Chapter 4, details of the test setup, loading, specimens' preparation, instrumentation and the data acquisition system are provided.

Chapter 5 reports the test results and observations obtained from the experimental program. Load-deflection relationship, concrete strain, GFRP strains, modes of failure and ultimate capacity are presented.

Chapter 6 contains the calibration of a finite element model using the experimental data (concrete properties and load-deformation behaviour) of the concrete beams. All the necessary steps to create the calibrated model are explained in detail. The general purpose finite element program ANSYS was used in the simulations. The chapter also contains the comparisons of the test results, and the finite element model predicted results in terms

of the linear region, initial cracking, the nonlinear region, ultimate load capacity and the maximum deflection of the test specimens.

Chapter 7 summarizes the findings from the experimental and analytical investigations and presents recommendations for future research.

Chapter 2

Literature Review

2.1. Introduction

Concrete made of Portland cement has certain characteristics. It is relatively strong in compression but weak in tension and tends to be brittle. The weakness in tension can be overcome using conventional rod reinforcement and to some extent, by the inclusion of a sufficient volume of certain fibres. The use of fibres also alters the behaviour of the fibre-matrix composite after it has cracked, thereby improving its toughness.

Brittle materials are considered to have no significant post-cracking ductility. Fibrous composites have been and are being developed to provide improved mechanical properties to otherwise brittle materials. When subjected to tension, these un-reinforced brittle matrices deform elastically. The elastic response is followed by micro-cracking, localized macro-cracking, and finally by fracture at relatively low strains. Introduction of fibre into concrete results in post-elastic property changes that range from subtle to substantial, depending upon a number of factors, including matrix strength, fibre type, fibre modulus, fibre aspect ratio, fibre strength, fibre surface bonding characteristics, fibre content, fibre orientation, and aggregate size effects (Johnston, 2000). For many practical applications, the matrix first-crack strength is not increased. In these cases, the most significant enhancement from the fibres is the post-cracking composite response. This is most commonly evaluated and controlled through toughness testing (such as measurement of the area under the load-deformation curve).

If properly engineered, one of the greatest benefits to be gained by using fibre reinforcement is improved long-term serviceability of the structure or product.

Serviceability is the ability of the specific structure or part to maintain its strength and integrity and to provide its designed function over its intended service life. One aspect of serviceability that can be enhanced by the use of fibres is the control of cracking. Fibres can prevent the occurrence of large crack widths that are either unsightly or permit water and contaminants to enter, causing corrosion of reinforcing steel or potential deterioration of concrete (Shah, 1991). In addition to crack control and serviceability benefits, use of fibres at high volume percentage (5 to 10% or higher with special production techniques) can substantially increase the matrix tensile strength (Shah, 1991).

The most important applications of fibres are generally to prevent or control the tensile cracking occurring in concrete structures by bridging these cracks and restraining them. In order to increase the deflection of the beam, additional forces and energies are required to pull out or fracture the fibres. This process improves the load carrying capacity beyond cracking. This improvement creates a long post-peak-descending portion in the load-deflection curve.

Recently, structurally efficient synthetic fibres have been developed. Synthetic fibres have high strength and high modulus of elasticity. The fibres exhibit structurally effective properties such as an increase of toughness and/or load-carrying capacity after cracking. These synthetic fibres have advantages compared to steel or other fibres in that they are corrosion-resistant and exhibit a high-energy absorption capacity.

2.2. Historical Background

Fibres are manufactured from many materials such as metal, glass, carbon and graphite, polymer, boron, ceramic, and silicon carbide (Mallick, 1993). The last three decades have seen a growing interest in the use of fibres in ready-mixed concrete, pre-

cast concrete and shotcrete. Currently, steel fibres are available in a variety of shapes, sizes and thickness; they may be round, flat, crimped or deformed with typical lengths of 6 mm to 150 mm and thickness ranging from 0.005 mm to 0.75 mm, as shown in Figure 2.1. They are added to the concrete during mixing. The main factors that control the performance of the composite material are:

1. The physical properties of fibres and matrix.
2. The strength of bond between fibres and matrix.

Although the basic governing principles are the same, there are several characteristic differences between conventional reinforcement and fibre systems:

1. The fibres are generally distributed throughout a given cross section, whereas reinforcing bars or wires are placed only where required.
2. Most fibres are relatively short and closely spaced as compared with continuous reinforcing bars or wires.
3. It is generally not possible to achieve the same area of reinforcement in an area of concrete using fibres as compared to using a network of reinforcing bars or wires.

Fibres are typically added to concrete in volume dosages and have been shown to be effective in reducing plastic shrinkage cracking. Fibres typically do not significantly alter free shrinkage of concrete. However, at high enough volume dosages, they can increase the resistance to cracking and decrease crack widths (Shah et al., 1998).

The Twentieth century interest in synthetic fibres as a component of construction materials was first reported in 1965. At that time synthetic monofilament fibres were used in the blast resistant structures for the US army corps of engineers.

2.3. Composition of Fibres

2.3.1. Steel Fibre Reinforced Concrete (SFRC)

The mechanical properties of steel fibre reinforced concrete (SFRC) mainly depend on the shape of fibres rather than the material (Johnston, 2000). ASTM A820 (2001) classifies steel fibres based upon the method used in their manufacture, in contrast with ACI 544.1R (1996) that considers the shape of fibres' cross-section in their classification.

A significant problem with using SFRC is its sensitivity to corrosion and subsequent loss of strength throughout its life time. Cracks in SFRC have been indicated to cause corrosion of fibres in laboratory and field testing when exposed to chloride environments due to fibres passing across the crack (Hoff, 1987). Appearance of the flexural or tensile cracking on SFRC can lead to catastrophic structural conditions, so that full consideration should be given to the possibility of corrosion at cracks (ACI 544.1R, 1996). Since SFRC is not in the scope of this thesis, the properties of such fibres will not be addressed in further details.

2.3.2. Synthetic Fibre Reinforced Concrete (SNFRC)

Synthetic fibres are man-made fibres resulting from research and development in the petrochemical and textile industries. Aramid (aromatic polyamide), a high-modulus polymeric material, was one of the first synthetic fibres used in the construction industry introduced for commercial application by late 1970s (Walton and Majumdar, 1978). The use of aramid fibres in Portland cement concrete based matrix was followed by acrylic, carbon, nylon, polyester, polyethylene, and polypropylene. For many of these fibres, there is little reported research or field experience; while others are found in commercial

applications and have been the subject of extensive reporting (Bentur and Mindess, 2007).

While durability in concrete in some respects relates specifically to the chemistry of each fibre type, some general physical considerations can be essential. All these polymers melt at a relatively low temperature between about 134°C for polyethylene and 257°C for polyester (ACI 544.1R, 1996), so they cannot be expected to perform under conditions where the concrete temperature approaches or exceeds these values, as in the case of fire in service.

The advantage of using synthetic fibres over SFRC is their corrosion resistance and according to ASTM CI 116 (2002) their compatibility with moisture, cement alkalis, and chemical admixtures. In addition, the use of synthetic fibres is advantageous over steel fibres due to the elimination of potential injuries caused by handling and placement. Polypropylene and polyethylene have been reported to be very resistant to strong alkalis, while polyester was not as resistant (Wang et al., 1987).

2.3.2.1. Polypropylene Fibres

Polypropylene fibres are produced from homo-polymer polypropylene resin in a variety of shapes and sizes, and with differing properties. Polypropylene has tended to be the most widely used polymeric form of fibre reinforcement in concrete because of its excellent resistance to moisture, acids and alkalis and the economy of the raw material on a volume basis compared with steel and other alternatives (Krenchel and Jensen, 1980; Larsen and Krenchel, 1991). Polypropylene fibres are generally used at low volume fractions, about 0.1%, to control plastic shrinkage cracking, and in larger amounts in

fibrillated form up to 0.7% to improve the hardened concrete mechanical properties (Johnston, 2000).

Fibrillated fibres were developed to increase mechanical bonding with the concrete by separation and branching of the fibrils in the polymer strand during the mixing stage. Monofilament form of polypropylene is also available to be used in concrete, in some cases with surface treatment or surface texturing to improve bonding between fibres and concrete resulting in an enhancement in pullout resistance and overall reinforcing effectiveness (Krenchel and Shah, 1985). Polypropylene fibres are not expected to bond chemically in concrete matrix, due to the nature of polypropylene that is hydrophobic so that there is difficulty of wetting the surface by the cement paste. However, bonding has been shown to occur by mechanical interaction. Figure 2.2 shows a picture of different Polypropylene fibres.

2.3.2.2. Polyethylene Fibres

There has been considerable interest in the use of polyethylene fibres in FRC (Bijen, 1990; Kobayashi and Cho, 1981) due to its higher elastic modulus and better mechanical properties than polypropylene fibres. However, from an economical point of view they have relatively higher price than polypropylene fibres. High-density polyethylene in monofilament forms (40×0.9 mm) with wart-like surface deformations along the length of the fibre at volume fraction of 0.2-0.4% have been used in Japan (Kobayashi and Cho, 1981). These deformations are intended to improve the mechanical bonding in cement paste and mortar. It has been reported that polyethylene fibres could be easily dispersed

in concrete mixtures in volume percentages of up to 4% using conventional mixing techniques (Kobayashi and Cho, 1981).

2.3.2.3. Macro-Synthetic Fibres

Macro-synthetic fibres are a blend of polypropylene/polyethylene. Table 2.1 illustrates that the elastic modulus of macro synthetic fibres is significantly higher than polyethylene and polypropylene, while the tensile strength is equivalent to the high range of the other two fibres. It is highly resistant to alkali, acid, and salt environments, and has almost the same specific gravity as polyethylene and polypropylene. Concrete reinforced with macro synthetic fibres have three-dimensional reinforcing with enhanced flexural toughness, impact and abrasion resistance and will also help mitigate the formation of plastic shrinkage cracking in concrete.

The primary applications for macro synthetic fibres are in shotcrete as ground support in underground works, concrete for footpaths, and for some ground supported slabs. Structural applications of macro synthetic fibres include: thin walled pre-cast (septic tanks, vaults, walls, etc.), shotcrete for tunnel linings, pool construction and slope stabilization, pavements and white-toppings, slab on Grade construction (distribution centers, warehouses, etc.), and elevated decking. Macro synthetic fibres have also been used in marine/coastal applications, and for non-magnetic applications such as track slabs. A further application is in composite steel floor decks as a suitable alternative to replace temperature and shrinkage steel reinforcement.

2.4. Fibre Reinforced Polymers (FRP)

Fibre Reinforced Polymers are composite materials consisting of a matrix and reinforcing fibres. Some FRP products are shown in Figure 2.3 (FRP sheets, 2D FRP grids, 3D FRP grids, FRP bars, pipes, tubes and other various shapes according to the different needs).

The fibres are usually made of glass, carbon, aramid and hybrid fibres. Polyester resin, Vinyl Ester resin, Epoxy resin, Polyimide resin and thermoplastic resins are used as Matrix. Fibres are used as reinforcement in FRP for strength, stiffness and dimensional stability. The matrix is used to provide lateral support to the fibres and to protect the fibre from physical and chemical trauma due to the surroundings. In addition, the matrix provides some important physical characteristic to the FRP such as stiffness, strength, fracture toughness, diffusivity, thermal susceptibility etc.

The fibres are stronger than the matrix. The strength of FRP composite depends on the strength of the fibre and matrix both. The mechanical properties of the final FRP product depend on the fibre quality, orientation, shape, volumetric ratio and adhesion to the matrix and on the manufacturing process. A qualitative stress-strain relation of fibre, matrix and FRP are depicted in Figure 2.4.

FRP bars have been successfully used as reinforcement for reinforced concrete members instead of the traditional mild-steel reinforcement. The main advantages of such a selection are: 1) corrosion resistance, 2) high tensile strength, 3) low mechanical relaxation, 4) good toughness, 5) high fatigue resistance, 6) dimensional stability, 7) particular electrical and magnetic properties (transparent to electromagnetic emissions),

and 8) light weight (specific gravity $1.8 \times 10^{-3} \text{ g/mm}^3$ compared to $2.8 \times 10^{-3} \text{ g/mm}^3$ for the Aluminum and $7.6 \times 10^{-3} \text{ g/mm}^3$ for steel).

Glass fibre reinforced bars are the most common type of FRP. The lower modulus of elasticity is a drawback in using the GFRP as reinforcing material. GFRP have been used for bridge decks, parking structures, marine structures and also used to strengthen masonry buildings and concrete members to resist flexure and shear.

2.5. Shear Strength of GFRP Reinforced Concrete Beams

There are several mechanisms by which shear force is transmitted between two planes in a concrete member. Joint ASCE-ACI Committee 445 (1998) reported that after the formation of diagonal cracks in members without stirrups, shear is carried by concrete as a combination of five mechanisms as shown in Figure 2.5: (1) shear resistance of uncracked concrete compression zone, V_{cz} , (2) vertical component, (V_{ay}), of the interface shear, (V_a) (aggregate interlock), (3) dowel force of longitudinal reinforcement, V_d , (4) arching action, and (5) residual tensile stress across the cracks (f_t). The total contribution to the shear resistance from the five mechanisms is termed as the concrete contribution to the shear resistance, V_c .

A database of published test results on shear strength of conventional steel reinforcement for simply supported rectangular beams without axial force was compiled by Brown et al. (2006). The database contained the test results of twelve hundreds beams failing in shear. In contrast, the results of less than one-hundred FRP reinforced concrete beams without web reinforcement are available in the literature (Sherwood et al., 2008; Hoult et al., 2008; El-Sayed et al., 2005; and Alam, 2010).

The mechanical behaviour of FRP bars differs from the behaviour of conventional steel bars. FRP bars have high tensile strength combined with low elastic modulus, and elastic brittle stress-strain relationship. When FRP bars are used as flexural reinforcement, additional complications arise due to their different behaviour, different bond, and surface characteristics. Consequently, the shear behaviour of FRP reinforced concrete members is different than that of steel reinforced concrete members (Alam, 2010).

The mechanisms of shear transfer discussed above for conventional steel reinforced members are expected to be affected when using FRP bars. In addition, the relative contribution from these mechanisms may not be the same as in conventional steel reinforced concrete.

Due to the lower elastic modulus of FRP bars, their axial rigidity would be smaller than conventional steel reinforcement. Therefore, the area of concrete under compression would be smaller than that developed in similar steel reinforced sections. Hence, it is expected that the contributions of the uncracked concrete will be reduced.

To sustain a given load, due to the higher strength of the bars, a smaller amount of FRP reinforcement is required compared to steel. This leads to higher strain in the FRP bars. This higher strain coupled with the lower stiffness of the bars reduces the total stiffness of the member and thus larger deflections and wider cracks are attained. Therefore, a smaller amount of shear force is expected to be carried by aggregate interlock in FRP-reinforced members. Wider cracks also reduce the contribution from residual tensile stresses.

The dowel strength of GFRP bar is 8.7% of the ultimate tensile strength, obtained in pure dowel strength test (Grieff, 1996). Consequently, for FRP reinforcement, which has a low transverse stiffness and strength, an even smaller load will be carried by dowel action. Hence, the dowel contribution from FRP reinforcement could be neglected.

The shear strength of FRP reinforced concrete beams has been the subject of several studies, for example Yost et al., 2001; Alkhrdaji et al., 2001; Tureyen and Frosch, 2002; Razaqpur et al., 2004; El- Sayed et al., 2006a, 2006b; and Alam, 2010.

The main objective of the current thesis is to investigate the enhancement of the macro-synthetic fibres to the shear strength of GFRP reinforced beams. For a comprehensive literature review on the shear behaviour of FRP reinforced concrete beams, the reader should refer to Alam (2010).

2.6. Shear Strength of FRC Beams

Shear failure can be sudden and catastrophic. This is true for critical sections where, due to construction constraints, little or no reinforcement may be placed. For more than three decades, fibre reinforced concrete (FRC) has been the object of studies dealing with shear in FRC members. Tests performed to study the shear behaviour of FRC can be categorized into two general groups: direct shear tests and tests on beams. The direct shear tests are required to understand the basic shear transfer mechanisms of FRC, while the tests on beams are necessary to understand the behaviour of FRC structural members.

2.6.1. Direct Shear Tests

The investigations on direct shear behaviour included those of Swamy et al., 1987; Barr, 1987; and Tan and Mansur, 1990. Valle and Buyukozturk (1993) reported the results of an investigation on the strength and ductility of fibre reinforced concrete under direct shear. Three parameters were investigated: (1) concrete type - high strength versus normal strength concrete, (2) type of fibre - steel versus polypropylene fibres, and (3) the presence of steel stirrups crossing the shear plane. The direct shear transfer behaviour of fibre reinforced concrete was investigated through testing of specimens that had dimensions of 75 mm × 250 mm × 525 mm. In general, fibres proved to be more effective in high strength concrete than in normal strength concrete. It increased both ultimate load and overall ductility. Shear strength increase was found with fibre reinforced high strength concrete specimens to be 60% with steel fibres and 17% with polypropylene fibres. Whereas, for fibre reinforced normal strength concrete specimens, the shear strength increase was 36% with steel fibres and there was no increase with polypropylene fibres when compared to the strength of their respective un-reinforced plain concrete specimens. The enhancement performance of fibres in high strength concrete is attributed to the improved bond characteristics associated with the use of fibres in conjunction with high strength concrete. For the specimens with steel fibres, significant increases in ultimate load and ductility were observed. With polypropylene fibres, a lower increase in ultimate load was obtained when compared to the increase due to steel fibres. Ductility of the polypropylene fibre reinforced specimens was greater than that of the steel fibre reinforced specimens. In the tests involving the combination of fibres and conventional stirrups, slight increase in ultimate load with major improvements

in ductility were observed in comparison to the corresponding values for plain concrete specimens with conventional stirrups.

Direct shear tests on FRC specimens for steel and synthetic fibres were also carried out by Majdzadeh et al. (2006). The results showed that the steel fibre performed better than the synthetic fibres. It was found that for all fibres' types, an almost linear increase in shear strength of the composite with increasing fibre volume fraction.

2.6.2. Shear in FRC Beams

In general, the shear failure of a reinforced concrete beam is directly related to the diagonal tensile cracking that develops in the direction perpendicular to the principal tensile stress axis. Once tensile cracking occurs, the tensile stress at the crack surfaces rapidly softens, which significantly reduces the shear strength of the beam.

Mansur et al. (1986) tested beams with $b = 152$ mm, $d = 197$ mm, and $a/d = 3.6$. The researcher found that adding 0.5% of hooked-end steel fibres by volume with length of 30 mm and aspect ratio of 60 increased the shear capacity by only 8%.

According to experimental results (Narayanan and Darwish, 1987; and Li et al., 1992), the addition of fibres to concrete effectively improved the shear strength of concrete. This is attributed to the effect of fibres transferring the tensile stress across crack surfaces that are called the crack-bridging stress. Due to such material characteristics of the fibres, the shear strength of a fibre reinforced concrete (FRC) beam increases. Furthermore, the failure mode of the beam is changed to be more ductile.

The ultimate shear strength of longitudinally reinforced fibre concrete beams without shear stirrups were examined (Li et al., 1992) to illustrate the effectiveness of

both steel and synthetic fibres as shear reinforcement. The test program employed four fibre types (steel, acrylic, aramid and polyethylene); shear span to effective depth ratio (a/d) ranging from 1.0 to 4.25; reinforcement ratios of 1.1%, 2.2% and 3.3%; and beam depths of 102 mm and 204 mm. In all beams with shear span to depth ratio (a/d) of 2.5 or greater, failure occurred suddenly when the first diagonal shear crack appeared. Fibre reinforced beams with a/d greater than 2.5 exhibited flexural-shear cracking, with diagonal shear cracks forming as an extension of flexural crack, a number of shear cracks formed along the beam span before ultimate load. This work showed correlations exist between the shear strength and a parameter that involved, moreover, demonstrates experimentally the dependence of shear structural properties on material tensile properties that can be efficiently modified by short random fibre reinforcement.

It was also suggested in earlier studies that the stirrups, as shear reinforcement in concrete members, can be partially or totally replaced using fibres (Mansur et al., 1986; and Lim et al., 1987). It should be noted that most of the work on shear in beams was limited to concrete of normal strength with steel fibres.

Noghabai (2000) performed shear tests on beams with $b = 200$ mm, $d = 180$ mm, and shear span to depth ratio (a/d) of 3.3. The researcher found that adding 0.5% and 0.75% of hooked-end steel fibres by volume with a length of 60 mm and aspect ratio of 86 increased the shear capacity by 20% and 25%, respectively.

Kwak et al. (2002) tested beams with hooked-end steel fibres with $b = 125$ mm, $d = 212$ mm, and $a/d = 3.0$. The results showed that adding 0.5% and 0.75% of the fibres by volume increased the shear capacity by 22% and 28% respectively.

Dupont and Vandewalle (2003) reported a test program in which beams with $b = 200$ mm, $d = 260$ mm, and $a/d = 3.5$ were tested. It was shown that using hooked-end steel fibres with a length of 60 mm and aspect ratio of 67 with volume fractions of 0.51% and 0.76% increased the shear strength of the beams by 35% and 65% respectively.

A detailed investigation on the shear behaviour of fibre reinforced self-consolidating concrete (FR-SCC) beams was carried out by Greenough and Nehdi (2008). FR-SCC mixtures were designed to study the influence of fibre type, fibre anchorage, fibre aspect ratio and fibre content on the shear performance of reinforced concrete slender beams without stirrups, and to determine the suitability of using fibres to satisfy minimum shear reinforcement requirements. It was observed that the short discrete fibres could significantly improve the shear behaviour of reinforced SCC slender beams and beams incorporating 1% steel fibre addition could achieve a 128% increase in shear capacity over that of the reference beam without fibres. Furthermore, the FR-SCC beams performed better under shear loading than conventional fibre-reinforced concrete (FRC) beams. The experimental results obtained on 13 FR-SCC slender beams indicated the possibility of using fibres as minimum shear reinforcement.

Choi et al. (2007) presented an interpretation of the variations of normal and shear stresses according to flexural deformation at cross section as shown in Figure 2.6. In reinforced concrete slender beams, the applied shear force is resisted mainly by the compression zone of intact concrete rather than by tension zone. On the other hand, in fibre reinforced concrete beams, because post-cracking tensile strength is developed by fibres, the applied shear force is resisted also by the tension zone. In the study done by the overall shear strength was defined as the sum of the contribution of compression and

tension zones. The contribution of the compression zone was evaluated considering the interaction with compressive stress developed by flexural moment. The contribution of tension zone was evaluated considering the effect of the post-cracking tensile strength of FRC. The magnitude and distribution of compressive stress in the compression zone vary according to the flexural deformation, which affects the shear capacity of a cross section.

A large database of test results for shear strength of steel fibre reinforced concrete (SFRC) beams obtained by many researchers was recently compiled by Parra-Montesions (2006).

2.6.3. Shear in FRC beams with Synthetic Fibres

Although the majority of the previous work on shear of FRC has been performed with steel fibres, there are few studies reported results on shear with synthetic fibres. Li et al. (1992) tested beams reinforced with flexural bars that contained several types of synthetic (acrylic, aramid and polyethylene) and steel fibres as mentioned earlier. Two of the three synthetic fibres (polyethylene and aramid) showed significant improvements in shear strength of the concrete beams.

Altoubat et al. (2007) investigated six large scale beams with $d = 400$ mm, $b = 280$ mm, $a/d = 3.5$ and macro synthetic fibres that have volumes of 0.5% and 0.75%. The test results showed that the addition of synthetic fibres enhanced the shear strength of the concrete beams by 12% and 25% by adding 0.5% and 0.75% respectively. The fibres modified the shear failure behaviour; in general the shear failure of the SNFRC beams was less brittle.

Altoubat et al. (2009) tested twenty-seven steel reinforced beams to determine the effect of a newly developed high-modulus macro synthetic fibres on the shear strength and failure behaviour of longitudinally reinforced concrete (RC) beams without stirrups. The results showed that the addition of macro synthetic fibres significantly improved the shear strength and ductility of the RC beams and modified the cracking and failure behaviour. The authors concluded that macro-synthetic fibres could be used as an alternative to minimum shear reinforcement as required by ACI 318-08.

The current research is focused on the effect of macro synthetic fibres on the shear behaviour of GFRP reinforced concrete beams. Since this type of fibre is relatively new; there is very little published research work available regarding the shear enhancement of such fibres. In addition, and to the best of the authors' knowledge, there was no investigation of the behaviour of macro-synthetic fibre reinforced beams with GFRP reinforcement.

2.7. Existing Shear Strength Models for FRC

Test results revealed that the material strength of FRC is significantly affected by the volume ratio, aspect ratio, and shape of the fibres. Like the shear strengths of reinforced concrete beams, as the compressive strength of concrete and the amount of longitudinal tensile reinforcement increase, the shear strengths of FRC beams increase. As the shear span to depth ratio increases, the shear strengths of FRC beams decrease. Therefore, the primary parameters that affect the shear strengths of FRC beams are the volume ratio, aspect ratio and shape of the fibres, the compressive strength of concrete, the ratio of flexural reinforcement, and the shear span to depth ratio. Based on the experimental

results, many researchers proposed design equations that were defined as functions of the primary design parameters. Existing shear strength models, however, do not accurately predict the strengths of both normal-strength FRC and high-strength FRC beams. Table 2.2 summarizes the different expressions that were proposed by several researchers to calculate the shear strength of FRC beams. Almost, all of those expressions were developed for FRC with steel fibres. From a code prospective, ACI Committee 544 (1996) recommended Sharma's model, but a code-based design equation for the shear strengths of FRC beams does not exist yet in the North American codes.

2.8. Design Codes Equations for FRP Reinforced Concrete Members

Most of the current design provisions for FRP-reinforced concrete beams follow the same approach as conventional steel reinforced concrete design methods; using the well-known ($V_c + V_s$) format to compute the shear resistance of FRP reinforced concrete members. Although, the specific manner in which the codes specify the contribution of concrete, V_c , may differ considerably, the steel contribution, V_s , is determined using the same equations as those for conventional steel reinforcement. This section summarizes the design equations used to compute V_c as recommended by the American Concrete Institute (ACI 440.1R-06) and the Canadian Standard Association (CSA S806-10). Nonetheless, both codes are used to give the shear strength of FRP reinforced concrete members that contain no fibres.

2.8.1. American Concrete Institute (ACI 440.1R-06)

To address some issues and to find a reasonable equation for calculating the shear strength of FRP reinforced concrete beams, the American Concrete Institute has revised the shear equation in ACI 440.1R-06 for a third time based on the work of Tureyen and Frosch (2002). According to this new revision, the concrete shear capacity, V_c , for flexural members with FRP as main reinforcement is given as:

$$V_c = \frac{2}{5} \sqrt{f'_c} b_w c \quad (2.1)$$

where b_w is the width of the web and c is the cracked transformed section neutral axis depth.

2.8.2. Canadian Standard Association (CSA S806-10)

According to the Canadian Standard Association (CSA S806-10) Code, the shear strength of a section, having either at least the minimum amount of transverse reinforcement as specified by the CSA standard or an effective depth not exceeding 300 mm and with no axial load acting on them is given by:

$$V_c = 0.045 \lambda \phi_c k_m k_r (f'_c)^{1/3} b_w d \quad (2.2)$$

where λ reflects the concrete density factor and ϕ_c represents the concrete material resistance factor. The factors k_m and k_r can be calculated as follows:

$$k_m = \sqrt{d \frac{V_f}{M_f}} \leq 1.0 \quad (2.3)$$

$$k_r = 1 + (E_f \rho_f)^{1/3} \quad (2.4)$$

It should be noted that V_c calculated according to Eq. (2.2) shall not be taken greater than $0.2\phi_c\sqrt{f'_c}b_wd$ nor less than $0.1\phi_c\sqrt{f'_c}b_wd$. In the determination of V_c , f'_c shall not be taken greater than 60 MPa. The quantity dV_f/M_f is equivalent to d/a , and shall not be taken as greater than 1.0, where V_f and M_f are the factored shear force and bending moment at the section of interest. This equation considers the effect of axial stiffness ($E_f\rho_f$), shear span-to-depth ratio (a/d), and concrete compressive strength (f'_c) for calculating the shear strength.

To account for the size effect for sections with an effective depth greater than 300 mm and with no transverse shear reinforcement or less transverse reinforcement than the minimum given by CSA standard, the value of V_c shall be multiplied by the factor k_s , as given by the following equation:

$$k_s = \frac{750}{450 + d} \leq 1.0 \quad (2.5)$$

This equation gives the concrete contribution to the shear strength of FRP reinforced concrete members regardless of the FRP type or the FRP reinforcement ratio, which is anomalous to the findings that the shear strength increases with an increase in the reinforcement ratio. Thus, the equation gives more conservative results for the beams with high axial stiffness ($E_f\rho_f$) of the longitudinal FRP bar (El-Sayed et al., 2006a). In addition, the equation neglects the shear transfer by arch action and it is quite conservative for beams with a/d less than 2.5 (Razaqpur and Isgor, 2006). The transition between the limits of shear strength is abrupt and unusual, and hence this issue should be considered in the future issues of the Code.

2.9. Finite Element Analysis

To model the nonlinear behaviour of concrete and its complex behaviour, such as cracking, aggregate interlock, bond, and dowel action, numerous finite element models have been developed (ASCE, 1982). Some of the available finite element models can simulate the nonlinear behaviour of traditional reinforced concrete beam in a realistic way. Various approaches of these finite element models differ in: a) material models, b) element formulations, and c) solution procedures.

Extensive research has been done on the application of finite element method to model the behaviour of reinforced concrete members. A comprehensive summary by Darwin (1993) gives a wide range of options available to perform a reliable finite element analysis of steel reinforced concrete. It concluded that there are both usefulness and limitations of finite element modeling of reinforced concrete. These limitations may be due to the nonlinear behaviour of reinforced concrete. Three major factors cause the nonlinear response of reinforced concrete, namely: (a) crushing in compression, (b) cracking of concrete in tension, and (c) yielding of reinforcement. It can generally be argued that a specific approach will be more suited to certain structure/loading situations and less to others; no single approach performs well over the entire range of structural details and loading conditions encountered in practice (Coronelli and Mulas, 2006).

Kachlakev et al. (2001) used ANSYS to study concrete beam members with externally bonded Carbon Fibre Reinforced Polymer (CFRP) fabric. One quarter of the beam was modeled as shown in Figure 2.7. Nonlinear Newton Raphson approach was utilized to trace the equilibrium path during the load-deformation response. It was found that convergence of solutions for the model was difficult to be achieved due to the

nonlinear behaviour of reinforced concrete. At certain stages in the analysis, load step sizes were varied from large (at points of linearity in the response) to small (when instances of cracking and steel yielding occurred). The load-deflection curve for the non-CFRP reinforced beam that was plotted showed a reasonable correlation with experimental data of McCurry and Kachlakev (2000), as shown in Figure 2.8. Furthermore, concrete cracking/crushing plots were created at different load levels to examine the different types of cracking that occurred within the concrete, as shown in Figure 2.9. The different types of concrete failure that can occur are flexural cracks, compression failure (crushing), and diagonal tension cracks. Flexural cracks (Figure 2.9a) form vertically up to the beam. Compression failures (Figure 2.9b) are shown as circles. Diagonal tension cracks (Figure 2.9c) form diagonally up to the beam towards the loading that is applied.

Tavarez (2001) discusses three techniques that exist to model steel reinforcement in finite element models for reinforced concrete (Figure 2.10), the discrete model, the embedded model, and the smeared model. The reinforcement in the discrete model (Figure 2.10a) uses bar or beam elements that are connected to concrete mesh nodes. Therefore, the concrete and the reinforcement mesh share the same nodes. The embedded model shown in Figure 2.10b overcomes the concrete mesh restriction because the stiffness of the reinforcing steel is evaluated separately from the concrete elements. The model is built in a way that keeps reinforcing steel displacements compatible with the surrounding concrete elements. When reinforcement is complex, this model is very advantageous. However, this model increases the number of nodes and degrees of freedom in the model. The smeared model shown in Figure 2.10c assumes that

reinforcement is uniformly spread throughout the concrete elements in a defined region of the FE mesh. This approach is used for large-scale models where the reinforcement does not significantly contribute to the overall response of the structure. Fanning (2001) modeled the response of the reinforcement using the discrete model and the smeared model for reinforced concrete beams. It was found that the best modeling strategy was to use the discrete model when modeling reinforcement.

FRP has different properties than those of steel reinforcement. Hence, the finite element modelling of shear critical FRP reinforced members may differ from that of steel reinforced members (Alam, 2010). The difference in the predicted behaviour of the GFRP reinforced beam can be attributed to the low modulus of elasticity, different bond characteristics, and difference in tension stiffening. Since FRP does not yield before failure, this will not create any nonlinearity. However, the interaction of the constituents of reinforced concrete, such as bond-slip between FRP and surrounding concrete, aggregate interlock at a crack, and dowel action of the longitudinal FRP at a crack, create nonlinearities.

Nour et al. (2007) investigated the nonlinear response of concrete members reinforced with internal and external FRP bars using finite element analysis. A 3D hypo-elastic concrete constitutive law that models the nonlinear behaviour of concrete using a scalar damage parameter was utilized in the investigation. In tension, the model adopted a macroscopic approach that was directly integrated into the concrete law. The proposed tension stiffening model was based on the nature of the reinforcement and varied as a function of the member strain. The model simulated the behaviour of internal and external FRP reinforced members, which agreed well with the experimental results.

Nonetheless, the investigation was carried out for beams that were designed to fail in flexure rather than in shear.

Alam (2010) carried out a finite element analysis to simulate the behaviour of shear critical FRP reinforced concrete beams with a wide range of design parameters such as shear span-to-depth ratio, depth of beam, reinforcement ratio, concrete strength, and reinforcement type. Two concrete material models were used. The models were a concrete damage plasticity model (Model-1) and a hypo-elastic concrete model (Model-2). An idealized tension-stiffening model was proposed based on the reinforcement type and varies as a function of the member strain. The models were implemented in general purpose finite element programs ABAQUS and ADINA, respectively. The models were used to simulate the experimental results of some of the beams tested in this investigation and to examine how well these models simulate the behaviour of shear critical FRP reinforced concrete members. The models predicted results were in a reasonable agreement with the experimental results. It was observed that a better prediction can be achieved using a proper tension-stiffening idealization.

The behaviour of FRC under tensile loading can be understood from Figure 2.11. A plain concrete member cracks in two pieces when the structure is subjected to the peak tensile load and cannot withstand further load or deformation. The fibre reinforced concrete structure cracks at the same peak tensile load, but does not separate and can maintain a load up to the point of very large deformation. The area under the curve shows the energy absorbed by the FRC when subjected to tensile load. This can be termed as the post cracking response of the FRC.

Despite the large number of experimental results available on the effectiveness of steel fibres in substituting the minimum code-required shear reinforcement in beams, only a few numerical studies have been published concerning fibre-reinforced concrete structures.

Minelli and Vecchio (2006) analyzed the behaviour of full-scale steel fibre-reinforced concrete (SFRC) elements using a finite element code based on the modified compression field theory (MCFT) and the disturbed stress field model (DSFM), and suitably adapted for steel fibre reinforcement. The numerical model was validated against the experimental results obtained on SFRC structural elements and was shown to adequately simulate the strength, stiffness, ductility, crack pattern development, and failure modes of all specimens tested, including those lightly reinforced or with fibres only.

Özcan et al. (2009) presented an experimental and finite element analysis of three SFRC beams. For this purpose, three SFRC beams with 250 mm × 350 mm × 2000 mm dimensions were produced using a concrete class of C20 with 30 kg/m³ dosage of steel fibres and steel class S420 with shear stirrups. SFRC beams were subjected to bending by a four-point loading setup in certified beam-loading frame. The tests were conducted in load control mode. The beams were loaded until failure and the loadings were stopped when the tensile steel bars were broken into two pieces. One of the SFRC beams was modeled by using nonlinear material properties adopted from experimental study and was analyzed till the ultimate failure cracks by ANSYS. Eight-node solid brick elements were used to model the concrete. Internal reinforcement was modeled by using 3D spar elements. A quarter of the full beam was taken into account in the modeling process. The

results obtained from the finite element and experimental analyses were compared to each other. It was seen from the results that the finite element failure behaviour indicated a good agreement with the experimental failure behaviour.

Table 2.1: Properties comparison of macro-synthetic, Polypropylene and Polyethylene fibres

Fibre Type	Macro synthetic ¹	Polyethylene ²	Polypropylene ²
Specific Gravity	0.92	0.92-0.96	0.90-0.91
Absorption	None	None	None
Modulus of Elasticity, GPa	9.5	5.0	3.4-4.8
Tensile Strength, MPa	620	76-586	138-689
Melting Point, °C	320	134	166
Ignition Point, °C	590	-----	593
Alkali Resistance	High	High	High

¹ Derived from Grace Company's Product Information.

² Derived from ACI 544.1R-96.

Table 2.2: Existing shear strength models for FRC beams without web reinforcement

Investigator	Shear strength models, MPa
Mansur et al. (1986)	$v_n = 0.41 \left(\tau V_f \frac{l_f}{d_f} \right) + \left(0.16 \sqrt{f'_c} + 17.2 \frac{\rho V d}{M} \right)$
Sharma (1986)	$v_n = k f_t \left(\frac{d}{a} \right)^{0.25}$ <p>Recommended by ACI Committee 544.1R-96</p> <p>$k = 1$ if f_t is obtained by direct tension test; $k = 2/3$ if f_t is obtained by indirect tension test; $k = 4/9$ if f_t is obtained using modulus of rupture; or $f_t = 0.79 \sqrt{f'_c}$, f'_c in MPa.</p>
Narayanan and Darwish (1987)	$v_n = e \left[0.24 f_{cp} + 80 \rho \frac{d}{a} \right] + 0.41 \tau F$ <p>$e = 1$ for $a/d > 2.8$ $e = 2.8 d/a$ for other case</p>
Ashour et al. (1992)	$v_n = \left(0.7 \sqrt{f'_c} + 7 F \right) \frac{d}{a} + 17.2 \rho \frac{d}{a}, f'_c \text{ in MPa.}$
Li et al. (1992)	<p>For FRC, d in m.</p> $v_n = 1.25 + 4.68 \left[(f_r f_{sp})^{3/4} \left(\rho \frac{d}{a} \right)^{1/3} d^{-1/3} \right] \text{ for } a/d > 2.5$ $v_n = 9.16 \left[(f_r)^{2/3} (\rho)^{1/3} \left(\frac{d}{a} \right) \right] \text{ for } a/d < 2.5$
Shin et al. (1994)	$v_n = 0.22 f_{sp} + 217 \rho \left(\frac{d}{a} \right) + 0.34 \tau F \text{ for } a/d < 3$ $v_n = 0.19 f_{sp} + 93 \rho \left(\frac{d}{a} \right) + 0.34 \tau F \text{ for } a/d \geq 3$
Khuntia et al. (1999)	$v_n = (0.167 + 0.25 F) \sqrt{f'_c}, f'_c \text{ in MPa.}$ $v_n = \left(0.418 \frac{d}{a} + 0.25 F \right) \sqrt{f'_c}, \text{ for } a/d < 2.5, f'_c \text{ in MPa.}$
Kwak et al. (2002)	$v_n = 2.1 e f_{sp}^{0.7} \left(\rho \frac{d}{a} \right)^{0.22} + 0.8 (0.41 \tau F)^{0.97}$ <p>$e = 1$ for $a/d > 3.5$ $e = 3.5 d/a$ for other case</p>
Greenough and Nehdi (2008)	$v_n = 0.35 \left(1 + \sqrt{\frac{400}{d}} \right) f_c^{0.18} \left((1 + F) \rho \frac{d}{a} \right)^{0.4} + 0.90 \eta_o \tau F$

Note: f_r = modulus of rupture; f_{sp} = splitting tensile strength; $F = V_f(L/D)$ β = fibre factor; V_f = volume ratio of fibre; L/D = aspect ratio of fibre; β = factor for fibre shape and concrete type; and τ = average interfacial bond stress of fibre matrix ($\tau = 4.15$ MPa).



Figure 2.1: Steel, glass, synthetic and natural fibres with different length and shape



Figure 2.2: Polypropylene fibres are produced either as (left) fine fibrils with rectangular cross section or (right) cylindrical monofilament



Figure 2.3: Available shapes of FRP products (ISIS, 2003)

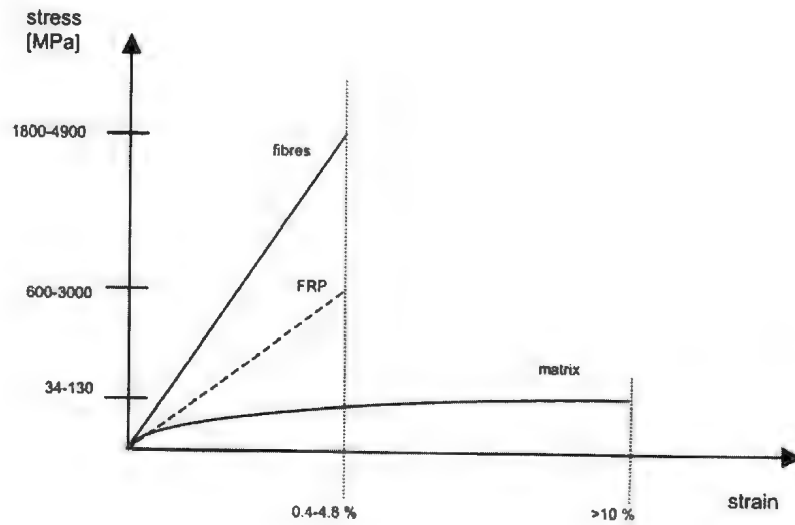


Figure 2.4: Stress vs. strain relationships for FRP reinforcement and matrix (ISIS, 2003)

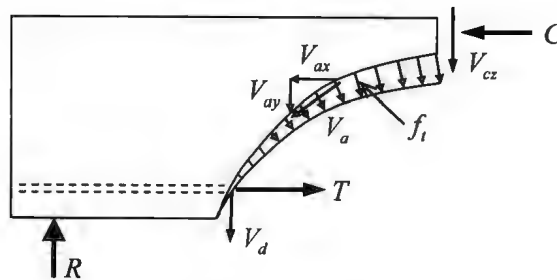


Figure 2.5: Internal forces in a cracked beam without stirrups

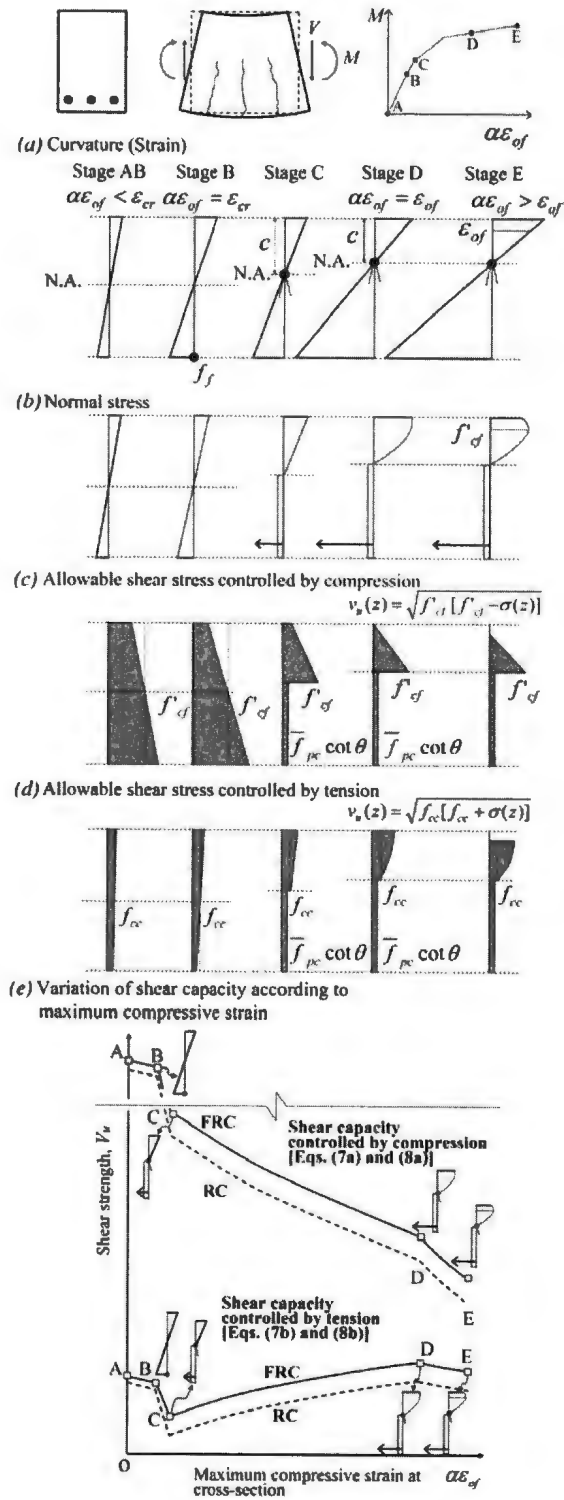


Figure 2.6: Variations of normal and shear stresses according to flexural deformation at cross section (Choi et al., 2007)

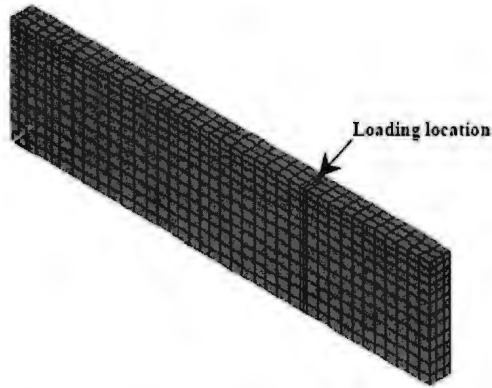


Figure 2.7: FEM discretization for a quarter of the beam (Kachlakev et al., 2001)

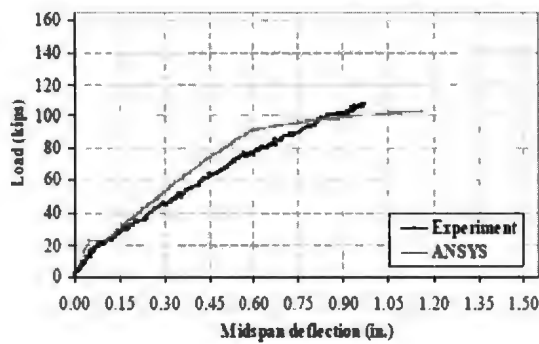


Figure 2.8: Load vs. deflection plot (Kachlakev et al., 2001)

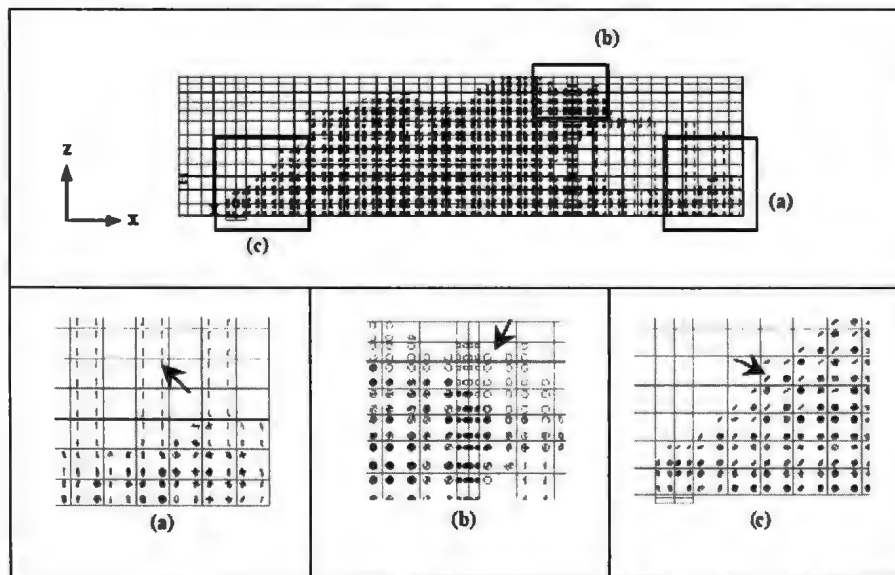
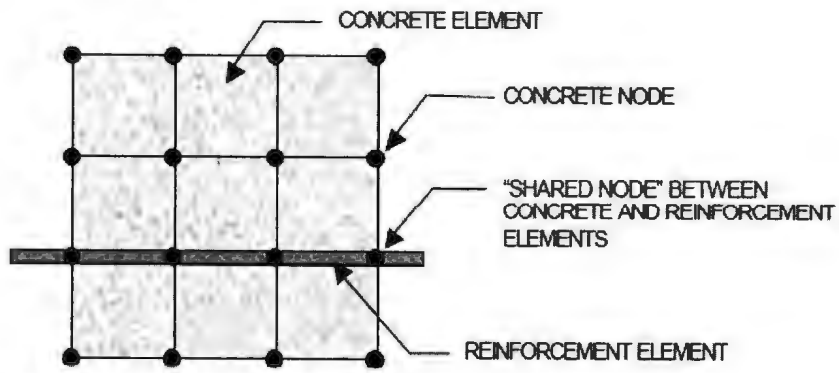
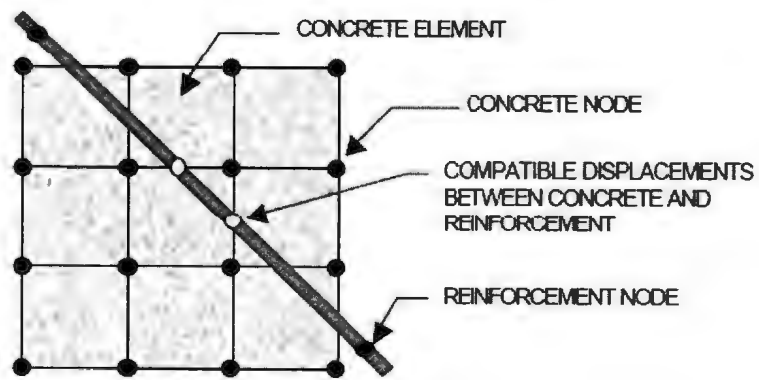


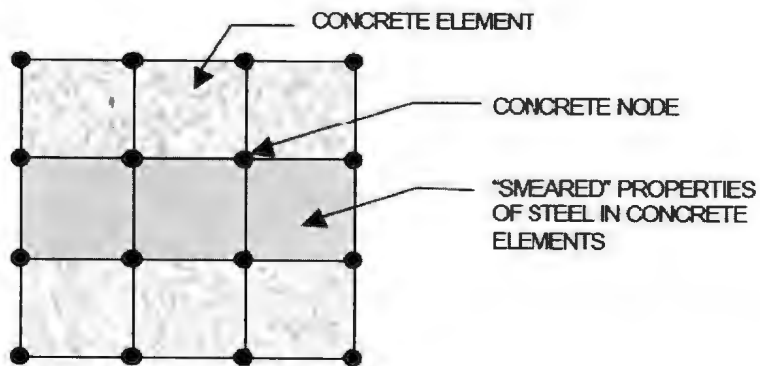
Figure 2.9: Typical cracking signs in finite element models: (a) Flexural cracks; (b) Compressive cracks; (c) Diagonal tensile cracks (Kachlakev et al., 2001)



(a) Discrete



(b) Embedded



(c) Smeared

Figure 2.10: Models for reinforcement in reinforced concrete: (a) Discrete; (b) Embedded; (c) Smeared (Tavarez, 2001)

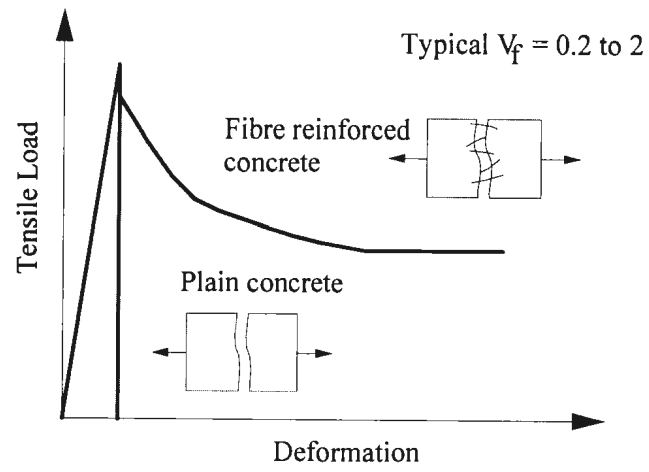


Figure 2.11: Tensile load vs. deformation for plain and fibre reinforced concrete

Chapter 3

Material Properties

3.1. Introduction

This chapter describes the different materials used in the current research work. The different concrete mixtures are presented. The properties of the macro-synthetic fibres and GFRP bars are also given as per the manufacturers' specifications.

Four different mixes were used in the current investigation. The main variable was the fibre ratio by volume. The four levels of fibre volume percentages were: 0%, 0.5%, 0.75% and 1.0%.

The mechanical properties of the hardened concrete were examined to develop a better understanding of the effect of the different macro-synthetic fibre volumes on the hardened concrete properties. Thirty two prisms (100 mm × 100 mm × 400 mm) and thirty six cylinders (100 mm × 200 mm and 150 mm × 300 mm) were cast to determine the mechanical properties of concrete. The examined mechanical properties were the compressive strength, indirect tension, modulus of rupture and flexure toughness. All tests were carried out in accordance with the appropriate ASTM standards.

3.2. Materials

3.2.1. Concrete

Ordinary Portland cement CSA type 10 was used. The coarse aggregate was mostly crushed sandstone with a maximum nominal size of 19 mm. The fine aggregate was identical in composition to the coarse aggregate. The water-cement ratio used for the present concrete mix was $w/c = 0.36$. The target compressive strength was 40 MPa.

Details of the concrete mix proportions are given in Table 3.1. The concrete used in casting the test beams was batched at a local batch plant and delivered to the concrete laboratory.

The concrete used in the beams was delivered at different times of the year. As a result, and due to the weather conditions in Newfoundland, there was a difference between the targeted and actual strength due to the difference in the moisture content in the fine aggregates. The setting of the batch plant was such that it ensured a uniform value of the compressive strength, which was acceptably satisfied for almost all the beams. It should be noted that it is practically impossible to replicate an identical batch with no tolerances from a batch plant.

The concrete mix proportions were maintained for all the different mixes. The fibres were added to the concrete mix at the batch plant. The fibres were added to the mix after the concrete was batched to the concrete truck. After the fibres were added, sufficient mixed time was used to ensure adequate dispersion of the fibres.

For the mixes with fibres ratio of 0.5% and 0.75%, a superplasticizer was added to improve the workability of the mix. The superplasticizer had a modified naphthalene sulfonate base and is commercially known as DARACEM[®] 19. The mix with 0.5% fibres ratio had an excellent workability while pouring the beams. On the other hand, the 0.75% fibres mix showed some balling and less workability. The operator accidentally added some water to improve the workability. That action was stopped and the workability was adjusted using the plasticizer. For the 1% mix, care was given to the mixing procedure and a polycarboxylate based high-range water-reducing admixture (commercially known

as ADVA[®] 190) was used. This mix showed excellent workability and uniformity when casting the test beams.

3.2.2. Synthetic Fibres

The synthetic fibres used in this investigation, as shown in Figure 2.2, were 40 mm long, with an aspect ratio of 90 and tensile strength of 620 MPa. It is commercially known as STRUX[®] 90/40. The fibres are composed of a polymer blend that partially fibrillates during mixing to increase its bond with the cement matrix, which improves the mechanical characteristics of the concrete.

3.2.3. GFRP Bars

The reinforcing materials used in this investigation were Glass Fibre Reinforced Polymer (GFRP). Two different sizes of the GFRP bars were used in this study. The bars were manufactured by Pultrall Inc. Quebec, Canada, and were sand coated to enhance the bond between the bars and the concrete.

Figure 3.1 shows GFRP bars used in the experimental investigation. The mechanical properties of GFRP bars are presented in Table 3.2, as provided by the manufacturer. Based on the pullout test provided by the manufacturer, the maximum bond stress is 11.6 MPa. The bond stress is an important factor that affects the cracking behaviour of concrete members.

3.3 Properties of Hardened Concrete

3.3.1. Compressive Strength

Six standard concrete cylinders (150 mm × 300 mm) and three small cylinders (100 mm × 200 mm) were prepared from each concrete mix at the time of casting of the concrete test beams. The cylinders were cured and kept at the same location as the test beams in the laboratory at temperature of around 20 °C. The cylinders were tested at the same time of testing the beams.

The test cylinders were capped with a high-strength sulphur compound on both ends and tested in accordance with ASTM C39 for determining the compressive strength. A picture of the compression test machine is depicted in Figure 3.2. The compression machine has a capacity of 2200 kN. The automatic loading cycle is controlled by a closed-loop microprocessor hydraulic system in load control. The results could also be shown in real time through a digital display system. A loading rate of 0.235 MPa/s was used until failure occurred as per the ASTM C39 standard.

The obtained values of the compressive strength of the different mixtures are shown in Table 3.3 based on the average results of three 150 mm × 300 mm cylinders. Comparing the results of mixes 2 (0.5%) and 4 (1%) indicated that there was an increase in the compressive strength as the fibre volume was increased. As mentioned earlier, the concrete was batched and mixed at a local batch plant. It was not possible to completely replicate the mixes produced by the plant without any tolerances. Therefore, there was some variation in the compressive strength of the different concrete mixtures. Hence, it was not possible to conclude, in the current study, whether increasing the fibre volume has an effect on the compressive strength of concrete. The apparent increase could have

been as a result in the variation in the compressive strength of the concrete produced at the batch plant.

The results of the compressive strength for the 100 mm × 200 mm and 150 mm × 300 mm cylinders, for mix no. 2 (0.5%), are given in Table 3.4. The results indicated that the 100 mm × 200 mm cylinders showed a higher compressive strength compared to the standard 150 mm × 300 mm cylinders. It should be noted that the fibres were 40 mm long and the smaller cylinders had a 100 mm diameter. It appears that the size of the specimen had an effect on the measured compressive strength. Hence, it was decided to use only the standard size cylinders to obtain the compressive strength of the different concrete mixtures.

3.3.2. Splitting Tensile Strength

The splitting tensile strength was measured using 150 mm × 300 mm cylinders. Three cylinders were tested, from each mix, in accordance with ASTM C496. The test method consisted of applying a diametric compressive force along the length of the specimen, as shown in Figure 3.3. The applied loading rate was 1333 N/s until failure occurred.

The obtained values of the splitting tensile strength of the different mixtures are shown in Table 3.3. Figure 3.4 shows the increase in tensile strength due to the addition of fibres. In general, it can be seen that the splitting tensile strength was increased with the addition of fibres. It can be noticed that the fibres increased the concrete splitting tensile strength by holding the concrete together after the cracking occurred and before failure, as shown in Figure 3.5. Hence, the fibres seem to increase the tensile strength

when compared to plain concrete. On the other hand, increasing the fibre volume beyond 0.5% did not result any significant increase in the splitting tensile strength.

3.3.3. Modulus of Rupture

Four concrete prisms (100 mm × 100 mm × 400 mm) were prepared from each concrete mix at the time of casting of the concrete test beams. The prisms were cured and kept under the same conditions as the test cylinders and were tested at the same time of testing the beams. The modulus of rupture (f_r) tests were carried out in accordance with ASTM C78, using simple beam with third-point loading, as shown in Figure 3.6. The loading rate was 1.0 MPa per minute.

The measured values of the modulus of rupture, for the different mixtures, are shown in Table 3.3. Figure 3.7 shows the increase in modulus of rupture due to the addition of fibres. In general, and as in the case of splitting tensile strength, the modulus of rupture was increased with the addition of fibres. The addition of fibres increased the modulus of rupture when compared to plain concrete. Nonetheless, increasing the fibre volume beyond 0.5% did not result any significant increase in the modulus of rupture.

The plain concrete prisms cracked in two pieces when the prism reached the peak load and could not withstand further load or deformation. The fibre reinforced concrete prisms did not separate when the peak load was reached and maintained some load up to the point of large deformation. The area under the curve shows the energy absorbed by the prisms, as shown in Figure 3.8.

Table 3.1: Mix proportions of one cubic meter of concrete

Cement (kg/m ³)	350
Coarse aggregate (kg/m ³)	825
Fine aggregate (kg/m ³)	1050
w/c ratio	0.36

Table 3.2: ISOROD Glass-Vinyl ester properties provided by the manufacturer

Bar Designation	Cross sectional area mm ²	Diameter mm	Tensile strength MPa	Modulus of elasticity GPa	Ultimate strain %
5/8 (16)	198	15.9	727	44	1.65 ± 0.03
1/2 (13)	127	12.7	756	45	1.70 ± 0.03

Table 3.3: Properties of hardened concrete

Mix No.	Fibre Volume %	Compressive strength* MPa	Splitting tensile strength MPa	Modulus of rupture MPa
1	0.0%	40	2.90	4.20
2	0.5%	44	4.01	6.20
3	0.7%	41	3.44	5.80
4	1.0%	47	4.21	5.94

*Based on 150 mm × 300 mm cylinders

Table 3.4: Concrete compressive strength of mix no. 2 for different cylinder sizes

Cylinder No.	100 × 200 mm MPa	150 × 300 mm MPa
1	47.72	44.19
2	44.14	43.49
3	47.01	45.28
Average	46.29	44.32



Figure 3.1: GFRP bars used in the test



Figure 3.2: Compressive strength test setup



Figure 3.3: Splitting tensile test setup

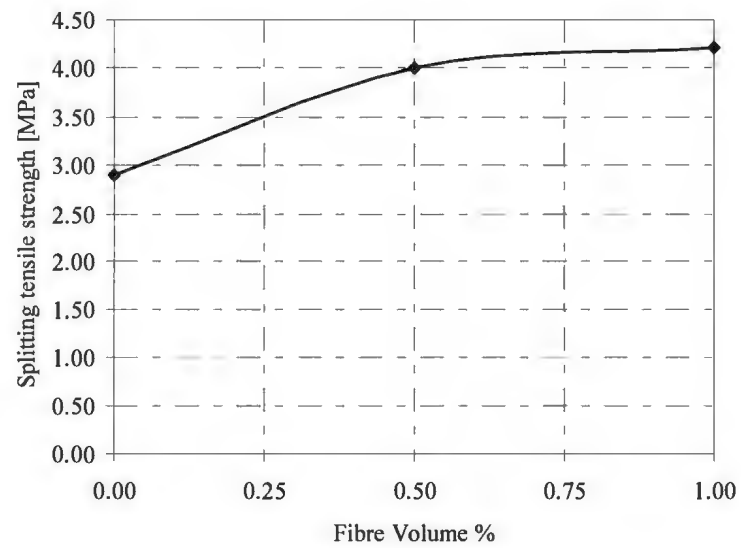
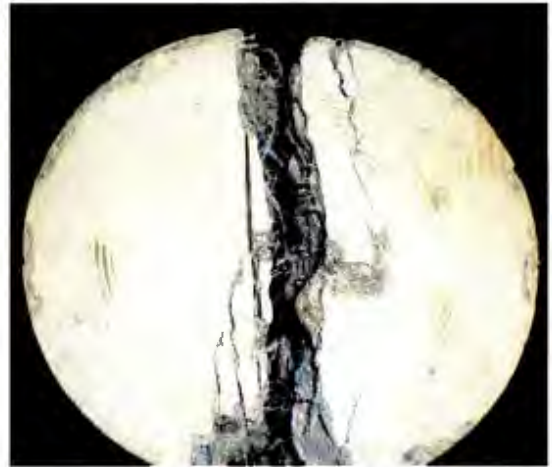


Figure 3.4: Relative increases in splitting tensile strength due to fibre addition



(a) Splitting tensile failure



(b) Compression failure

Figure 3.5: Fibres holding the concrete on test cylinder: (a) Splitting tensile failure; (b) Compression failure



Figure 3.6: Modulus of rupture test setup

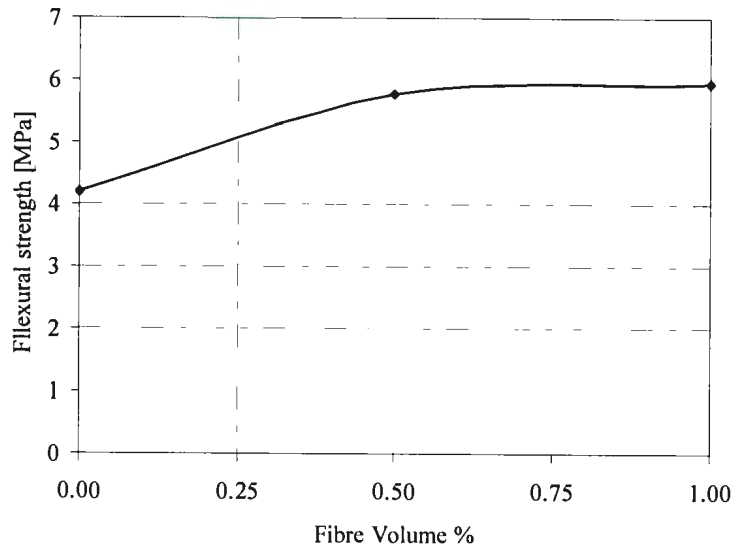


Figure 3.7: Relative increases in flexural tensile strength due to fibre addition

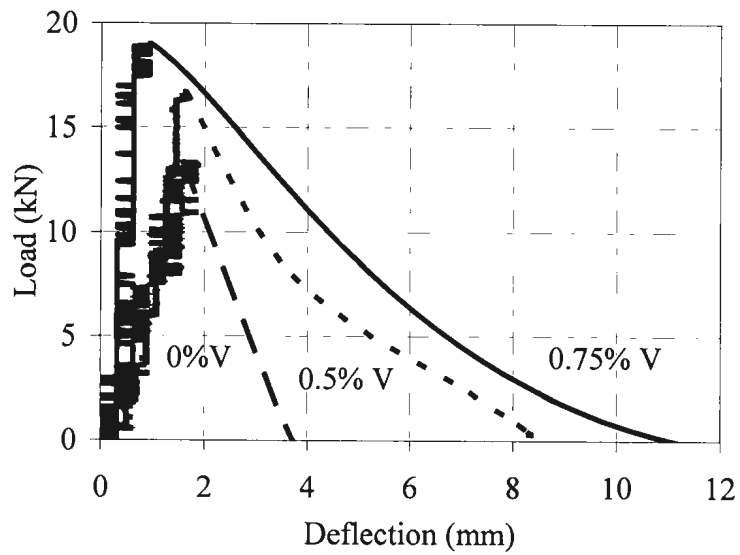


Figure 3.8: Flexural strength and energy absorption capacity due to fibre addition

Chapter 4

Experimental Program

4.1. Introduction

This chapter describes the details of the experimental program that was carried out, at the structural lab of Memorial University (MUN), to investigate the shear behaviour of macro synthetic fibre-reinforced concrete beams with Glass Fibre Reinforced Polymer (GFRP) bars. The experimental program consisted of casting, testing and evaluation of the structural performance of sixteen beams. The details of the test specimens and the procedure used in preparing the specimens are discussed in this chapter. The test set-up and the different equipments used to measure the load, deformations and strains, throughout the testing program, are also described in this chapter.

4.2. Test Specimens

The test specimens were divided into four groups. The first group has no fibre that is a fibre volume percentage of 0%. This was the reference group. The other three groups had three levels of fibre volume equal to 0.5%, 0.75% and 1.0%. The main test variables were the fibre volume (V), reinforcement ratio (ρ_f), effective depth (d) and shear span to depth ratio (a/d). The definition of the variables is shown in Figure 4.1. A summary of the test program with the parameters investigated is shown in Figure 4.2.

The specimens were divided into four groups. Each group consisted of four specimens. Within the same group, the beams had different fibre volumes of 0%, 0.5%, 0.75% and 1.0%. The beams in the first group had the following dimensions ($b \times h \times L$): 250 mm \times 350 mm \times 2840 mm. The reinforcement ratio (ρ_f) was 0.87% and the shear

span to depth ratio (a/d) was 2.5. The beam depth (d) was calculated from the extreme fibres in compression to the centroid of the flexural reinforcement based on a 40 mm clear cover, as shown in Figure 4.2. The beams in the second group had $b \times h \times L$ equal to 250 mm \times 350 mm \times 2840 mm, ρ_f equal to 1.45% and a/d ratio of 2.6. The beams in the third group had $b \times h \times L$ equal to 250 mm \times 500 mm \times 3540 mm, ρ_f equal to 0.87% and a/d ratio of 2.6. The beams in the fourth group had $b \times h \times L$ equal to 250 mm \times 350 mm \times 3540 mm, ρ_f equal to 0.87 and a/d ratio of 3.5. The design of the experiment was such that to examine the effect of the different variables (ρ_f , d and a/d) for a given volume of fibre, where V was equal to 0%, 0.5%, 0.75% and 1.0%.

All of the beams were over-reinforced as recommended by the FRP codes and guidelines. The balanced reinforcement ratio, ρ_b , was calculated assuming that crushing of concrete occurs simultaneously at the same time as the rupture of the reinforcement. The balanced reinforcement ratio was calculated according to CSA S806-10 as follows:

$$\rho_b = \frac{\alpha_1 \beta_1 f'_c}{f_u} \frac{0.0035}{0.0035 + f_u/E_f} \quad (4.1)$$

where f'_c is the compressive strength of concrete (MPa), f_u and E_f are the tensile strength and modulus of elasticity of the reinforcement (MPa), respectively. The parameters α_1 and β_1 are the equivalent stress block parameters, as shown in Figure 4.3. Based on CSA S806-10, $\alpha_1 = 0.85 - 0.0015 f'_c \geq 0.67$ and $\beta_1 = 0.97 - 0.0025 f'_c \geq 0.67$.

A section with a reinforcement ratio of $\rho_f/\rho_b < 1.0$ is defined as tension-controlled failure and a section with a reinforcement ratio $\rho_f/\rho_b > 1.0$ is defined as compression-controlled failure (over-reinforced). The general design approach for FRP reinforced

beams is to use a compression-controlled failure in the concrete. However, in some rare cases, GFRP reinforced sections could be designed for tension-controlled failure.

That test beams were over reinforced at the section capacity level. The minimum reinforcement ratio was 0.87% that was equivalent to $1.3 \rho_b$ and the maximum reinforcement ratio was 1.45% that corresponded to $2.0 \rho_b$ within Group 2.

4.3. Formwork and Fabrication

The formwork was designed and constructed using 25 mm thick plywood sheets. The sides of the formwork were cut according to the height of each beam. A sufficient number of vertical supports and top bracings were used to maintain the integrity of the formwork during casting, and to ensure that the dimensions of the beams remained unchanged. Figure 4.4 shows a typical formwork and reinforcement layout for a single formwork. The bars were placed on plastic chairs to maintain uniform clear concrete cover. The longitudinal bars were tied using several cross bars of the same diameter and the same width of the beam to maintain uniform side concrete cover.

4.4. Casting and Curing of the Specimens

Four beams were cast from batch depending on the fibre volume. For example, beams B1, B5, B9 and B13 were poured from the same batch where $V = 0\%$. The same casting sequence was used for all beams. First, some concrete was poured in the formwork to form a layer that extend just above the level of the reinforcement. The concrete, which poured for this layer, was spread throughout the whole length of the beam and vibrated to ensure the proper compaction of the concrete within the

reinforcement area. The remaining portion of the beam was poured in layers depending on the depth of the beam. Test cylinders were prepared from the same batch of concrete according to the ASTM-C192. At the end of the pour, the surface of each beam was finished with a steel trowel.

After casting the beams in one batch, the beams were covered with plastic sheets to prevent moisture loss. Curing of test specimens is an essential way to avoid evaporation from the surface of the beam and to achieve the design properties. Without proper curing, significant shrinkage can be found in the specimen. This could lead to a large number of shrinkage cracks on the surface of the beams. It was noticed that covering test specimens with plastic sheets after casting was an effective way to reduce shrinkage. After 18 hours, the concrete mixture began to harden and produced a lot of heat due to the chemical reaction. Spraying water on the specimens at this stage reduced the heat of hydration and did not impair the concrete strength development. The specimens were watered 2-3 times a day. The test specimens were cured in this way for seven days and then kept in the laboratory until the day of testing.

4.5. Test Setup

The tests were performed in the structural engineering laboratory of Memorial University of Newfoundland. Figure 4.5 shows the detail of the test setup. The frame consists of two vertical columns of W310 × 107 sections. The columns were braced using two C310 × 45 sections on both sides. The bottoms of the columns were stiffened using 15 mm thick plates, and the columns were supported on two 20 mm thick plates to avoid any possible bending. The columns were mounted with 1000 mm thick reinforced

structural floor, using four bolts with 40 mm diameter for each column. The front column was braced at the bottom, using two 152 mm × 152 mm angles on both sides, to spread the loads and to facilitate the use of 4 more bolts, as this column will experience tensile force. The beam supporting the actuator consists of two C460 × 86 sections that were bolted to the columns. Both of the channels were stiffened using 15 mm thick plates to avoid the warping of the flange. The channels were connected to each other using horizontal plates at both top and bottom of the channels to provide more stiffness to the channels.

4.6. Instrumentation

During the test, each beam was instrumented with six electrical resistance strain gauges, as shown in Figure 4.6. Four electrical strain gauges designated as RS were placed on the reinforcement. For protection against any possible water damage during casting, the strain gauges were coated with a protective sealant and then covered with a shrink tube waxed at the ends. The strain gauges were bonded to the outside bars equally spaced from the faces of the beam. For ease of fabrication, the strain gauges were placed on the outer bars. Two of the gauges were placed at the mid span of the beam. One gauge was placed at the center of each shear span. Two strain gauges designated as CS were placed on the top surface of the beam at mid span to measure the concrete strains. The locations of the concrete strain gauges were marked on the compression surface of the beam. The concrete surface was smoothed using a hand grinder and then a very thin film of epoxy resin was placed on the concrete surface. After drying, each strain gauge was

placed in a position located, as shown in Figure 4.6. All of the strain gauges were 10 mm long. The resistance of the strain gauges was 120Ω with a gauge factor of $2.07 \pm 0.5\%$.

Three Linear Variable Differential Transformers (LVDTs) were placed at the same location of the reinforcement strain gauges to measure the deflections of the beam at the centre of the beam and at the centre of each shear span. These LVDTs were also used to check the symmetry of the loading on the beam. It should also be noted that the mid-span displacement measurements from the built-in LVDT of the MTS actuator were also recorded. However, such measurements would be susceptible to any settlement in the set-up that would also be recorded in addition to the deflection of the beam.

4.7. Data Acquisition System

The electrical strain gauges, LVDT's and the load readings were logged to a computerized data acquisition system. This system can be divided into two broad categories, analog systems and digital systems. In analog systems, the measurement information is processed and displayed in analog form. In digital systems, the original information may also be acquired in the form of an analog electrical signal, but the signal is then converted to a digital signal for further processing and display. A digital electrical signal has the form of a group of discrete and discontinuous pulses. Typically, the instrument first subjects the analog signal to amplification. Next, the amplified signal is converted into digital form by an analog-to-digital (A/D) conversion circuit. Finally, the digital signal is either displayed on a digital display device or is made available for transmission to other digital instruments such as a computer for further processing and display. All measurements were stored in Microsoft Excel files. The software (Lab-

VIEW, 2005) was used and the data scanning and saving rate was set to record the readings every 3 seconds.

4.8. Test Procedure

All beams were simply supported and loaded with four-point loading. Figure 4.7 shows a photograph of the test setup and data acquisition system. The loading was applied using a 670 kN servo-hydraulic MTS actuator in displacement control. The load was applied gradually using the 407 Controller. A spreader beam was used to divide the load into two points. Each beam was preloaded to approximately 10 kN to minimize the settlement of the beam. The preload was released prior to starting the test. During a test, the load was applied in increments of approximately 10 kN to 20 kN. The load increment was chosen depending on the beam dimensions. Smaller load increment was used at the beginning of the test to capture the load that caused the first cracking in the beam. At each load increment, the beam was inspected and the cracks were monitored and mapped until failure load was reached, as shown in Figure 4.8. The applied load, deflections, and strains from the different sensors were recorded using a high speed data acquisition system. The data was monitored by a personnel computer using LABVIEW program and stored on the hard disk of the computer. The frequency of the data sampling was 2.0 Hz.

Table 4.1: Details of test specimens

Test series No.	Beam No.	Fibre volume, V (%)	f'_c MPa	Reinforcement ratio ρ_f %	ρ_f/ρ_b	Effective depth, d mm	Shear span to depth ratio a/d
1	B1	0.00	40	0.87	1.3	302	2.5
	B2	0.50	44	0.87	1.3	302	2.5
	B3	0.75	41	0.87	1.3	302	2.5
	B4	1.00	47	0.87	1.3	302	2.5
2	B5	0.00	40	1.45	2.0	291	2.6
	B6	0.50	44	1.45	2.0	291	2.6
	B7	0.75	41	1.45	2.0	291	2.6
	B8	1.00	47	1.45	2.0	291	2.6
3	B9	0.00	40	0.87	1.3	441	2.5
	B10	0.50	44	0.87	1.3	441	2.5
	B11	0.75	41	0.87	1.3	441	2.5
	B12	1.00	47	0.87	1.3	441	2.5
4	B13	0.00	40	0.87	1.3	302	3.5
	B14	0.50	44	0.87	1.3	302	3.5
	B15	0.75	41	0.87	1.3	302	3.5
	B16	1.00	47	0.87	1.3	302	3.5

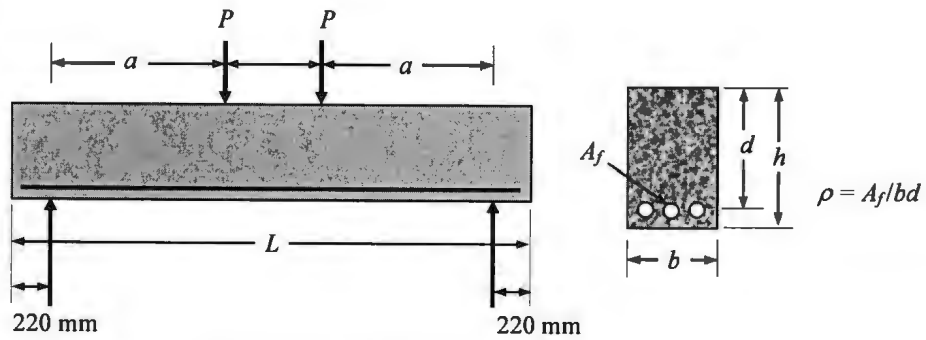


Figure 4.1: Definition of variables

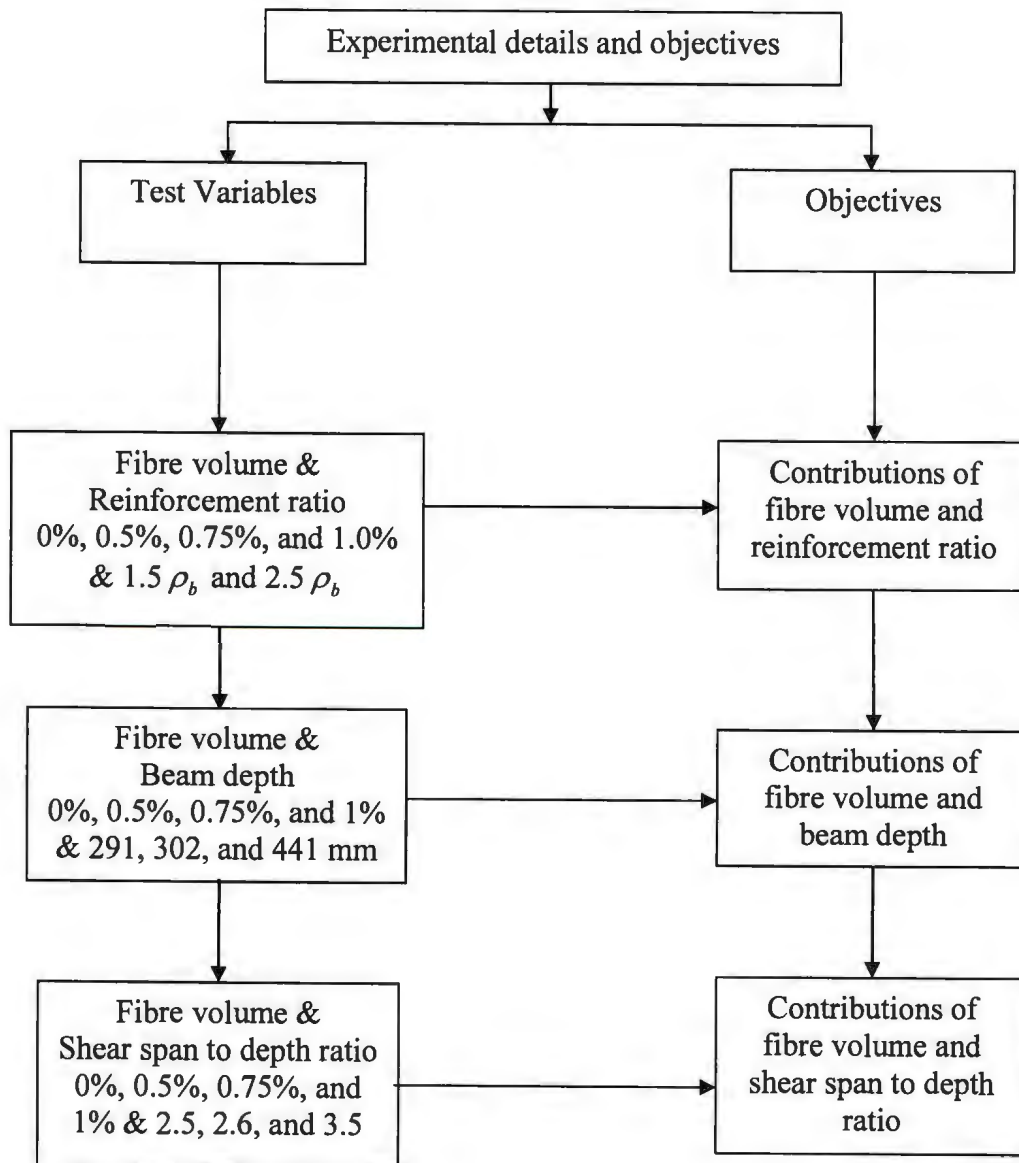


Figure 4.2: Experimental details and objectives

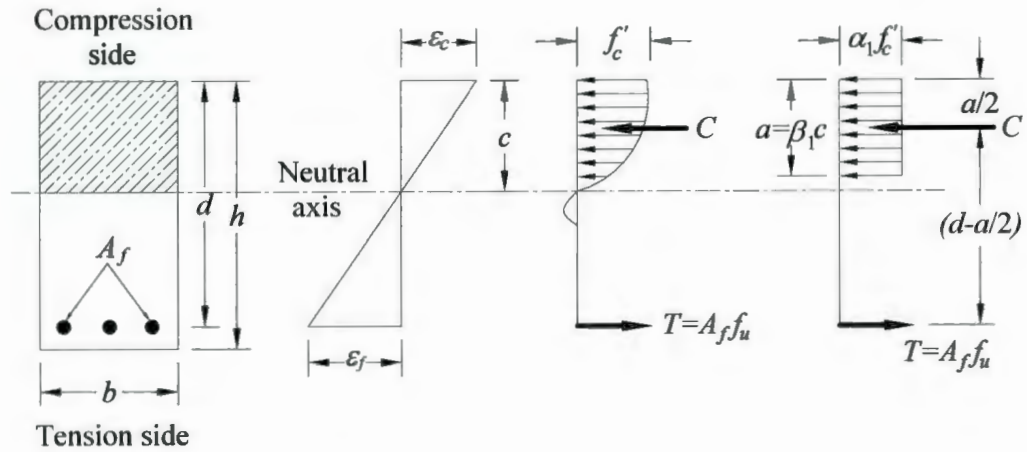


Figure 4.3: The equivalent stress block

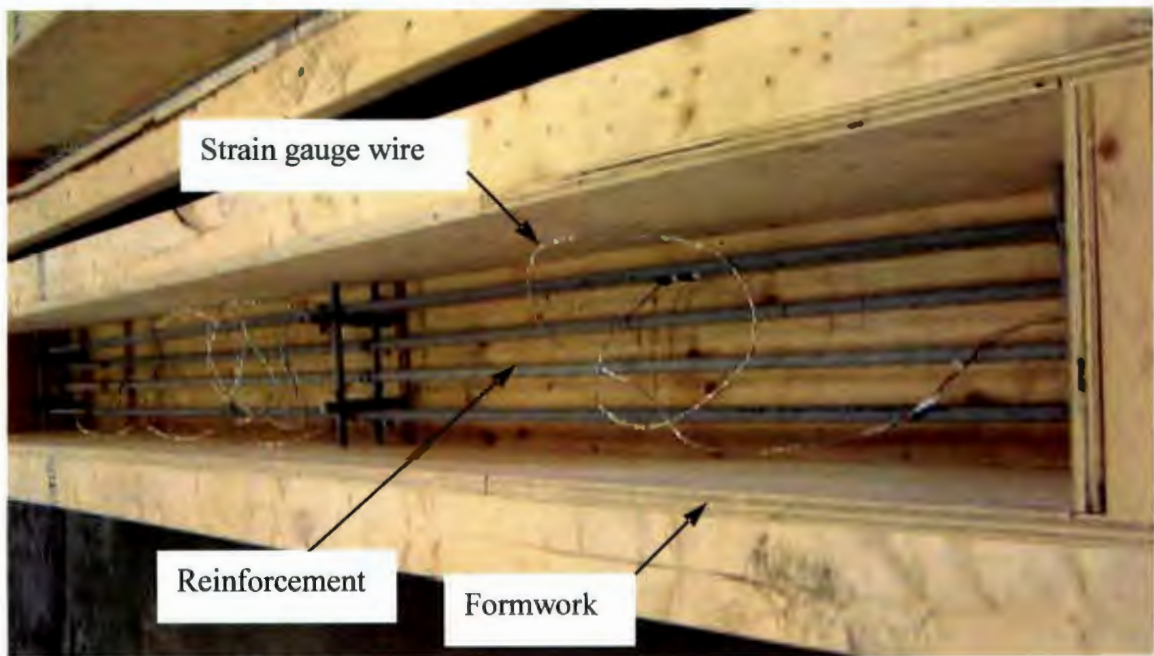


Figure 4.4: Typical formwork and reinforcement layout (Top view of typical formwork and reinforcement layout (before placing the top cross bracing for the formwork))

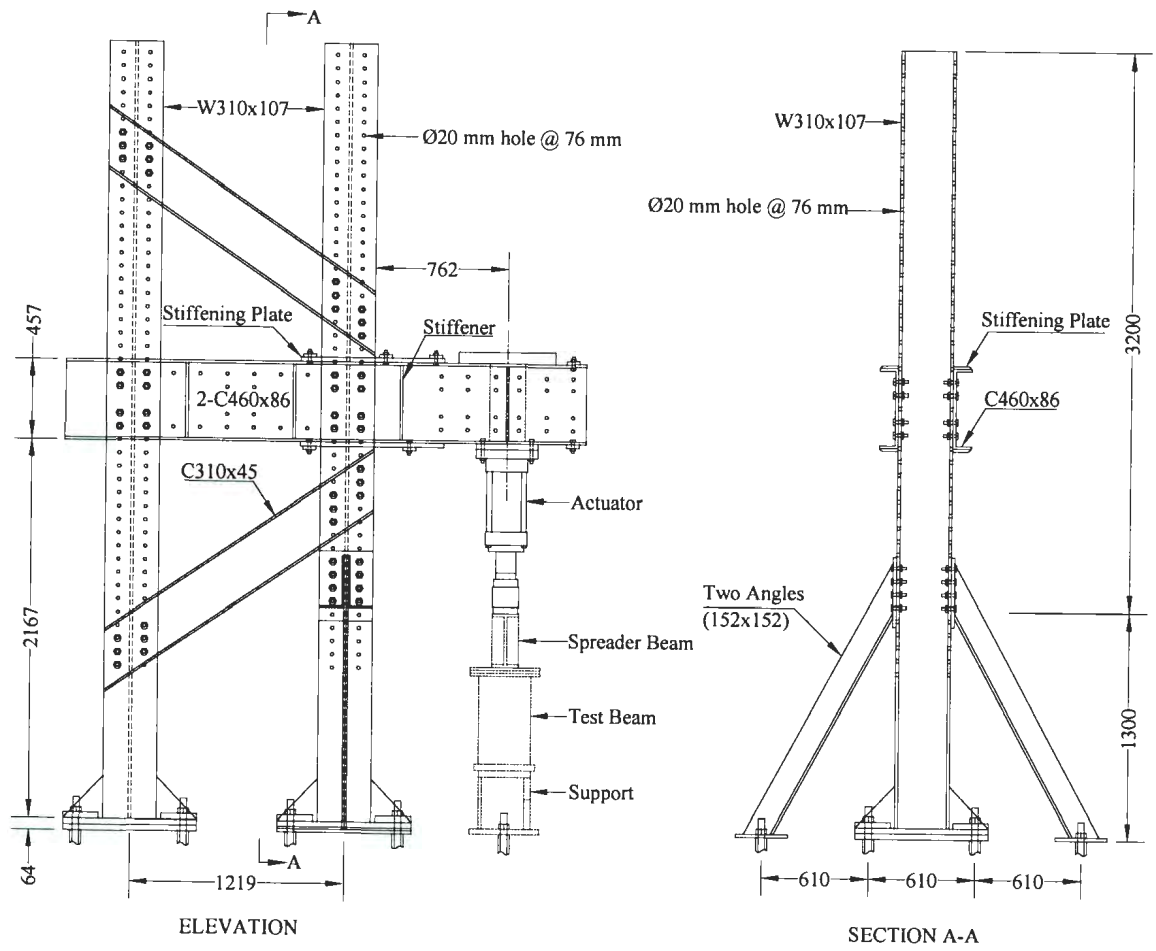


Figure 4.5: Test setup

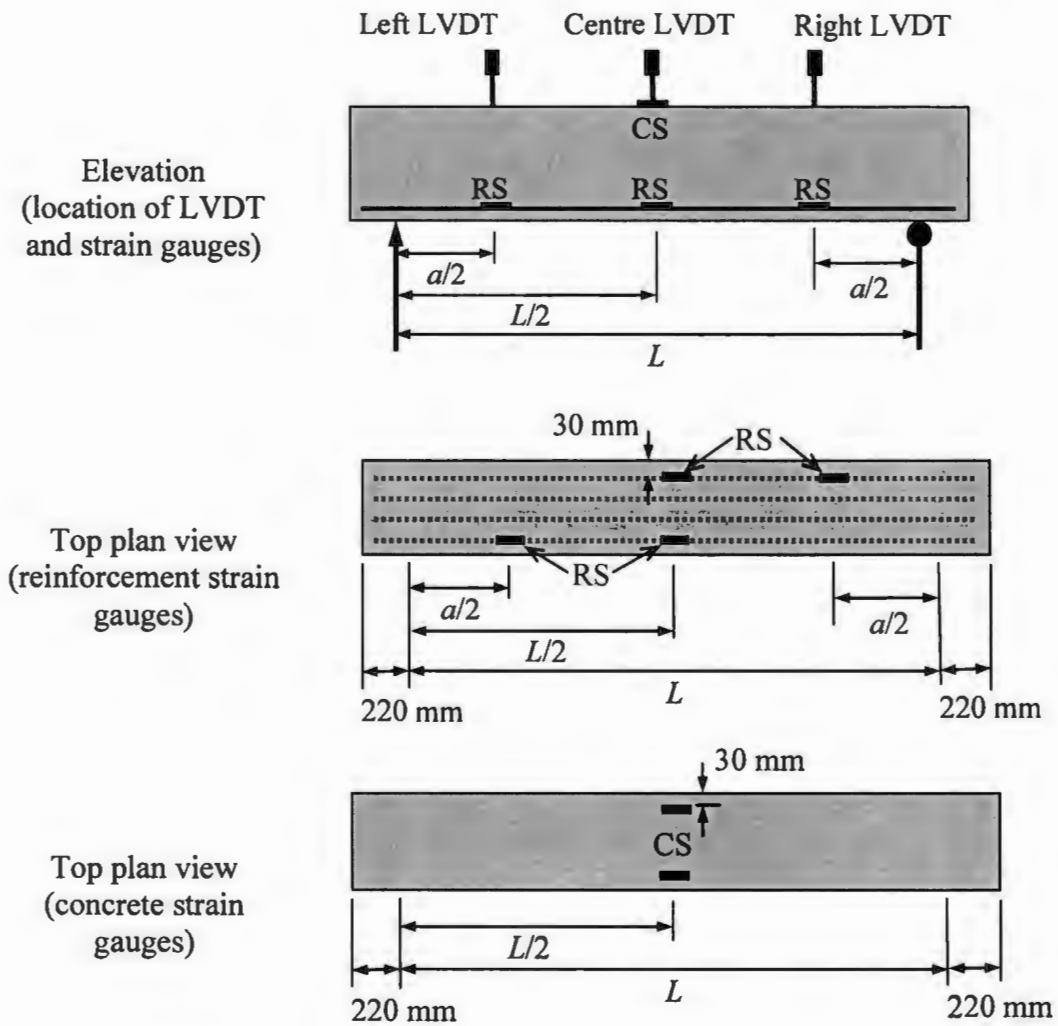


Figure 4.6: Instrumentation used during a test (Note: CS refers concrete strain gauges and RS refers reinforcement strain gauges)



Figure 4.7: Test setup and data acquisition system



Figure 4.8: Cracks mapping

Chapter 5

Test Results and Discussion

5.1. Introduction

The test results and observations obtained from the experimental program are presented in this chapter. The four macro-synthetic fibre concrete mixes mentioned in Chapter 4 were used in casting the test beams. Sixteen full-size normal strength concrete beams reinforced with GFRP bars were tested. The test beams were divided into four series according to their fibre volume percentages. Details of the test beams are given in Table 4.1. The test results are arranged in a manner that illustrates the influence of the fibre volume, V , 0%, 0.5%, 0.75%, and 1.0%; the ratio of the reinforcement ratio to the balanced reinforcement ratio, ρ_f/ρ_b , 1.5 and 2.5; the effective depth of the beam, d , 291 mm, 302 mm, and 441 mm; and the shear span to depth ratio, a/d , 2.5, 2.6 and 3.5 on the behaviour of the beams. The structural behaviour of the beams is presented in terms of load-deflection characteristics; concrete strains; GFRP reinforcement strains; crack patterns; failure modes and ultimate capacity. Due to the large quantity of experimental data, only representative results are presented in this chapter. All test data are presented in Appendix A. Finally, the capacity of the beams are compared with the predictions of some of the models that are available in the literature.

5.2. Load-Deflection Characteristics

As mentioned in Section 4.6, three Linear Variable Differential Transformers (LVDTs) were used to measure the deflections of the beam at the centre of the beam and at the centre of each shear span, as shown in Figure 4.6. During the test, the load was

paused at certain intervals to map the cracks. When the system was put on hold, the readings of the load decreased slightly due to relaxation of the beams' internal stresses. Thus, the load deflection graphs were not very smooth. However, this did not affect the behaviour and the capacity of the beam.

The load versus deflection curves of each test beam are shown in Appendix A. The results are presented for the deflection measurements at mid-shear span and at mid span (Figure 4.6) for all beams.

Typically, the shape of the load-deflection diagram for mid-shear span (presented in Appendix A) was approximately the same as the load-deflection diagram for mid-span. However, at a certain load level, the deflection at mid-shear spans was, as expected, less than the deflection at mid-span. The deflection measurements obtained from the two LVDTs that were placed at the center of each mid-shear span were very close. This indicated that the beams were symmetrically loaded.

In the following sections, the load-deflection curves obtained only from the mid-span LVDT are discussed for all of the beams in different test series. Figures 5.1 to 5.3 show the load versus central deflection curves for all test beams. In general, the load-deflection behaviour of the beams can be defined by three stages; before cracking, transition from uncracked to cracked stage, and after cracking. The first and third stages of a typical load deflection curve can be represented by two straight lines with different slopes. The first line has a steep slope corresponding to the stiffness of the uncracked beam. This indicates the higher stiffness of the uncracked beam. As the applied load was increased, initial cracks formed and the test beams experienced a slight gradual loss in stiffness at this transition stage and the slope of the load-deflection curve was changed to

another straight line that represented the stiffness of the cracked beam. The transition between these two lines was not abrupt; it was rather a smooth transition. This indicates that the beam did not completely lose its uncracked stiffness once the first crack was formed.

It should be noted that the beams with fibre volume of 0.5%, i.e. beams B2, B6, B10 and B14, were tested using different LVDTs than those used in testing all other beams. It appears that the load-deflection curves for those beams did not conform to the trends observed from the results of other beams. Hence, the beams of those beams are excluded in the current discussion.

The load that caused the first crack in the beam was observed with the naked eye. In general, the addition of the fibres increased the first crack-load for all beams as can be noticed from Table 5.1. The stiffness, load and deflection values at the first crack and at failure are presented in Table 5.1. The stiffness of a beam represents the amount of load needed for unit displacement at the centre of a beam. The initial stiffness, K_i , is the tangential value of the slope of the load-deflection curve at the uncracked stage. The cracked stiffness, K_{cr} , is calculated as the average tangential value of the slope of the load-deflection curve after the transition stage has ended. The values of K_i and K_{cr} are tabulated in Table 5.1. From the table, it is apparent that the beams had a stiffer response before and after cracking when the reinforcement ratio and the beam depth increased. Among all variables, changing of the depth of the beam yielded the most prominent influence on the stiffness. There were no consistent trends that could be observed from the uncracked stiffness results. The cracked stiffness of the beams increased with

increasing the fibre volume. Also, the change in fibre volume has no effect on beams with a/d ratio equal to 3.5.

The load deflection curves can give an indication of the failure mode of the beam. From the load deflection curves shown in Figures 5.2 and 5.3, one can notice that all the beams have a positive slope up to failure and that failure is abrupt due to shear. This means that the load deflection curve for the test beams is not complete, since the beams did not develop its full flexural capacity; instead the load deflection curve is triggered by sudden shear failure. Hence, the effect of macro synthetic fibre on the flexural ductility of the beams can not be obtained from the current study.

The load-deflection curves for beams that have different reinforcement ratios are shown in Figure 5.2. In general, it could be noted that increasing the flexural reinforcement ratio resulted in increasing the ultimate failure load but at the same time did not result in increasing the maximum deflection. In general, for the same fibre volume, increasing the reinforcement always resulted in increasing the ultimate failure load.

The load-deflection curves for beams that have different effective depths are shown in Figure 5.3. It could be noted that increasing the beams effective depths resulted in increasing the ultimate shear failure load. In general, for the same fibre volume increasing the beam effective depth by 46% resulted in increasing the ultimate failure load by 33%. However, a significant increase was achieved in the ultimate shear failure load for the same fibre volume of 1.0% when the beam effective depth was increased. Test results revealed that for the same fibre volume of 1.0%, increasing the beam effective depth by 46% resulted in increasing the ultimate shear failure load by 82%.

Table 5.1 presents the load and deflection, at the first crack and at failure, for the different test beams. In general, it could be noted that the addition of synthetic fibre resulted in increasing the ultimate shear failure load when the same reinforcement ratio, the same effective depth, and the same shear span to depth ratio were used, respectively.

5.3. Strain Behaviour

The measured applied loads are plotted as a function of the concrete and reinforcement strains for all beams. Typical load versus strain plots for concrete and reinforcement are shown in Figure 5.4. In the pre-cracking stage, all strain gauges exhibited a linear behaviour. The strains in the longitudinal bars were very small. After cracking, the strain in the bars at mid-span increased as a portion of the concrete was not able to carry tension.

The following sections show the relation between load and concrete and GFRP reinforcement strains for the reinforced concrete beams. The concrete strain here was the strain at the extreme compression fibre of the mid span and GFRP strain at the tension zone of the mid-span.

5.3.1. Concrete Strains

The concrete strains were measured at the central location by using the strain gauges shown in Figure 4.6. This location was selected to measure the concrete strains at mid-span of the beam. The load versus concrete strain strains is shown in Figure 5.4 for all beams. The concrete strains did not reach 3500 $\mu\epsilon$, which is the concrete crushing strain, in any of the test beams. In addition, there was no physical damage at any location that

could be identified by the naked eye, which would indicate crushing of the concrete. This indicates that none of the test beams reached its flexural capacity.

5.3.2. GFRP Strains

The strain gauge locations on the GFRP reinforcement were described in Chapter 4 (Figure 4.6). The strain gauge locations were selected and placed at a distance of $L/2$ and $a/2$ to measure the maximum strain in GFRP reinforcement during the test. The load versus mid-span GFRP strain plots are shown in Figure 5.5 for all beams. The load versus mid shear-span GFRP strain curves are shown in Figure 5.6 for all beams.

All the beams had an over reinforced section capacity. The ultimate strain that a GFRP bar can reach, before rupture, is around $15000 \mu\epsilon$. The recorded maximum strain in the GFRP bars was around $5000 \mu\epsilon$ which is less than the ultimate tensile strain of GFRP bars.

In general, it could be noted that the shape of the load versus mid-shear span strain is approximately the same as the load versus mid-span strain that is bilinear. Also, the transition between the two lines is smooth, and this could be due to the existence of macro synthetic fibre that bridged the formed cracks. The slope of the first line is steeper compared to the slope of the first line of load versus mid-span strain. Before cracking, the reinforcement strains in the left and right shear spans also showed a similar trend as the mid-span strain. While the GFRP strains at mid-span of the beam increased gradually, the strains in the mid-shear span increased rapidly after cracking. This could be due to the rapid opening up of the cracks near the strain gauge location. It could be noted also, that the increase in load after cracking near the mid-shear span was small. This behaviour

suggests that the beam failed shortly after the formation of the cracks at the vicinity of that location.

5.4. Crack Patterns

The cracks were marked manually at the end of each load increment; the growth of cracks was marked on each test beam. This was done to identify the direction of crack propagation and to determine the different crack patterns. Figures 5.7 to 5.10 show the crack patterns for different test beams. The extent of a crack at the end of each loading increment was marked by a short horizontal line. The loads shown at each crack tip corresponds to the actuator loads. The actuator loads were twice the test loads; the load was applied by the actuator on the spreader beam and hence the load was divided into two point loads.

For all beams, the first flexural crack initiated at the tension side of the beam in the constant moment region, where the flexural tension stress was the highest and the shear stress was equal to zero. The observed flexural cracks propagated vertically upward to the level of the neutral axis that reflected the absence of shear stress. As the load was increased, additional flexural cracks were developed within the shear span. Due to the presence of shear stresses, the flexural cracks became progressively more inclined and propagated towards the load points. These types of cracks are known as flexural-shear cracks. These cracks extended rapidly through the beam leading to the so-called a diagonal-tension failure. In general, the slope of the inclined crack decreased as the shear span to depth ratio (a/d) of the beam increased for all reinforcement ratios as can be observed by comparing Figures 5.7 and 5.10.

It is clear from different crack patterns that the amount of fibre volume affected the cracks spacing. In general, the crack spacing was decreased and hence cracks width as the amount of fibre by volume was increased. Also, the existence of fibres enhanced the post-cracking behaviour and delayed the opening of shear cracking in a similar way to the existence of shear reinforcement. The addition of macro synthetic fibre changed the mode of failure of short beams from web-shear cracking to flexural shear cracking. However, despite the existence of synthetic fibre, concrete beams eventually collapsed due to localized shear stresses.

5.5. Failure Modes

Figures 5.17 to 5.10 show the observed failure modes for different test beams. Unfortunately, the picture that represents the final failure mode of test beam B8 was lost, rather a photo that represents the crack pattern of the mentioned beam just before failure (i.e. at 82% of the failure load) is shown in Figure 5.8(d).

In general, the failure modes of the beams were either by shear-tension, or shear-compression, or diagonal tension, as shown in Figure 5.11. The slope of the inclined shear cracks decreased as the shear span to depth ratio (a/d) was increased. Also, it was observed that the increase in shear span to depth ratio (a/d) resulted in a more ductile behaviour.

For some beams, a secondary bond/anchorage failure was observed within the shear span, as shown in Figures 5.7(a) and 5.9(a). All Beams in series 4 that have shear span to depth ratio of 3.5 failed by bond failure between the bars and the concrete cover, which resulted in pulling off the bars from one end of the beam (see Figure 5.10).

Test beams in series 3 that had a 500 mm thickness and shear span to depth ratio of 2.5 failed a more brittle manner. For these beams, few inclined cracks were observed in the shear span zone. These cracks propagated and merged into one diagonal crack, which started from the support and penetrated in a straight line into the compression side of the beam at the inner side of the loading point. As a result, an arch action formed in the compression strut between the loading point and the support above the inclined crack. This beam failed by crushing of the concrete near the loading point (see Figure 5.9).

In general, as the amount of fibre by volume was increased, the number of flexural cracks was increased. However, the existence of macro synthetic fibre did not affect the final failure modes. All test beams experienced brittle failure modes. The test results showed that macro synthetic fibre did not change the failure mode, instead the existence of fibre slowed down the propagation and widening of the diagonal shear crack and thus increased the load at which the major diagonal crack fully developed.

5.6. Shear Capacity

The shear investigation of fibre reinforced concrete beams was made for different fibre volumes (0%, 0.5%, 0.75%, and 1.0%) and the same variables (reinforcement ratio, effective depth and shear span to depth ratio) to observe the enhancement of the macro synthetic fibre to the shear capacity of the fibre reinforced concrete beams. Moreover, the effect of reinforcement ratio, effective depth, and shear span to depth ratio on the shear capacity of FRC for the same fibre volume was also examined. The contribution of fibre to shear capacity can be calculated by comparing the beams with different fibre volumes to those with no fibres added.

The reactions at the supports were equal to the applied load that was one-half of the actuator loads. The shear force in a beam was equal to the reactions. Hence, in the following discussion of the results, the term shear capacity ($V_{c,test}$) is used to refer to the ultimate shear that a beam carries as shown in Table 5.2. The nominal shear strength of a beam, v_n , is obtained by dividing $V_{c,test}$ by bd , where b is the width of the beam and d is the depth of the beam (Table 5.3). As mentioned in Chapter 4, there was some slight difference in the compressive strengths of the beams. Hence, to make the comparison between the shear strength relevant for different beams, the nominal shear strength was normalized with respect to the square root of the compressive strength. This is referred to as the normalized shear strength, $v_n / \sqrt{f'_c}$ (Table 5.4)

5.6.1. Effect of Reinforcement Ratio

In general, it could be noted that increasing the flexural reinforcement ratio resulted in increasing the normalized shear strength. The normalized shear strength, for the same fibre volume was increased from 0.16, 0.16 and 0.17 to 0.19, 0.21 and 0.19, for fibre volumes of 0.5%, 0.75%, and 1.0%, respectively, when the reinforcement ratio was increased from $1.3 \rho_b$ to $2.0 \rho_b$.

This means, that increasing the reinforcement ratio by 67% resulted in increasing the average shear capacity by about 21% when the same amount of fibre volume was used. In general, this is due to the reduced size of cracks and the possible increase in the total dowel force prior to failure.

5.6.2. Effect of Shear Span to Depth Ratio

In general, it could be noted that increasing the shear span to depth ratio did not result in a significant change in the normalized shear strength of the beams with fibres. For beams that have no fibre, increasing the shear span to depth ratio (a/d) from 2.5 to 3.5 resulted in decreasing the normalized shear strength from 0.13 to 0.09 but it was not enough to change the shear failure mode.

5.6.3. Effect of Effective Depth

In general, it could be noted that increasing the beam effective depth resulted in a slight decrease in the normalized shear strength and at the same time resulted in a slightly more brittle failure. For the beams with no fibres, increasing the effective depth from 302 mm to 441 mm resulted in decreasing the normalized shear strength from 0.13 to 0.11. For beams with fibres, increasing the effective depth from 302 mm to 441 mm resulted in no significant change in the nominal shear strength, which is around 6.7% on the average.

5.6.4. Effect of Fibre Volume

Test results indicated that the addition of the macro synthetic fibre enhanced the shear strength of the GFRP concrete beams as shown in Figure 5.12.

Figures 5.12(a) and 5.12 (b) present the influence of fibre volume on the normalized shear strength of the FRC beams that have the same reinforcement ratio of $1.3 \rho_b$ and $2.0 \rho_b$, respectively. It can be noted that increasing the volume of synthetic fibre from 0.0% to 1.0% resulted in an increase in the normalized shear strength from 0.13 to 0.17 and from 0.14 to 0.19 for the beams with $1.3 \rho_b$ and $2.0 \rho_b$, respectively. This means that the

contribution to the normalized shear strength of 1.0% fibre by volume was about 35% on the average the same reinforcement ratio was used.

Figure 5.12(c) represents presents the influence of fibre volume on shear capacity of FRC beams that have the same shear span to depth ratio (a/d) of 3.5. It can be noted that increasing the volume of synthetic fibre from 0.0% to 1.0% resulted in an increase in the normalized shear strength from 0.09 to 0.17. This means, that the maximum contribution of 1.0% fibre by volume was about 90% when the shear span to depth ratio (a/d) of 3.5 was used.

Figure 5.21(d) presents the influence of fibre volume on shear capacity of FRC beams that have the same effective depth of 441 mm. It can be noted that increasing the volume of synthetic fibre from 0.0% to 1.0% resulted in an increase in the normalized shear strength from 0.11 to 0.15. This means, that the maximum contribution of 1.0% fibre by volume was about 39% when the same effective depth of 441 mm was used. The enhancement of the shear capacity was not noticeable when the fibre volume was increased from 0.5% to 1.0%, for beams that had the effective depth of 441 mm.

As mentioned earlier and as observed from the experimental program, the beams with synthetic fibre continued to resist higher loads after the appearance of the first diagonal shear crack. The addition of macro synthetic fibre modified the shear failure behaviour of the reinforced concrete beams. In general, the shear failure of the SNFRC beams was less brittle compared to the sudden brittle failure of control beams.

5.7. Test Results versus Design Models Predictions

Many researchers proposed design equations that were defined as functions of the primary design parameters (Table 2.2). Existing shear capacity models, however, were developed for steel fibre reinforced concrete and not for macro synthetic fibres. Hence, they should be used with caution as they may not be fully applicable. ACI Committee 544 recommended Sharma's model, but a code-based design equation for the shear capacities of FRC beams does not exist yet.

To account for the real material properties and section dimensions, the average shear capacity of the RC beams was calculated from the ultimate loads using actual dimensions of the beams. The average shear capacity was then normalized to the square root of the compressive strength. It is well established that the shear capacity of concrete beams is directly proportional to the square root of concrete compressive strength. In addition, the existing equations were applied with the adjustment of the axial rigidity of the reinforcing bars by replacing ρ with $\rho_f E_f/E_s$ in the equations, where ρ_f is the reinforcement ratio of the longitudinal bars, E_f is the modulus of elasticity of the GFRP bars and E_s is the modulus of Elasticity of steel.

The normalized results are shown in Figure 5.13 for all beams tested in this program. The graph shows that the addition of macro-synthetic fibres has minimum normalized shear strength of 0.15, on the average. The results obtained from this study show that beams with macro synthetic fibre of 0.5% and more by volume can enhance the shear capacity lower limit established by CSA S806-10 for normal concrete.

A comparison of the predicted shear capacity using the experimental measured failure shear capacity, as reported by seven different existing formulas, is shown in Table

5.5 and Figure 5.14. In general, it could be noted that available shear capacity models overestimated the shear capacity of test beams except for the model proposed by Greenough and Nehdi (2008) which gave the best results. This is expected, as those empirical equations are developed using data obtained from beams with steel fibres and reinforced with traditional steel reinforcement.

Table 5.1: Load*, deflection and stiffness values at first crack and at failure

Test series No.	Beam No.	f'_c (MPa)	Fibre volume $V\%$	First Crack		Failure		K_r (kN/mm)	K_{cr} (kN/mm)
				Load (kN)	Deflection (mm)	Load (kN)	Deflection (mm)		
1	B1	40	0.00	27.0	0.38	122.0	15.73	53.0	5.9
	B2	44	0.50	60.0	1.30	158.7	13.50	62.9	11.1
	B3	41	0.75	44.5	1.48	158.9	20.30	35.3	7.3
	B4	47	1.00	45.0	0.88	176.8	18.22	54.6	7.0
2	B5	40	0.00	26.3	0.89	130.9	9.71	23.7	6.5
	B6	44	0.50	53.9	1.01	182.0	13.36	49.5	10.3
	B7	41	0.75	66.7	1.41	200.1	19.29	75.4	9.4
	B8	47	1.00	69.2	2.42	191.5	18.76	35.4	9.7
3	B9	40	0.00	36.7	0.57	154.3	15.20	70.2	7.2
	B10	44	0.50	–	–	214.9	13.32	–	–
	B11	41	0.75	65.7	1.22	217.6	16.07	58.0	7.7
	B12	47	1.00	66.9	1.36	232.3	27.50	43.9	9.8
4	B13	40	0.00	25.6	1.47	87.3	22.31	25.2	3.2
	B14	44	0.50	39.0	2.40	147.8	31.35	29.5	3.3
	B15	41	0.75	35.6	2.05	164.1	43.11	24.9	3.0
	B16	47	1.00	35.6	2.68	180.4	51.11	21.3	3.3

*Loads reported in this table are actuator loads. The actuator loads were twice the test loads; the load was applied by the actuator on the spreader beam and hence the load was divided into two point loads.

Table 5.2: Shear Capacity of beams ($V_{c, test}$)

Fibre volume ($V\%$)	$V_{c, test}$ (kN)			
	1.3 ρ_b	2.0 ρ_b	d (441 mm)	a/d (3.5)
0.00	61.2	65.5	77.2	43.7
0.50	79.4	91.0	107.5	73.9
0.75	79.5	100.1	108.8	82.1
1.00	88.4	95.8	116.2	90.2

Table 5.3: Nominal shear strength of beams ($v_n = V_{c, test} / bd$)

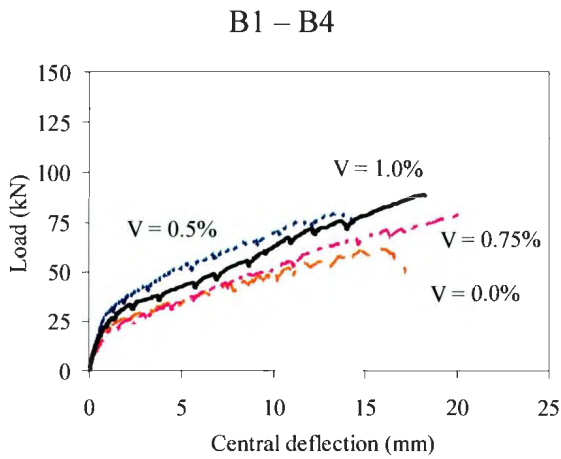
Fibre volume ($V\%$)	v_n (MPa)			
	1.3 ρ_b	2.0 ρ_b	d (441 mm)	a/d (3.5)
0.00	0.81	0.90	0.70	0.58
0.50	1.05	1.25	0.97	0.98
0.75	1.05	1.38	0.99	1.09
1.00	1.17	1.32	1.05	1.19

Table 5.4: Normalized shear strength w. r. t. $\sqrt{f'_c}$ ($v_n / \sqrt{f'_c}$)

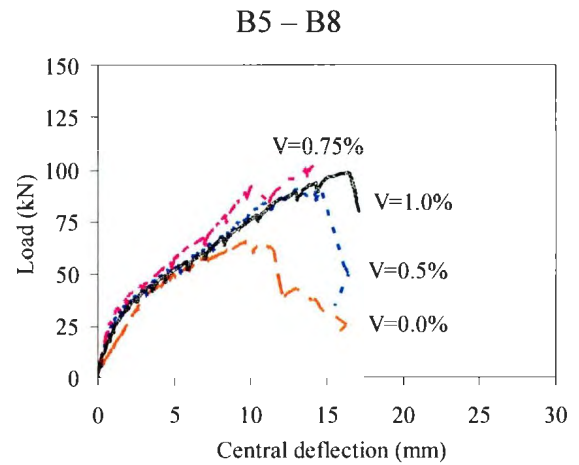
Fibre volume ($V\%$)	$v_n / \sqrt{f'_c}$			
	1.3 ρ_b	2.0 ρ_b	d (441 mm)	a/d (3.5)
0.00	0.13	0.14	0.11	0.09
0.50	0.16	0.19	0.15	0.15
0.75	0.16	0.21	0.15	0.17
1.00	0.17	0.19	0.15	0.17

Table 5.5: Strength predictions by existing models

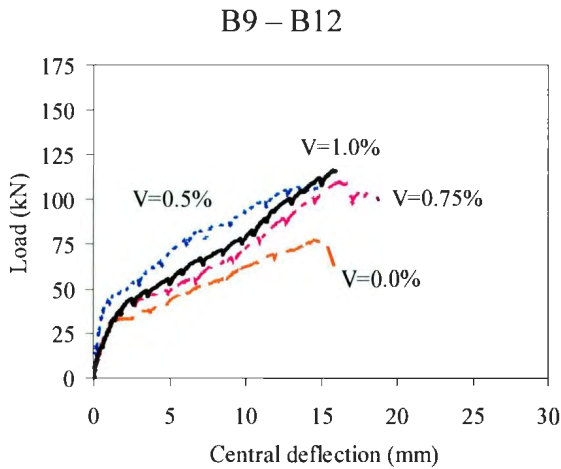
Beam No.	Fibre volume $V\%$	$V_{c,test}$ kN	$V_{c,equation} / V_{c,test}$							
			Li et al. (1992)	Ashour et al. (1992)	Khuntia et al. (1999)	Sharma (1986)	Shin et al. (1994)	Kwak et al. (2002)	Greenough and Nehdi (2008)	CSA S806-10 (2010)
B1	0.00	61	2.06	2.21	1.30	1.83	0.97	1.56	0.62	0.98
B2	0.50	79	1.87	3.13	1.84	2.09	1.39	1.90	0.98	0.78
B3	0.75	80	1.77	3.73	2.16	1.95	1.47	1.94	1.21	0.76
B4	1.00	88	1.68	4.07	2.44	1.80	1.64	2.09	1.32	0.72
B5	0.00	66	1.94	1.93	1.17	1.64	0.98	1.50	0.68	1.00
B6	0.50	91	1.68	2.54	1.55	1.74	1.24	1.69	0.92	0.74
B7	0.75	100	1.43	2.76	1.65	1.48	1.19	1.56	1.03	0.66
B8	1.00	96	1.60	3.49	2.17	1.58	1.53	1.95	1.28	0.74
B9	0.00	77	2.31	2.50	1.51	2.11	1.12	1.74	0.65	0.97
B10	0.50	108	1.93	3.29	1.99	2.24	1.49	2.00	1.00	0.72
B11	0.75	109	1.81	3.88	2.30	2.07	1.56	2.02	1.23	0.70
B12	1.00	116	1.78	4.40	2.72	1.98	1.82	2.28	1.40	0.68
B13	0.00	44	2.81	2.21	1.82	2.36	1.29	1.45	0.76	1.16
B14	0.50	74	1.94	2.40	1.98	2.06	1.44	1.50	0.98	0.71
B15	0.75	82	1.65	2.58	2.09	1.74	1.38	1.44	1.11	0.62
B16	1.00	90	1.58	2.85	2.39	1.62	1.57	1.59	1.22	0.59
Average			1.87	3.00	1.94	1.89	1.38	1.76	1.02	0.78
Standard deviation			0.33	0.74	0.43	0.25	0.24	0.26	0.25	0.16
Coeff. of variation			0.18	0.25	0.22	0.13	0.17	0.15	0.24	0.20



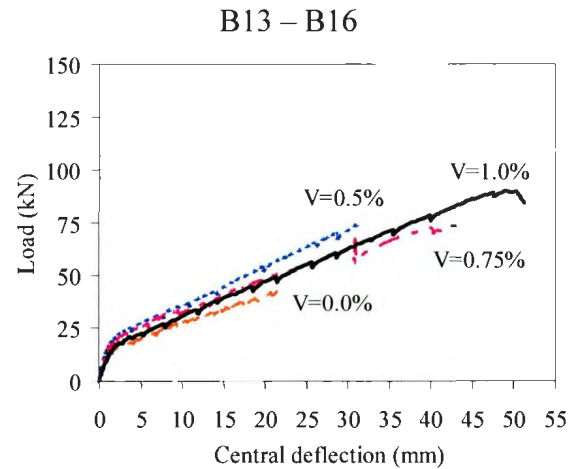
(a) Different fibre volume and same reinforcement ratio ($1.3\rho_b$)



(b) Different fibre volume and same reinforcement ratio ($2.0\rho_b$)

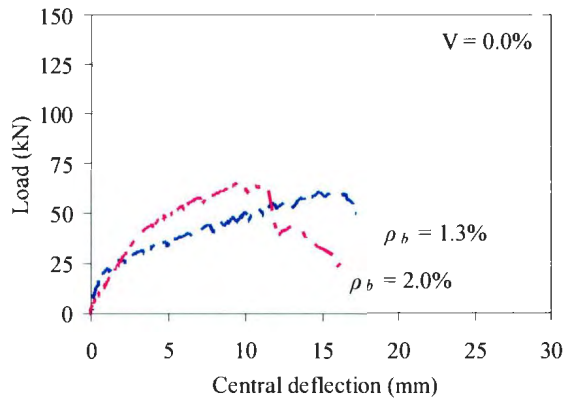


(c) Different fibre volume and same effective depth (441 mm)

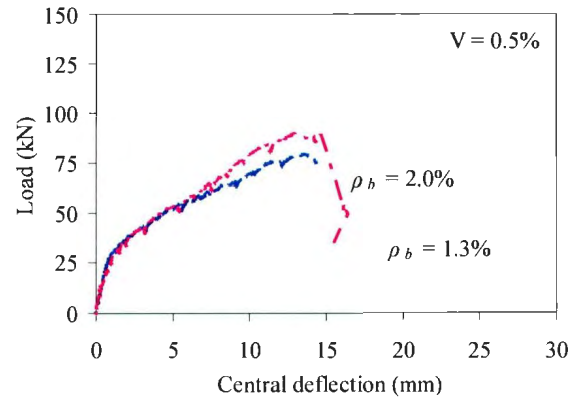


(d) Different fibre volume and same span to depth ratio (3.5)

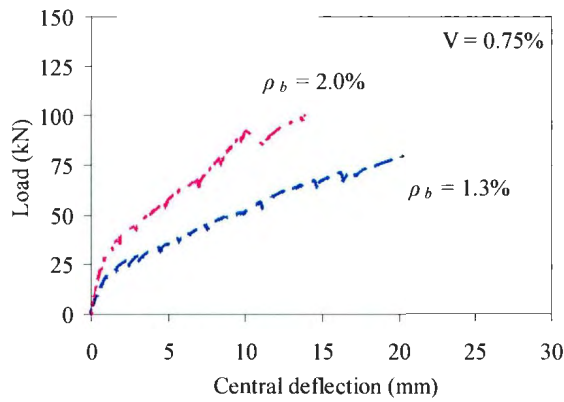
Figure 5.1: Load vs. deflection curves for the different fibre volumes and the same variables (reinforcement ratio, effective depth and shear span to depth ratio)



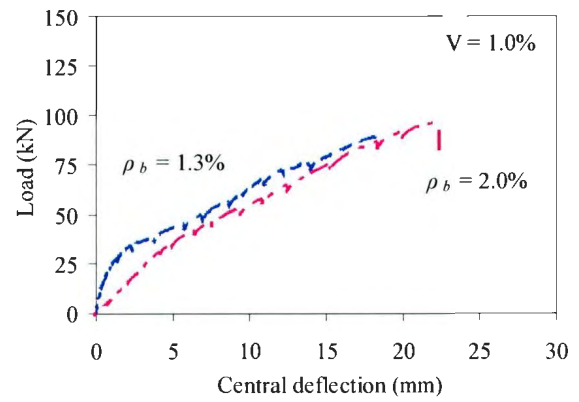
(a) Beams B1 and B5



(b) Beams B2 and B6

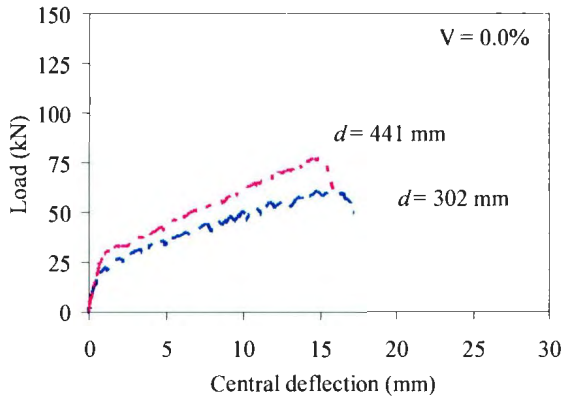


(c) Beams B3 and B7

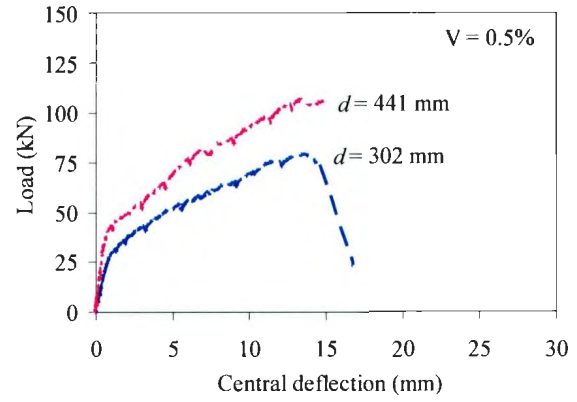


(d) Beams B4 and B8

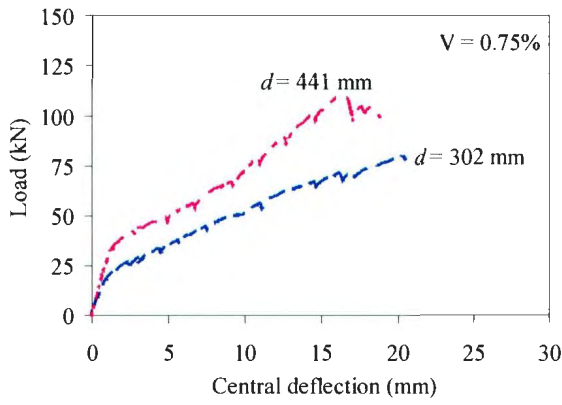
Figure 5.2: Load vs. deflection curves for the different reinforcement ratios and the same variables (fibre volume, effective depth and shear span to depth ratio)



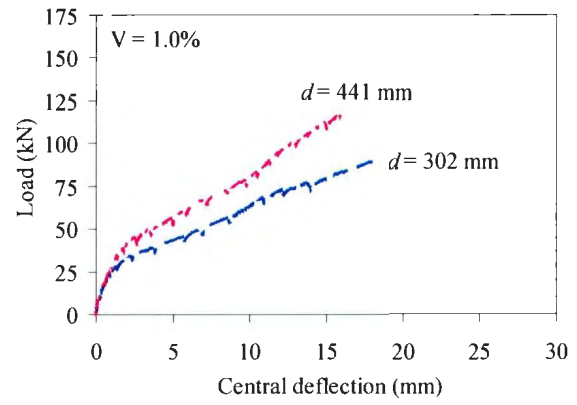
(a) Beams B1 and B9



(b) Beams B2 and B10

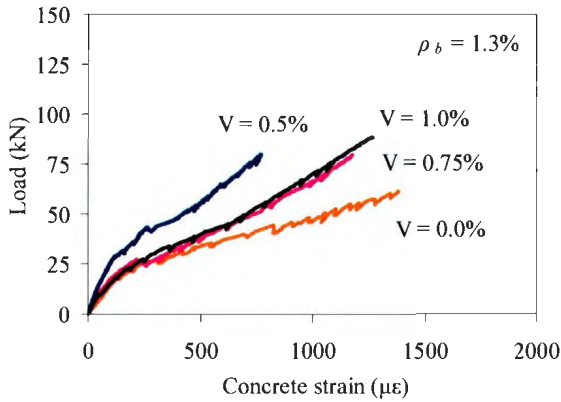


(c) Beams B3 and B11

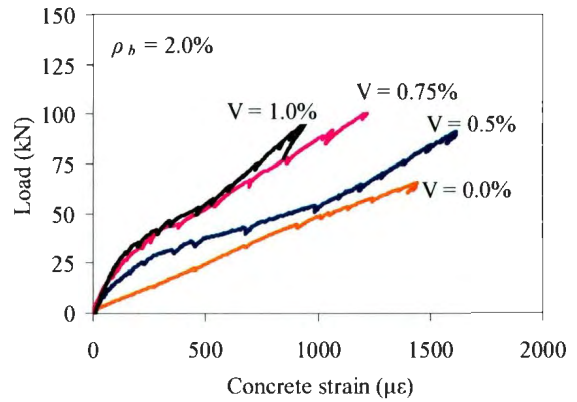


(d) Beams B4 and B12

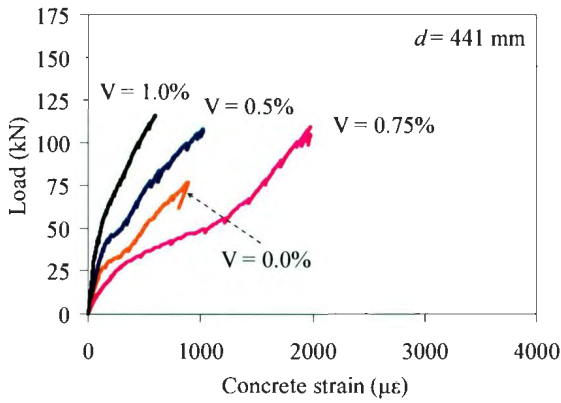
Figure 5.3: Load vs. deflection curves for the different effective depths and the same variables (fibre volume, reinforcement ratio and shear span to depth ratio)



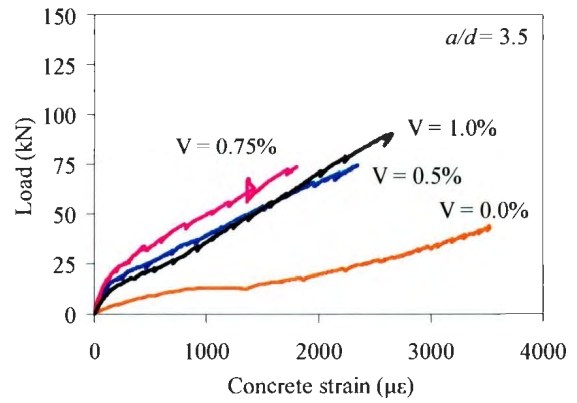
(a) Beams with the same reinforcement ratio (Group 1)



(b) Beams with the same reinforcement ratio (Group 2)

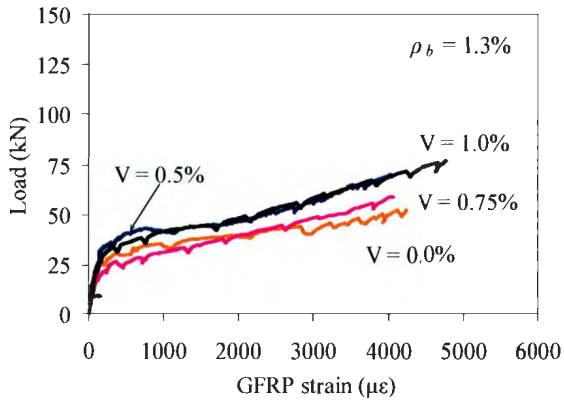


(c) Beams with same effective depth (Group 3)

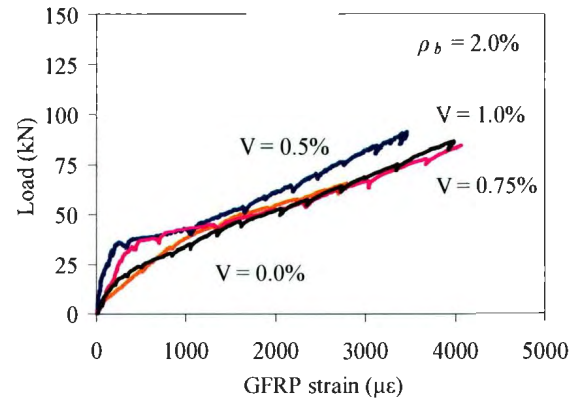


(d) Beams with same shear span to depth ratio (Group 4)

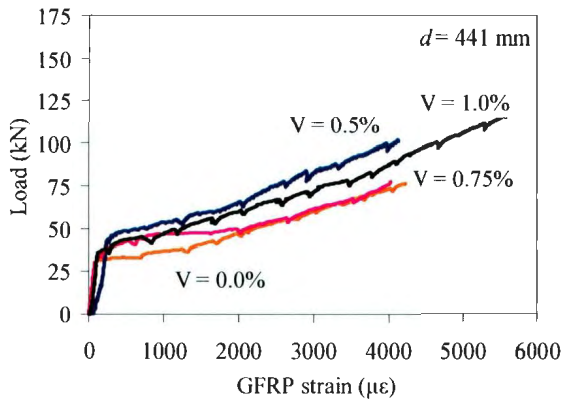
Figure 5.4: Load vs. concrete strains



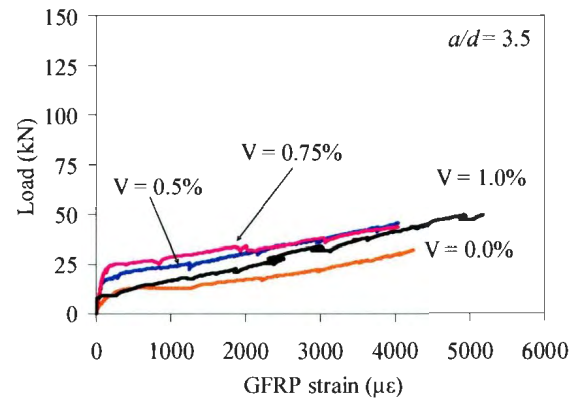
(a) Load vs. GFRP strain for the same reinforcement ratio (Group 1)



(b) Load vs. GFRP strain for the same reinforcement ratio (Group 2)

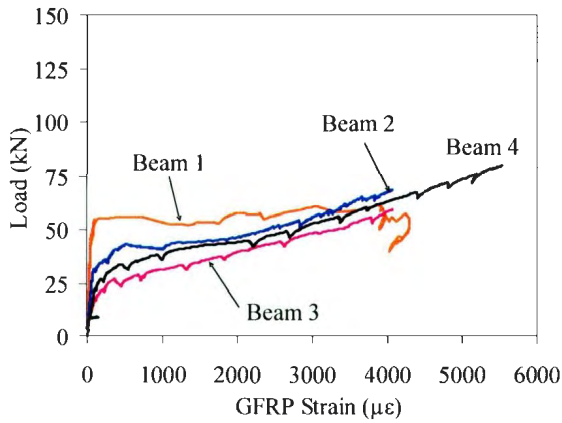


(c) Load vs. GFRP strain for the same effective depth (Group 3)

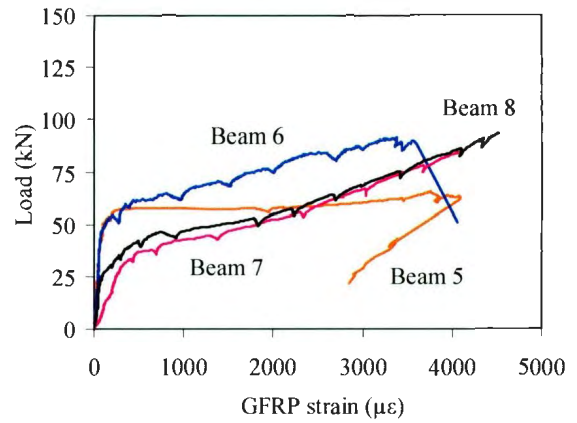


(d) Load vs. GFRP strain for the same shear span to depth ratio (Group 4)

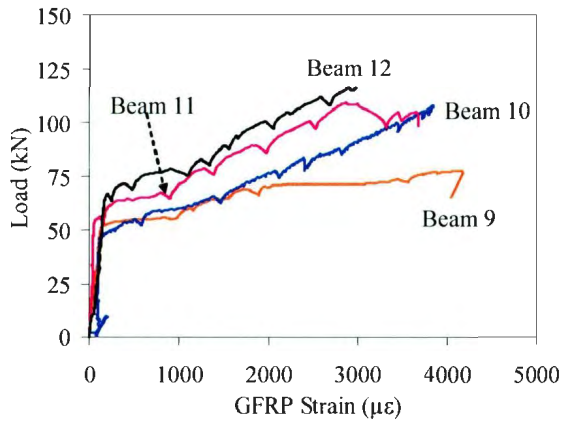
Figure 5.5: Load vs. mid-span GFRP strain for all beams



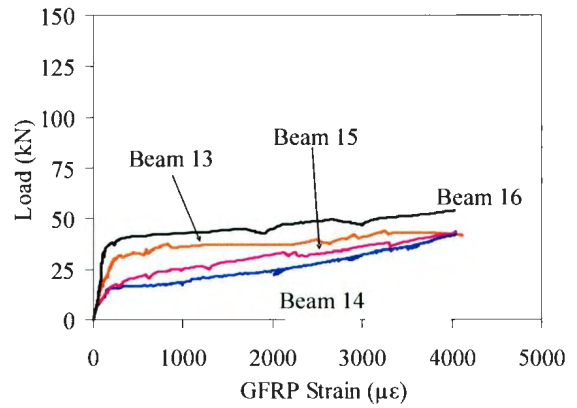
(a) Load vs. mid-shear span GFRP strain
(Group 1)



(b) Load vs. mid-shear span GFRP strain
(Group 2)

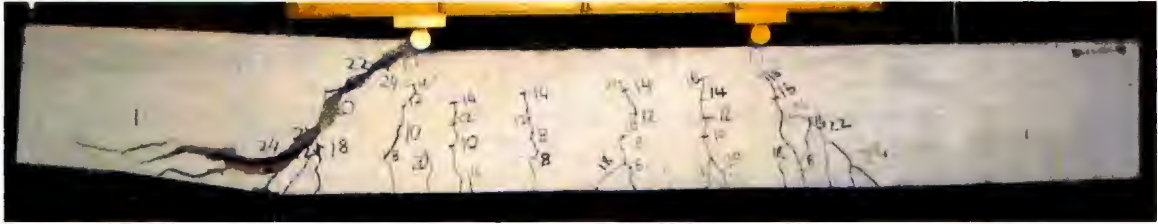


(c) Load vs. mid-shear span GFRP strain
(Group 3)

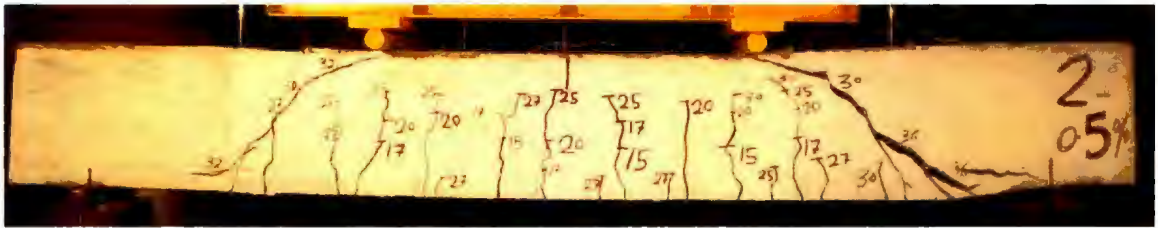


(d) Load vs. mid-shear span GFRP strain
(Group 4)

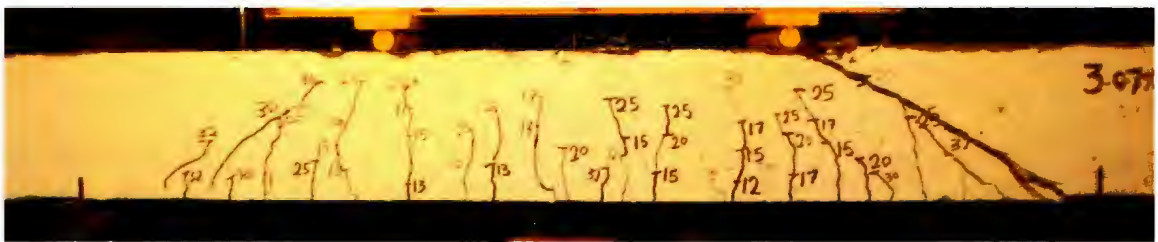
Figure 5.6: Load vs. mid-shear span GFRP strain for all beams



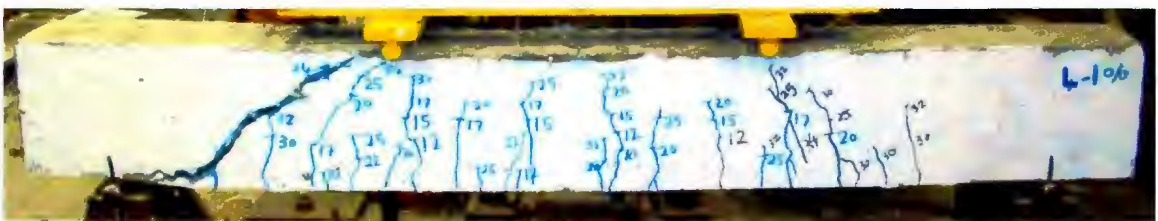
(a) B1



(b) B2



(c) B3

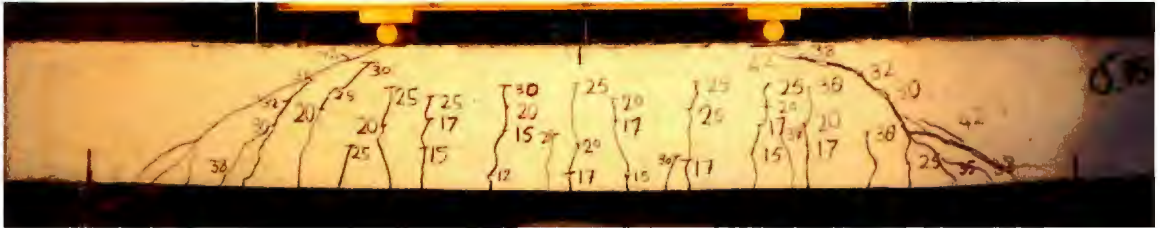


(d) B4

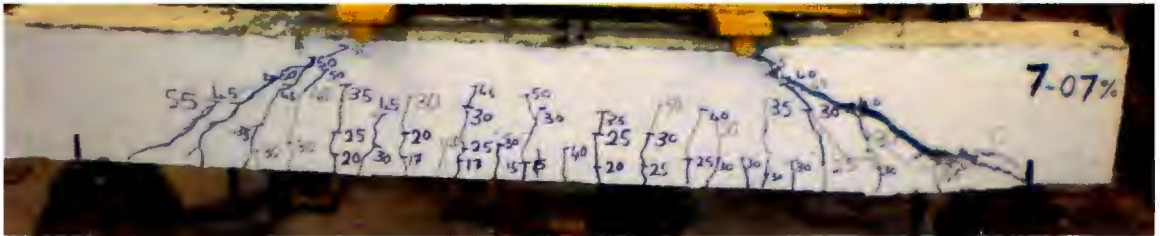
Figure 5.7: Crack patterns for beams of Group 1 ($a/d = 2.5$)



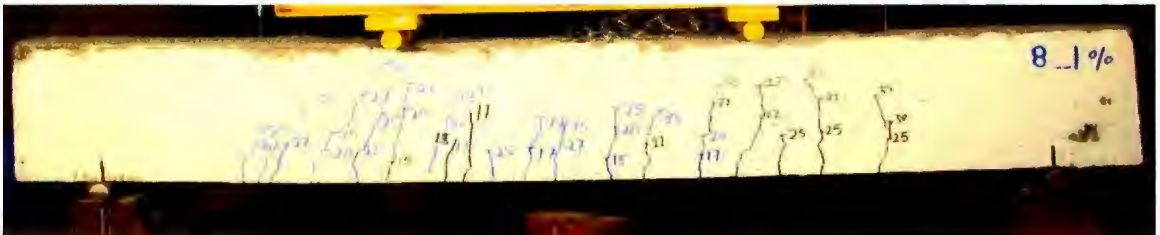
(a) B5



(b) B6



(c) B7

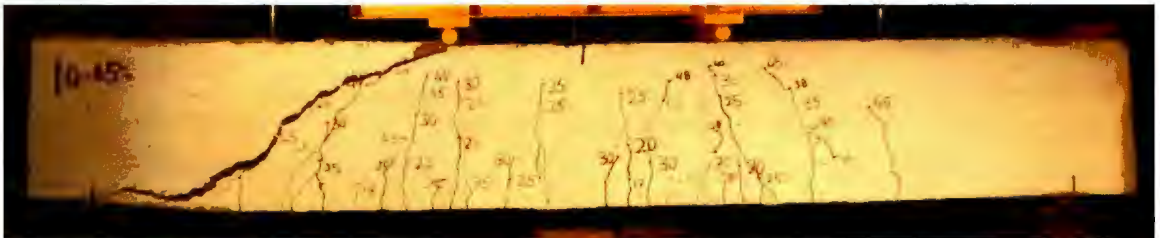


(d) B8

Figure 5.8: Crack patterns for beams of Group 2 ($a/d = 2.6$)



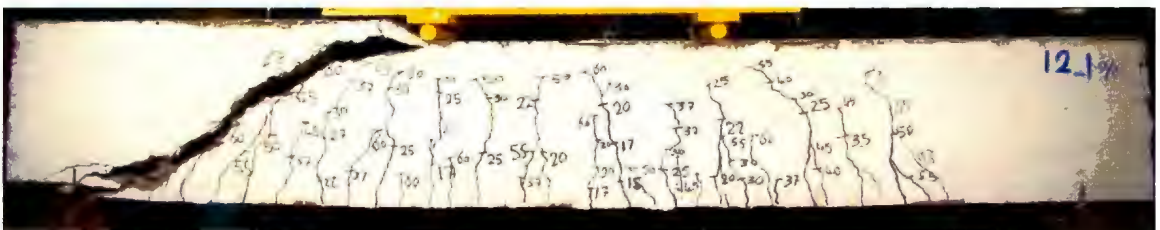
(a) B9



(b) B10

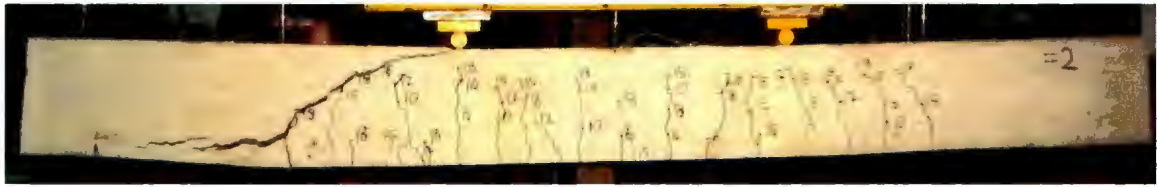


(c) B11

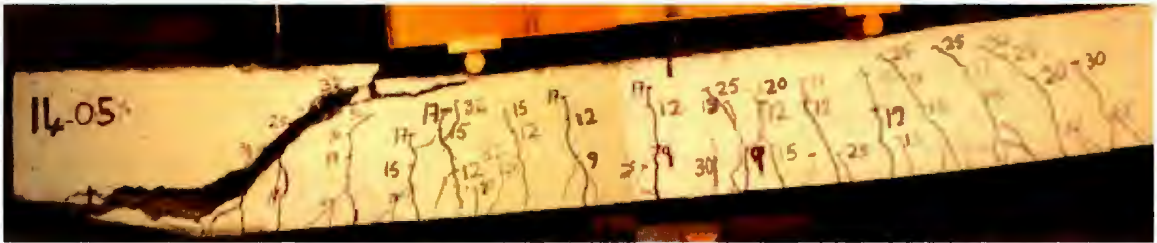


(d) B12

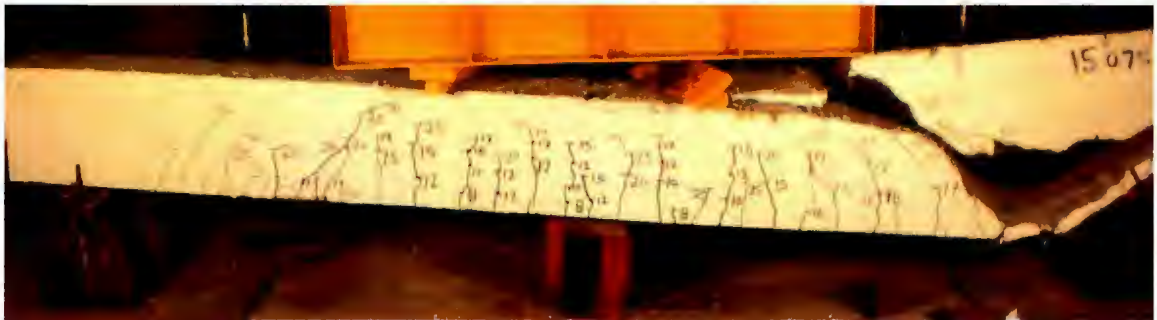
Figure 5.9: Crack patterns for beams of Group 3 ($a/d = 2.5$)



(a) B13



(b) B14



(c) B15

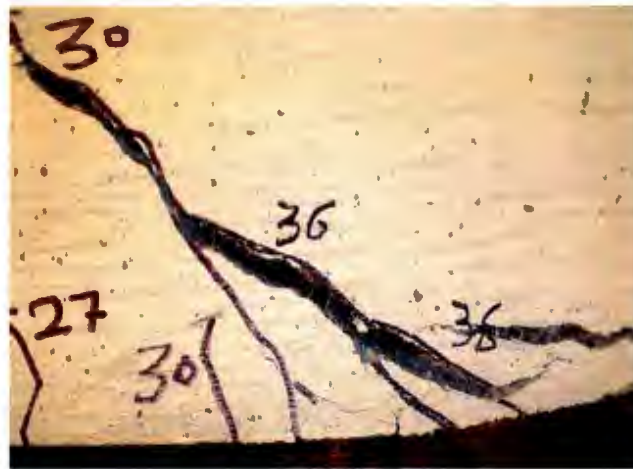


(d) B16

Figure 5.10: Crack patterns for beams of Group 4 ($a/d = 3.5$)



(a) Flexural and diagonal shear cracks

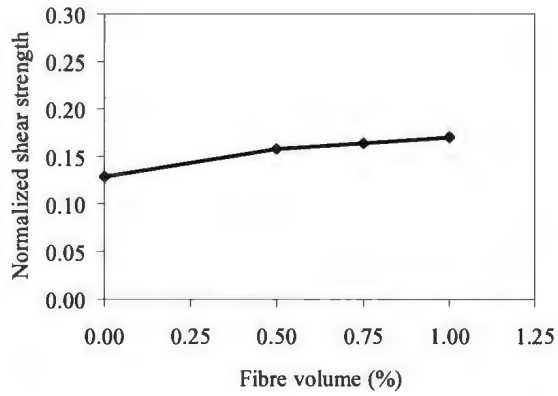


(b) Shear flexural crack

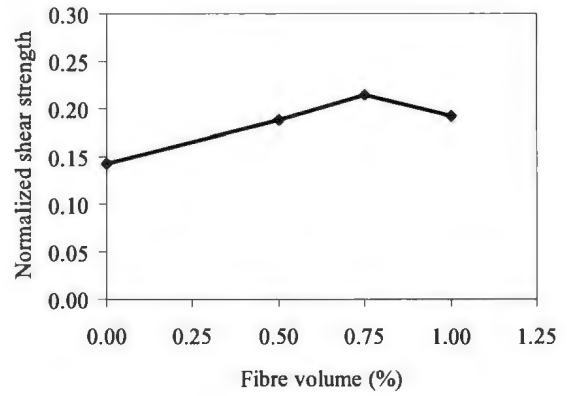


(c) Bond/anchorage crack

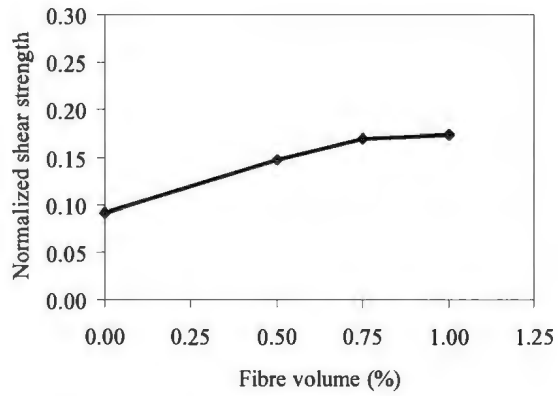
Figure 5.11: Typical cracks: (a) Flexural and diagonal shear cracks; (b) shear flexural crack, and (c) bond/anchorage crack



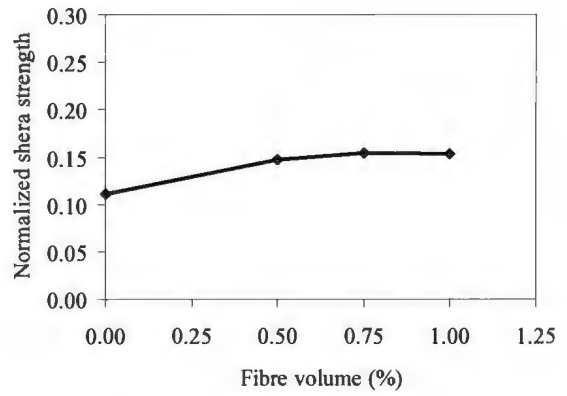
(a) Reinforcement ratio of $(1.3 \rho_b)$



(b) Reinforcement ratio of $(2.0 \rho_b)$



(c) Shear span to depth ratio (a/d) of 3.5



(d) Effective depth of 441 mm

Figure 5.12: Influence of fibre volume on the normalized shear strength (shear strength is normalized with respect to $\sqrt{f'_c}$)

Chapter 6

Finite Element Analysis

6.1. Introduction

This chapter presents a numerical approach to model the fibre reinforced concrete beams with GFRP bars that were tested in the experimental program. The focus of the finite element (FE) analysis is to develop a numerical model to predict the response of such beams in terms of first crack, load-deflection behaviour and ultimate load capacity. A three-dimensional non-linear FE model was constructed to simulate the behaviour of the beams from linear through nonlinear response and up to failure. The model was constructed in the general-purpose FE program ANSYS (2005). A description of the FE model and the calibration of the model are discussed. Finally, a comparison between the experimental and finite element results is presented.

6.2. Constitutive Models

6.2.1. Concrete Model

The three-dimensional element “Solid65” from the ANSYS library was used. The element is capable of simulating plastic deformation, cracking and crushing of the concrete. This element was used to model the concrete and is shown in Figure 6.1. It has eight nodes with three translational degrees of freedom at each node. A Gaussian integration scheme over the element faces and the smeared crack approach are used with the element. Cracking may develop in up to three orthogonal directions at each integration point when the predefined tensile capacity of the concrete is exceeded, as

shown in Figure 6.1, a combination of an angle θ in the xy plane and an angle of ϕ in the three-dimensional space define a smeared band of the cracks.

In addition to cracking, the concrete constitutive model has a yield and failure surfaces in uniaxial, biaxial, or triaxial compression. The concrete is assumed to crush under that condition. A three-dimensional failure surface for concrete is shown in Figure 6.2. The most significant nonzero principal stresses are represented by σ_{xp} and σ_{yp} , respectively. The failure surfaces under different conditions are shown as the projections on the σ_{xp} - σ_{yp} plane (see Figure 6.2). The mode of failure is a function of the sign of σ_{zp} (the principal stress in the z direction).

The occurrence of cracks in a concrete structure reduces the shear stiffness. This is taken into account by using shear transfer coefficients. The shear transfer coefficient, β_t , represents conditions of an open crack. Typical shear transfer coefficients range from 0.0 to 1.0, with 0.0 representing a smooth crack and 1.0 representing a rough crack.

In general, the cracking criterion of concrete in tension is expressed in terms of principal tensile stresses or strains. Concrete in tension is assumed to behave in a linear elastic fashion prior to cracking. The initial tangent modulus E_c determines the maximum positive (tensile) stress. Once cracking occurs, a smeared model is used to represent the discontinuous macro crack behaviour. The cracked concrete can still carry some tensile stress perpendicular to the crack, which is termed tension stiffening. Figure 6.3 shows the cracking model for concrete used in the present analysis. One disadvantage of the ANSYS model is the default value of the strain at which the tension stiffening stress reduced to zero. The default values cannot be changed and it is set to a value equal to six times the strain that corresponds to the maximum elastic tensile stress.

6.2.2. Reinforcement

The element Solid65 is capable of describing the reinforcing bars. However, in this study an additional element, Link8, was used to investigate the stress along the reinforcement rather than using the smeared reinforcement used in the element. The link element is a three-dimensional spar element that carries a uniaxial tension-compression and it has two nodes with three degrees of freedom, translations in the nodal x , y , and z directions. Based on the experimental observations, no reinforcement slip was assumed. The link elements were superposed on the mesh that was used to model the concrete. The constitutive model for FRP bar was assumed to be linear elastic. The dowel action of the FRP reinforcement is neglected.

6.3. Finite Element Model

6.2.3. Finite Element Mesh

Due to symmetry in the x direction, only one half of a beam was used assuming symmetric boundary conditions. Hence, the modelled beams were 1420, 1770 and 1770 mm long, with a cross-section of 250 mm \times 350 mm, 250 mm \times 500 mm and 250 mm \times 350 mm, respectively. Figure 6.4 shows the finite element mesh used to model the beams.

The FE concrete model approximates the actual stress distribution depending on the selection of the mesh size. Therefore, it is important to choose an appropriate mesh size to meet the requirements of accuracy and to avoid having convergence problems due to cracking. To obtain reasonable results, the use of a square mesh is recommended. The typical mesh size was selected to be equal to 50 mm \times 50 mm \times 50 mm that was approximately twice the aggregate size. This also follows the recommendations of Shah

(2010) that were based on a mesh sensitivity analysis for beams reinforced with GFRP bars.

The internal reinforcement for the beams was modelled using the spare element link 8, embedded in the solid mesh. This option was favoured over the alternative smeared mesh, since it allowed the reinforcement to be precisely located where it was needed.

Figure 6.5 shows the applied displacement and boundary conditions. The boundary conditions were applied at points of symmetry and where the supports and loadings exist. The supports were modeled as pins supports where translations were constrained in y and z directions. A beam was loaded through an applied displacement to simulate the actual tests where all beams were loaded through the hydraulic actuator in displacement control.

6.2.4. Material Properties

The actual material properties, obtained from the material investigation presented in Chapter 4, were used. Typical parameters used to define the material models could be found in Table 6.1. As presented in Table 6.1, there are multiple parts of the material model for each element.

Material Model Number 1 refers to the concrete elements. An element requires linear isotropic and multi-linear isotropic material properties to properly model concrete. The multi-linear isotropic material uses the Von Mises' failure criterion. E_x is the modulus of elasticity of the concrete E_c , and PRXY is the Poisson's ratio, ν . The modulus of elasticity was based on the following equation:

$$E_c = 4500\sqrt{f'_c} \quad (6.1)$$

The values of f'_c were set based on the cylinder test results for the beams. Poisson's ratio is assumed to be equal to 0.17. The compressive uniaxial stress-strain relationship for the concrete model is obtained using the following equations by Collins and Mitchell (1991):

$$f = \frac{E_c \varepsilon}{1 + \varepsilon / \varepsilon_o} \quad (6.2)$$

$$\varepsilon_o = \frac{2f'_c}{E_c} \quad (6.3)$$

$$E_c = \frac{f}{\varepsilon} \quad (6.4)$$

where:

f = stress at any strain ε ,

ε = strain at stress f , and

ε_o = strain at the ultimate compressive strength.

Nonetheless, an elastic-perfectly plastic concrete material model with defining the concrete crush stress limit was applied in the FE model as shown in Figure 6.6.

Typical shear transfer coefficients range from 0.0 to 1.0, with 0.0 representing a smooth crack and 1.0 representing a rough crack. The shear transfer coefficients for open and closed cracks were determined using the work of Kachlakev (2001) as a basis. Convergence problems occurred when the shear transfer coefficient for the open crack dropped below 0.2. No deviation of the response occurred with the change of the coefficient. Therefore, the coefficient for the open crack was set to 0.3. The shear transfer coefficient for the concrete with macro-synthetic fibres was set equal to that of

plain concrete since the macro-synthetic fibres will have negligible contribution to the shear transferred across the crack as it has not bending stiffness.

The biaxial crushing stress refers to the ultimate biaxial compressive strength. There are no data available in the literature to define the biaxial stress envelopes for concrete with macro-synthetic fibres. As a result, the biaxial values were taken as recommended by Kupfer et al. (1969) that is widely accepted for normal concrete.

The density of the concrete is not added in the material model. For the control beam, the LVDTs that were used to measure the deflection at the center were placed above the beams as in the experimental test setup. Deflections were taken relative to a zero deflection point after the self-weight was introduced. Therefore, the self-weight is not introduced in the model.

Material Model Number 2 refers to the FRP reinforcement. An elastic modulus equal to 40 GPa (as discussed in Chapter 4) was used.

6.2.5. Analysis Type

The finite element model for this analysis is a simple beam under transverse loading. For the purpose of this model, static analysis was used. The Newton-Raphson equilibrium iterations were applied for the nonlinear analysis. A displacement controlled incremental loading was applied. This approach was used to simulate the experimental loading method. In order to obtain fast and accurate convergence, the convergence tolerance was set as 2.5%. A small initial step was used to detect the first crack in the connection. Afterwards, an automatic time stepping was used to control the load step sizes. The line search approach and the predictor-corrector method were also used in the nonlinear

analysis to accelerate the convergence. The failure of the beams was assumed when the solution for a small displacement increment did not converge or when a rigid body motion occurred.

6.4. Finite Element Model Predictions

The objectives of comparing the results of the FE model to the experimental test results was to ensure that the elements, material properties, real constants and convergence criteria were adequate to model the response of the beams. The different components that were studied were: the linear region, the initial cracking, the nonlinear region and the failure region.

6.4.1. Load-Deformation Response

The full load-deformation response can be seen in Figures 6.7 (a) and (b). The selected beams have fibre volumes of 0.0% and 0.5%; thus representing all beams in groups 1 and 2. The response predicted using the FE is plotted along with the experimental response. From Figure 6.7, it can be seen that the predicted response by the FE model was in reasonable agreements with the test results.

6.4.2. Behaviour at First Cracking

Comparisons were carried out in the linear region to ensure that deflections and loads in the FE model were consistent with the test results and followed the same pattern in terms of stiffness, load and deflection when first cracking occurred. Before cracking

occurs, the beam behaved as linear elastic. A reasonable prediction of the model was observed in that region.

A typical first crack, as predicted by the model, can be seen in Figure 6.8. The first crack always occurred in the constant moment region. The crack was a flexural vertical crack. The first cracks predicted by the model were similar to those observed from the experiments. A comparison of the values obtained from the FE model and experimental observations are presented in Table 6.2. The results indicate that the FE model of the beam prior to cracking is acceptable and there was reasonable correlation between the model predictions of the first cracks and the experimental observations.

6.4.3. Behaviour beyond First Cracking

In the non-linear region of the response, subsequent cracking occurred as the additional load was applied to the beam. Cracking increased in the constant moment region and the cracks started to propagate towards the supports. Significant flexural cracking occurred in the beam. Furthermore, diagonal tension cracks began to form in the model. These diagonal cracks caused a sudden drop in the applied load, usually regained as the displacement continued. As the load was increased more cracks formed in the constant moment region, cracking started to reach the top of the beam. At this stage, the beam continued to lose its stiffness until failure occurred. Typical cracking pattern can be seen in Figure 6.9.

6.4.4. Ultimate Capacity

As the load was increased, severe cracking propagated throughout the entire beam. At failure, the beam was no longer able to support the additional loads, as indicated by the convergence failure. Figure 6.10 shows typical cracking patterns at failure.

The predicted load and deflection at failure are compared with the experimental values. The results are presented in Table 6.3. For the beams, the ratios of predicted-to-measured ultimate loads ranged from 0.6 to 1.1. The mean value was 0.91 with a COV of 0.18. The ratios of the corresponding deflections at the center of the beams varied from 0.6 to 1.4; and the mean value was 0.88 with COV of 0.23. It should be noted that the deformation of the beam was measured at the center of the beam only. In general, the mode of failure that was predicted using the FE model was a shear failure that was consistent with the experimental test results.

Table 6.1: Typical material parameters used in the model

Material model number	Element type	Material properties		
1	Solid65	Linear isotropic		
		Ex	28460 N	
		PRXY	0.17	
		Multi-linear Isotropic		
			Strain	Stress MPa
		Point1	0.000444	12.67
		Point2	0.000705	17.1
		Point3	0.001040	23.7
		Point4	0.001360	28.0
		Point5	0.001700	31.0
		Concrete		
		ShrCf-Op	0.3	
ShrCf-CI	0.8			
UnTensSt	3.5			
UncompSt	-1			
Bicompst	0			
HydroPrs	0			
UntensSt	0			
TenCrFac	0			
BicompSt	0			
2	Link8	Linear Isotropic		
		Ex	40000 N	
		PRXY	0.25	

Table 6.2: Load-deflection comparison at first cracking

Beam No.	Load (kN)		Deflection (mm)		FEM/Experimental	
	FEM	Experimental	FEM	Experimental	Load	Deflection
B1	25.5	27.0	0.35	0.38	0.94	0.94
B2	56.0	60.0	1.06	1.30	0.90	0.81
B3	52.6	44.5	0.91	1.48	1.20	0.62
B4	49.4	44.9	0.98	0.88	1.10	1.12
B5	29.9	26.3	0.44	0.89	1.14	0.50
B6	54.7	53.9	0.82	1.01	1.01	0.81
B8	55.3	69.3	1.93	2.42	0.80	0.79
B9	33.8	36.7	0.53	0.57	0.92	0.93
B11	60.2	65.4	1.05	1.22	0.92	0.86
B13	23.9	25.6	1.32	1.47	0.93	0.89
B14	41.3	39.0	2.17	2.40	1.05	0.90
B15	41.3	35.6	1.98	2.05	1.20	0.97
B16	39.2	35.6	2.23	2.68	1.10	0.83

Table 6.3: Comparison between experimental and FE model at failure

Model No.	Load (kN)		Deflection (mm)		FEM/Experimental	
	FEM	Experimental	FEM	Experimental	Load	Deflection
B1	135.0	122.0	16.1	15.7	1.10	1.01
B2	168.8	158.7	19.2	13.5	1.06	1.40
B3	158.7	158.9	19.7	20.3	1.00	0.97
B4	169.3	176.8	17.4	18.2	0.95	0.95
B5	131.9	130.9	9.1	9.7	1.00	0.93
B6	200.5	182.0	13.4	13.7	1.10	1.00
B8	175.6	191.5	16.7	18.8	0.92	0.89
B9	146.6	154.3	10.8	15.2	0.95	0.70
B11	220.3	217.6	15.7	16.1	1.01	0.98
B13	70.2	87.3	19.3	22.3	0.81	0.86
B14	98.8	147.8	19.5	31.4	0.70	0.60
B15	112.0	164.1	29.3	43.1	0.68	0.68
B16	160.9	180.4	41.2	51.1	0.89	0.80
Mean					0.91	0.88
Coefficient of Variation					0.18	0.23

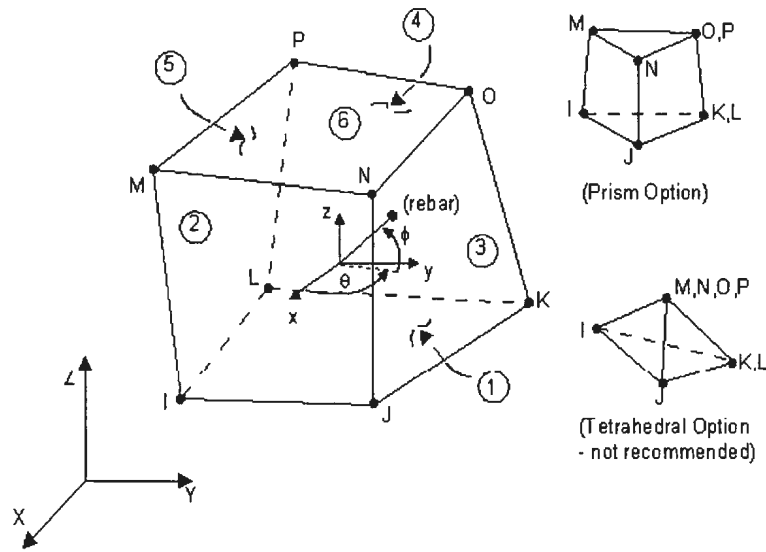


Figure 6.1: Solid 65 element (ANSYS, 2005)

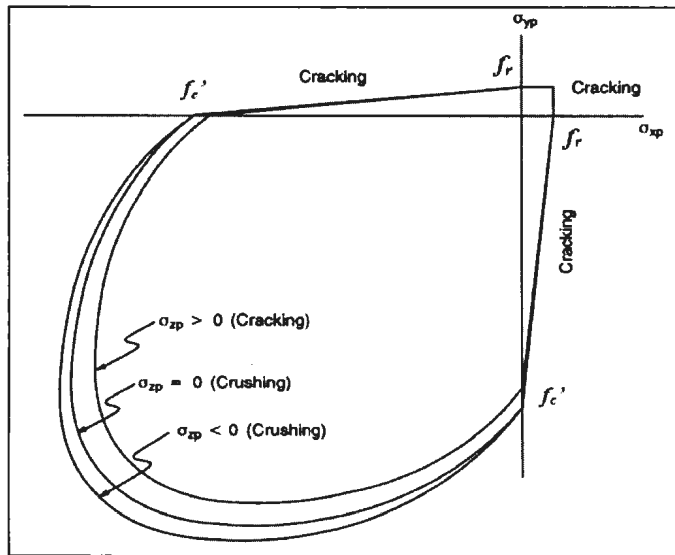


Figure 6.2: Failure surface in principal stress space (ANSYS, 2005)

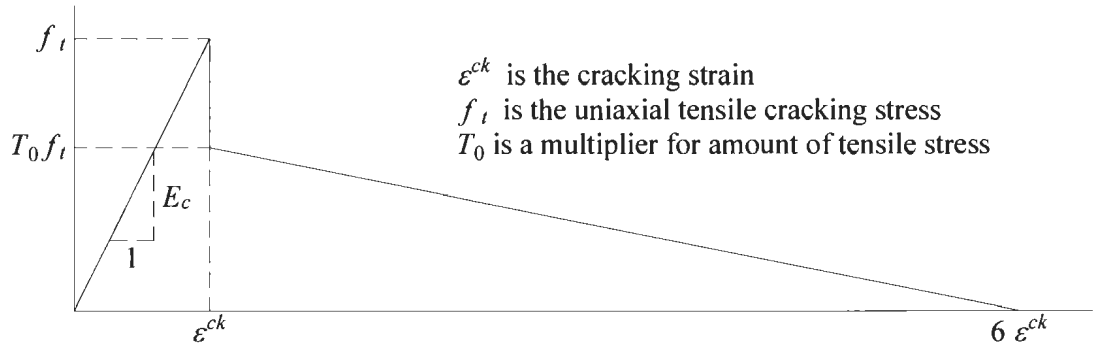


Figure 6.3: Concrete cracking model

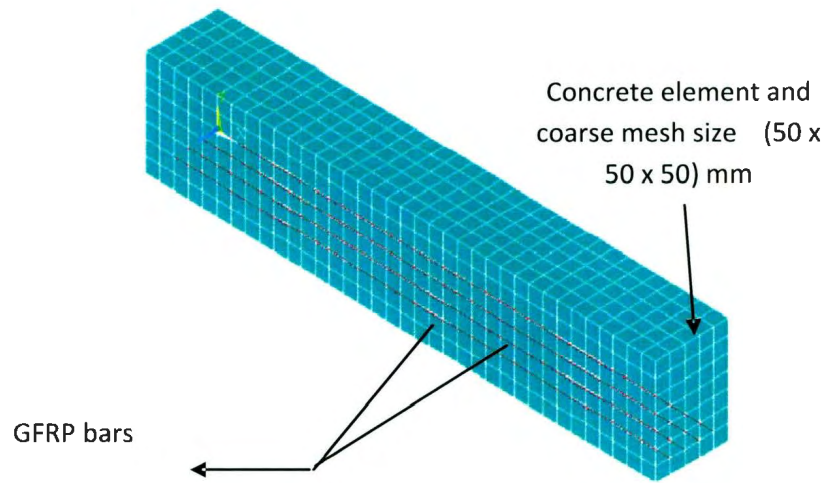


Figure 6.4: Used mesh; concrete elements and the GFRP reinforcement

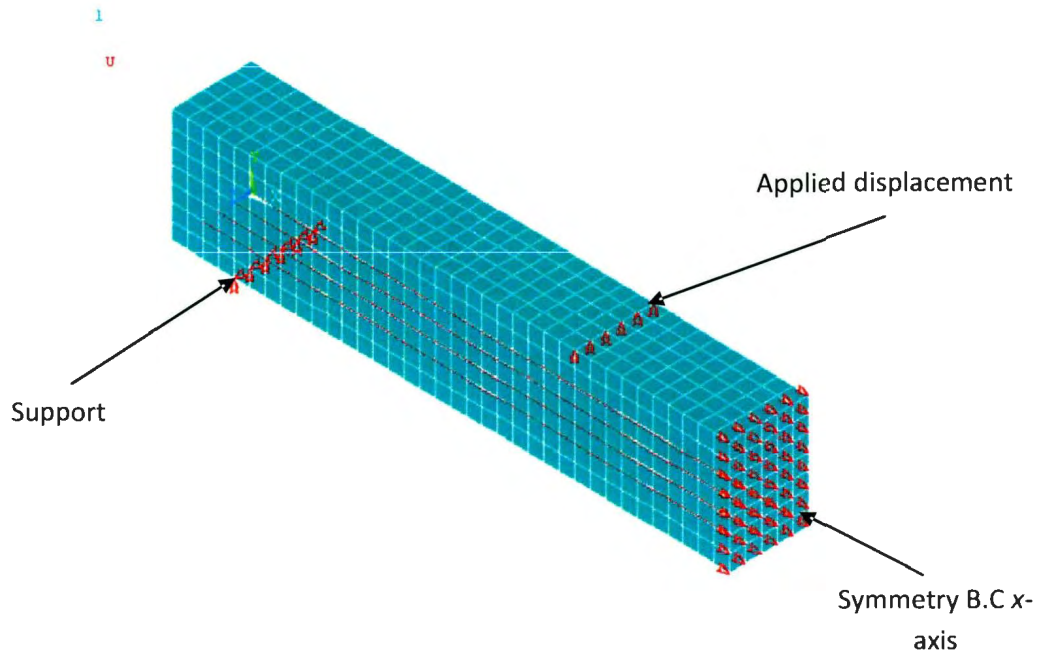


Figure 6.5: Applied displacement and boundary conditions

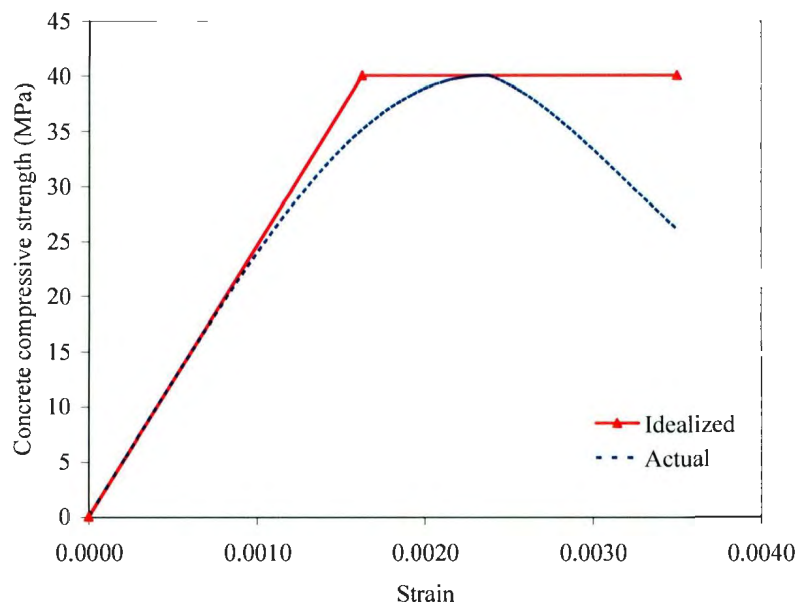
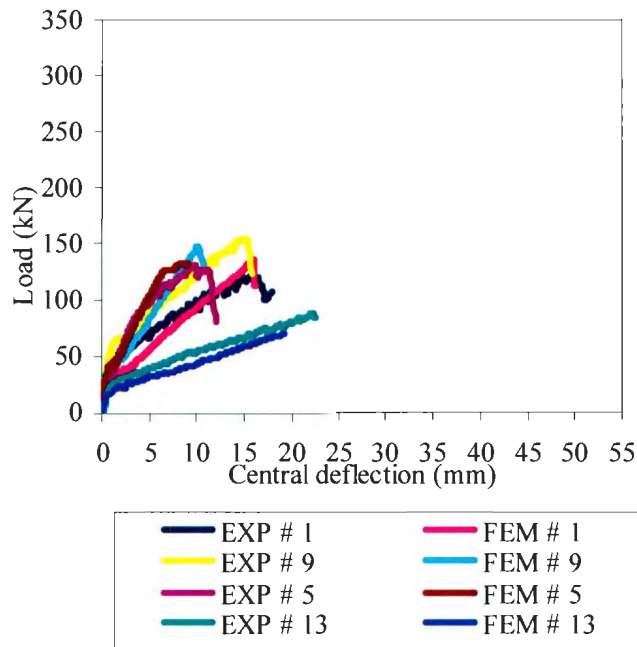
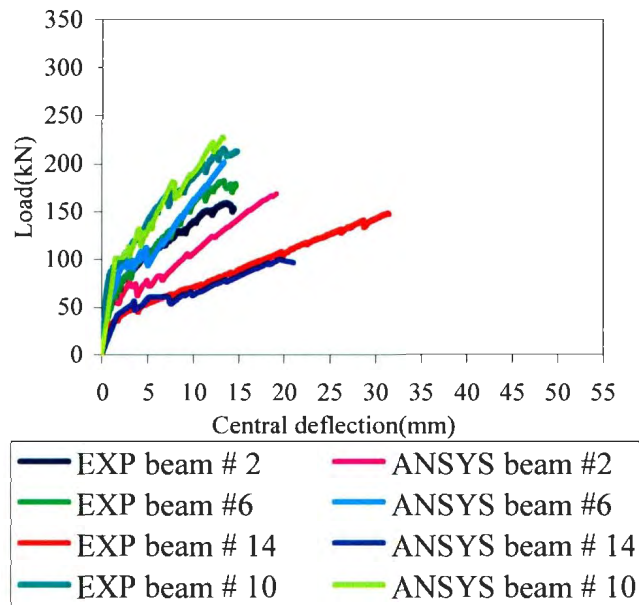


Figure 6.6: Uniaxial stress-strain curve for concrete

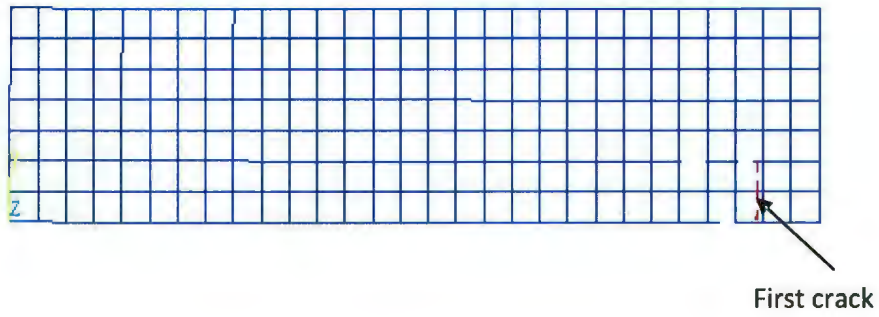


(a) Beams in group 1: 0% fibre volume and different variables (ρ , d and a/d)

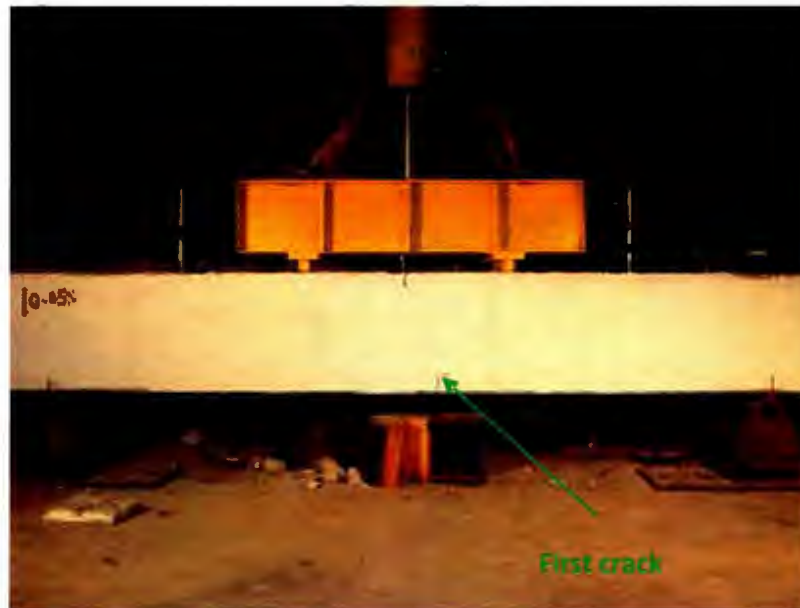


(b) Beams in group 2: 0.5% fibre volume and different variables (ρ , d and a/d)

Figure 6.7: Predicted and experimental load versus deflections

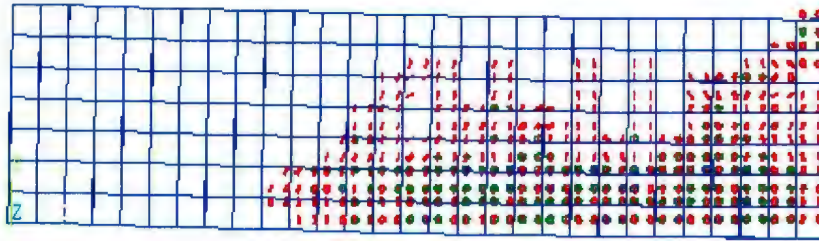


(a) First crack (FE model)

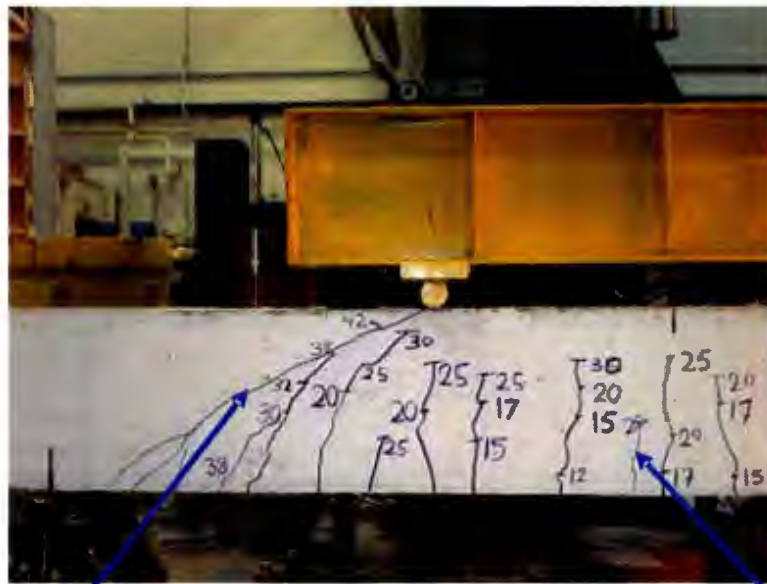


(b) First crack (experimental)

Figure 6.8: First crack: model prediction and experimental observation



(a) Flexural and diagonal shear cracks (FE model)



Diagonal shear crack

Flexural crack

(b) Flexural and diagonal shear cracks (experiment)

Figure 6.9: Significant flexural and diagonal shear cracks

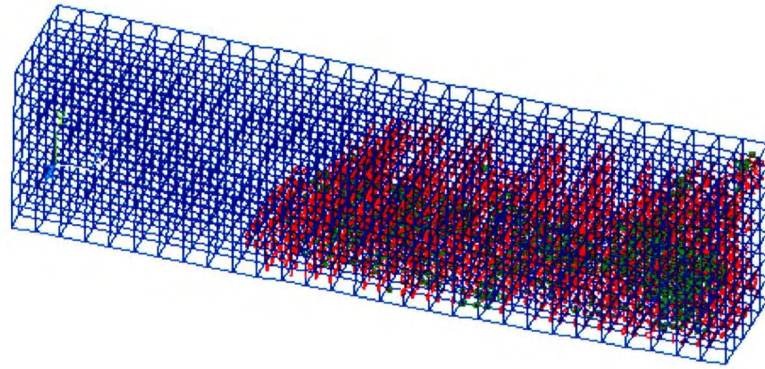


Figure 6.10: Severe cracking near failure (model prediction)

Chapter 7

Summary and Conclusions

Structural testing of sixteen scale beams reinforced with GFRP bars with additional macro synthetic fibre was conducted. The purpose of the investigation was to determine whether the macro synthetic fibre could be added to enhance the shear strength of longitudinally reinforced concrete beams. Four sets of beams were tested; the control set without fibre and another three sets included macro synthetic fibre with volume fractions of 0.5%, 0.75% and 1%. Moreover, material investigation was carried out by testing thirty two prisms and thirty six cylinders to examine the effect of fibre on the concrete properties.

Results of the experimental investigation showed that the addition of the macro synthetic fibre enhanced the shear strength and slightly modified the shear failure behaviour of reinforced concrete beams. Furthermore, the shear capacity was affected by increasing the reinforcement ratio, effective depth and shear span to depth ratio. The formation of the first shear crack led to complete failure of the control beams, whereas the beams with macro synthetic fibre continued to resist higher loads after the appearance of the first diagonal shear crack. From the investigation of the two phases, structural and material, the following conclusions can be drawn:

1. Adding the fibre to concrete, improved the splitting tensile strength and flexural tensile strength of the concrete by enhancing the toughness. The addition of fibre significantly increased the flexural toughness and toughness indices of concrete.
2. The deflections of the beams showed typical bilinear-elastic behaviour up to the failure with a transition stage. Also, the GFRP strain was measured and reported from

the test beams at the mid span and mid-shear span. The strains at midspan showed typical bilinear-elastic behaviour up to the failure and were similar to the load deflection curve. The strain variation can be divided into two segments before and after cracking. The maximum strains occurred at the center of the beam. The recorded maximum strain in the GFRP bars was $4200 \mu\epsilon$ in beams of Group 2, which had 0.5% fibre by volume, $1.3 \rho_b$ reinforcement ratio and 350 mm beam depth. This value is less than the ultimate tensile strain of GFRP bars, which is approximately $15000 \mu\epsilon$; based on the reinforcement strain values provided by the manufacturer. It should be noted that there was no rupture of the GFRP bars in any of the test beams.

3. The GFRP strains in the mid-shear span increased rapidly after cracking. This could be due to the rapid opening up of the cracks near the strain gauge location. The associated increase in load after cracking near the mid-shear span was small which suggests that the beam failed shortly after the formation of the cracks at the vicinity of that location.
4. The maximum concrete strain recorded on the compression side of the beams did not reach the crushing concrete strain. Moreover, there were no signs observed during the experiments indicating that the phenomenon had occurred.
5. The addition of macro synthetic fibre modified the shear failure behaviour of reinforced concrete beams and increased the cracked stiffness of the beams.
6. Increasing the flexural reinforcement ratio resulted in increasing the normalized shear strength. The normalized shear strength, for the same fibre volume was increased from 0.16, 0.16 and 0.17 to 0.19, 0.21 and 0.19, for fibre volumes of 0.5%, 0.75%,

and 1.0%, respectively, when the reinforcement ratio was increased from $1.3\rho_b$ to $2.0\rho_b$.

7. Increasing the shear span to depth ratio did not result in a significant change in the normalized shear strength of the beams with fibres. However, for beams that have no fibre, increasing the shear span to depth ratio (a/d) from 2.5 to 3.5 resulted in decreasing the normalized shear strength from 0.13 to 0.09.
8. For the beams with no fibres, increasing the effective depth from 302 mm to 441 mm resulted in decreasing the normalized shear strength from 0.13 to 0.11. For beams with fibres, increasing the effective depth from 302 mm to 441 mm resulted in no significant change in the nominal shear strength, which is around 6.7% on the average.
9. Increasing the volume of synthetic fibre from 0.0% to 1.0% resulted in an increase in the normalized shear strength from 0.13 to 0.17 and from 0.14 to 0.19 for the beams with $1.3\rho_b$ and $2.0\rho_b$, respectively. This means that the contribution to the normalized shear strength of 1.0% fibre by volume was about 35% on the average the same reinforcement ratio was used.
10. Increasing the volume of synthetic from 0.0% to 1.0%, for beams that have the same shear span to depth ratio (a/d) of 3.5, resulted in an increase in the normalized shear strength from 0.09 to 0.17. That is, an increase of 90% when in the normalized shear strength.
11. Increasing the volume of synthetic fibre from 0.0% to 1.0%, for beams with effective depth of 441 mm, resulted in an increase in the normalized shear strength from 0.11

to 0.15. This means, that the maximum contribution of 1.0% fibre by volume was about 39% when the same effective depth of 441 mm was used.

12. The enhancement of the shear capacity was not noticeable when the fibre volume was increased from 0.5% to 1.0%, for beams that had the effective depth of 441 mm.
13. The energy absorption capacity was slightly increased as the reinforcement ratio was increased, approximately increased by 14% by increasing the beam effective depth and increasing the shear span to depth ratio.

A finite element study was carried out to analyze the test beams. In the model, proper elements, boundary conditions, mesh size and nonlinear solution strategies were implemented. The reinforced concrete beams models were calibrated based on the data obtained from the material tests. The initial cracking load and the failure load of the beams were compared to the experimental results in terms of load deflection curve, initial cracking load, deflection at the cracking load and the values of the load and deflection at the failure point. The following conclusions can be reached:

1. The load-deflection characteristics obtained from the finite element solution at the center of the beam were in close agreement with the experimental test results at first cracking stage and at failure stage.
2. The initial crack and progressive cracking of the finite element model compared well to the experimental data obtained.
3. The failure mechanism of the reinforced concrete beams models was very close to the failure load measured during experimental testing.

References

- ACI Committee 318, "Building Code Requirements for Structural Concrete (ACI 318-08) and Commentary (ACI 318M-08)," ACI 318-08, American Concrete Institute, Farmington Hills, Michigan, 2008.
- ACI Committee 440, "Guide for the Design and Construction of Structural Concrete Reinforced with FRP Bars (ACI 440.1R-06)," Farmington Hills, Michigan, 2006.
- ACI Committee 544, State-of-the-Art Report on Fibre Reinforced Concrete, ACI 544.1R-96, American Concrete Institute, Farmington Hills, Michigan, 1997.
- ACI-ASCE Committee 445, "Recent Approaches to Shear Design of Structural Concrete," ASCE Journal of Structural Engineering, Vol. 124, No. 12, 1998, pp. 1375-1417.
- Alam, S., "Influence of Different Parameters on Shear Strength of FRP Reinforced Concrete Beams Without Web Reinforcement," PhD Thesis, Memorial University of Newfoundland, Canada, 2010.
- Alkhrdaji, T., Wideman, M., Belarbi, A., and Nanni, A., "Shear Strength of GFRP-RC Beams and Slabs," Composites in Construction. Edited by Figueiras et al. Swets and Zeitlinger, Lisse, 2001.
- Altoubat, S., Yazdanbakhsh, A., and Rieder, K., "Effect of Synthetic Macro Fibres on Shear Behaviour of Concrete Beams," Deflection and Stiffness Issues in FRC and Thin Structural Elements, SP-248, P. H. Bischoff and F. Malhas, eds., American Concrete Institute, Farmington Hills, MI, 2007, pp. 41-52.
- Altoubat, S., Yazdanbakhsh, A., and Rieder, K., "Shear Behaviour of Macro-Synthetic Fibre-Reinforced Concrete Beams without Stirrups," ACI Materials Journal, Vol. 106, No. 4, 2009, pp. 381-389.
- Ashour, S., Hasanain, G., and Wafa, F., "Shear Behaviour of High-Strength Fibre-Reinforced Concrete Beams," ACI Structural Journal, Vol. 89, No. 2, 1992, pp. 176-184.
- Balaguru, P., "Fibre-Reinforced Rapid Setting Concrete," Concrete International, Vol. 14, No. 2, 1992, pp. 64-67.
- Barr, B., "Fracture Characteristics of FRC Materials in Shear," Fibre Reinforced Concrete Properties and Applications, American Concrete Institute, Detroit, MI, 1987, pp. 27-53. (ACI SP-105).
- Banthia, N., and Trottier, J., "Concrete Reinforced with Deformed Steel Fibres, Part I: Bond-slip mechanisms," ACI Materials Journal, Vol. 91, No. 5, 1994, pp. 435-446.

- Bayasi, Z., and Celik, T., "Application of Silica Fume in Synthetic Fibre-Reinforced Concrete," *Transportation Research Record*, No. 1382, 1993, pp. 89-98.
- Bayasi, Z., and Zeng, J., "Properties of Polypropylene Fibre Reinforced Concrete," *ACI Materials Journal*, Vol. 90, No. 6, 1993, pp. 605-610.
- Bentur, A., Mindess, S. (second edition) "Fibre Reinforced Cementitious Composites", *Modern Concrete Technology Series*, published by Taylor & Francis Group, New York, USA, 2007, 601p.
- Bijen, J., "Improved Mechanical Properties of Glass Fibre Reinforced Cement by Polymer Modification," *Cement & Concrete Composites*, Vol. 12, 1990, pp. 95-101.
- Canadian Standard Association, "Design and Construction of Building Components with Fibre Reinforced Polymers," CSA S806-10, Rexdale, Ontario, Canada, 2010.
- Choi, K., Park, H., and Wight, J., "Shear Strength of Steel Fibre-Reinforced Concrete Beams without Web Reinforcement," *ACI Structural Journal*, Vol. 104, No. 1, 2007, pp. 12-22.
- Collins, M., and Mitchell, D., "Prestressed Concrete Structures," Prentice-Hall, 1991, 760 p.
- Daniali, S., "Development Length for Fibre-Reinforced Plastic Bars," *Advanced Composite Materials in Bridges and Structures*, K. W. Neale and P. Labossiere, eds., Sherbrooke, Canada, 1992, pp. 179-188.
- Dupont, D., and Vandewalle, L., "Shear Capacity of Concrete Beams Containing Longitudinal Reinforcement and Steel Fibres," *ACI Special Publication*, 216, 2003, pp. 79-94.
- El-Salakawy, E., Benmokrane, B., El-Ragaby A., and Nadeau, D., "Field Investigation on the First Bridge Deck Slab Reinforced with Glass FRP Bars Constructed in Canada," *Journal of Composites for Construction*, Vol. 9, No., 6, 2005, pp. 470-479.
- El-Sayed, A., El-Salakawy, E., and Benmokrane, B., "Shear Strength of FRP-Reinforced Concrete Beams without Transverse Reinforcement. *ACI Structural Journal*, Vol. 103, No. 2, 2006a, pp. 235-243.
- El-Sayed, A., El-Salakawy, E., and Benmokrane, B., "Shear Capacity of High-Strength Concrete Beams Reinforced with FRP Bars," *ACI Structural Journal*, Vol. 103, No. 3, 2006b, pp. 383-389.
- Fanning, P., "Nonlinear Models of Reinforced and Post-Tensioned Concrete Beams," *Electronic Journal of Structural Engineering*, Vol. 2, 2001, pp. 111-119.
- Fattuhi, H., "SFRC Corbel Tests," *ACI Structural Journal*, Vol. 84, No. 2, 1987, pp. 119-123.

- Greenough, T., and Nehdi, M., "Shear Behaviour of Fibre-Reinforced Self-Consolidating Concrete Slender Beams," *ACI Materials Journal*, Vol. 105, No. 5, 2008, pp. 468-477.
- Hara, T., and Kitada, Y., "Shear Strength of Reinforced Concrete Corbels and Steel Fibres as Reinforcement," *Transactions of the Japan Concrete Institute*, Vol. 2, 1980, pp. 279-286.
- Hoff, G., "Durability of Fibre Reinforced Concrete in a Severe Marine Environment," *Fiber Reinforced Concrete Properties and Applications*, SP-105, American Concrete Institute, Detroit, 1987, pp. 997- 1041.
- Hoult, N., Sherwood, E., Bentz, E., and Collins, M., "Does the Use of FRP Reinforcement Change the One-Way Shear Behaviour of Reinforced Concrete Slabs?," *Journal of Composites for Construction*, Vol. 12, No. 2, 2008, pp. 125-133.
- Johnston, C., "Fibre Reinforced Cement and Concretes," LT249, Gordon & Breach, Amsterdam, 2000, 368 p.
- Johnston, C., and Zemp, R., "Flexural Fatigue Performance of Steel Fibre Reinforced Concrete-Influence of Fibre Content, Aspect Ratio and Type," *ACI Materials Journal*, Vol. 88, No. 4, 1991, pp. 374-383.
- Kachlakev, D., Miller, T., Yim, S., Chansawat, K., and Potisuk, T., "Finite Element Modelling of Reinforced Concrete Structures Strengthened with FRP Laminates," PhD dissertation, California Polytechnic State University, San Luis Obispo, USA, 2001.
- Khuntia, M., Stojadinovic, B., and Goel, S., "Shear Strength of Normal and High-Strength Fiber Reinforced Concrete Beams without Stirrups," *ACI Structural Journal*, Vol. 96, No. 2, 1999, pp. 282-289.
- Kobayashi, K., and Cho, R., "Flexural Behaviour of Polyethylene Fibre Reinforced Concrete," *The International Journal of Cement Composites and Lightweight Concrete*, Vol. 3, No. 1, Construction Press, 1981.
- Krenchel, H., and Jensen H., "Organic Reinforcing Fibres for Cement and Concrete, in Fibrous Concrete," in *The Concrete Society, Proceeding of the Symposium on Fibrous Concrete*, Lancaster, The Construction Press, 1980, pp. 87-98.
- Krenchel, H., and Shah, S., "Fracture Analysis of the Pullout Test," *Materials and Structures*, Vol. 18, No. 6, 1985, pp. 439-446.
- Kwak, Y., Eberhard, M., Kim, W., and Kim, J., "Shear Strength of Steel Fibre Reinforced Concrete Beams without Stirrups," *ACI Structural Journal*, Vol. 99, No. 4, 2002, pp. 530-538.

- Larson, E., and Krenchel, H., "Durability of FRC-materials," Fibre-reinforced Cementitious Materials Symposium, Sidney Mindess, Jan Skalny (Eds.), Boston, Massachusetts, Proceedings, Vol. 211, Materials Research Society Symposium Society, Pittsburgh, 1991, pp. 119-124.
- Li, V., Ward, R., and Hamza, A., "Steel and Synthetic Fibres as Shear Reinforcement," ACI Materials Journal, Vol. 89, No. 5, 1992, pp. 499-508.
- Lim, T., Paramasivam, P., and Lee, S., "Shear and Moment Capacity of Reinforced Steel-Fiber-Concrete Beams," Magazine of Concrete Research, Vol. 39, No. 140, 1987, pp. 148-160.
- Majdzadeh F., Soleimani, S., and Banthia, N., "Shear Strength of Reinforced Concrete Beams with a Fibre Concrete Matrix," Canadian Journal Of Civil Engineering, Vol. 33, No. 6, 2006, pp. 726-734.
- Mallick, P., "Fibre Reinforced Composites: Materials, Manufacturing and Design," 2nd Ed. Marcel Dekker Inc., New York, 1993, 566 p.
- Mansur, M., Ong, C., and Paramasivam, P., "Shear Strength of Fibrous Concrete Beams without Stirrups," Journal of Structural Engineering, Vol. 112, No. 9, 1986, pp. 2066-2079.
- Minelli, F., and Vecchio, F., "Compression Field Modeling of Fiber-Reinforced Concrete Members Under Shear Loading," ACI Structural Journal, Vol. 103, No. 2, 2006, pp. 244-252.
- Narayanan, R., and Darwish, I., "Use of Steel Fibres as Shear Reinforcement," ACI Structural Journal, V. 84, No. 3, 1987, pp. 216-227.
- Noghabai, K., "Beams of Fibrous Concrete in Shear and Bending; Experiment and Model," Journal of Structural Engineering, ASCE, Vol. 126, No. 2, 2000, pp. 243-251.
- Otter, D., and Naaman, A., "Fibre Reinforced Concrete under Cyclic and Dynamic Compression Load," Research Report, No. UMCE 88-9, Department of Civil Engineering, University of Michigan, Ann Arbor, 1988, 178 p.
- Özcan, D., Bayraktar, A., Sahin, A., Haktanir, T., and Türker, T., "Experimental and Finite Element Analysis on the Steel Fiber-Reinforced Concrete (SFRC) Beams Ultimate Behavior," Journal of Construction and Building Materials, Vol. 23, 2009, pp. 1064-1077.
- Parra-Montesions, G., "Shear Strength of Beams with Deformed Steel Fibres," Concrete International, Vol. 28, No. 11, 2006, pp. 57-67.
- Ramakrishnan, V., Gallapudi, S., and Zellers, R., "Performance Characteristics and Fatigue Strength of Polypropylene Fibre Reinforced Concrete," Fibre Reinforced

- Concrete Properties and Applications, American Concrete Institute, Detroit, MI, 1989, pp. 159-177. (ACI SP-105).
- Ramakrishnan, V., Oberling, G., and Tatnall, P., "Flexural Fatigue Strength of Steel Fibre Reinforced Concrete," Fibre Reinforced Concrete Properties and Applications, SP-105, American Concrete Institute, Detroit, 1987, pp. 225-245.
- Razaqpur, A., Isgor, B., Greenway, S., and Selley, A., "Concrete Contribution to the Shear Resistance of Fibre Reinforced Polymer Reinforced Concrete Members," Journal of Composites for Construction, Vol. 8, No. 5, 2004, pp. 452-460.
- Razaqpur, A., Isgor, O., "Proposed Shear Design Method for FRP-Reinforced Concrete Members without Stirrups," ACI Structural Journal, Vol. 103, No. 1, 2006, pp. 93-102.
- Romualdi, J., and Mandel, J., "Tensile Strength of Concrete Affected by Uniformly Distributed and Closely Spaced Short Lengths of Wire Reinforcement," ACI Journal, Proceedings Vol. 61, No. 6, 1964, pp. 657-671.
- Shah, S., "Do Fibres Increase the Tensile Strength of Cement Based Matrixes?" ACI Materials Journal, Vol. 88, No. 6, 1991, pp. 595-602.
- Shah, S., Weiss, W., and Yang, W., "Shrinkage Cracking - Can it Be Prevented?" Concrete International, Vol. 20, No. 4, 1998, pp. 51-55.
- Sharma, A., "Shear Strength of Steel Fibre Reinforced Concrete Beams," ACI Journal Proceedings Vol. 83, No. 4, 1986, pp. 624-628.
- Shin, S., Oh, J., and Ghosh, S., "Shear Behaviour of Laboratory-Sized High-Strength Concrete Beams Reinforced with Bars and Steel Fibres," Fibre Reinforced Concrete Developments and Innovations, SP-142, American Concrete Institute, Farmington Hills, 1994, pp. 181-200.
- Swamy, R., Jones, R., and Chiam, T., "Shear Transfer in Steel Fibre Reinforced Concrete," Fibre Reinforced Concrete Properties and Applications, American Concrete Institute, Detroit, MI, 1987, pp. 565-592. (ACI SP-105).
- Tan, K., and Mansur, M., "Shear Transfer in Reinforced Fibre Concrete," Journal of Materials in Civil Engineering, Vol. 2, No. 4, 1990, pp. 202-214.
- Trottier, J., and Mahoney, M., "Innovative Synthetic Fibres," Concrete International, Vol., 23, No. 6, 2001 pp. 23-28.
- Tureyen, A., and Frosch, R., "Concrete Shear Strength: Another Perspective," ACI Structural Journal, Vol. 100, No. 5, 2002, pp. 609-615.
- Valle, M., "Shear Transfer in Fibre Reinforced Concrete," MSc Thesis, Department of Civil and Environmental Engineering, Massachusetts Institute of Technology, 1991.

- Valle, M., and Buyukozturk, O., "Behaviour of Fibre Reinforced High-Strength Concrete under Direct Shear," *ACI Materials Journal*, Vol. 90, No. 2, 1993, pp. 122-133.
- Walton, P., and Majumdar, A., "Properties of Cement Composite Reinforced with Kevlar Fibres," *Journal of Materials Science*, Vol. 13, 1978, pp. 1075-1083.
- Wang, Y., Backer, S., and Li, V., "An Experimental Study of Synthetic Fibre Reinforced Cementitious Composites," *Journal of Materials Science*, Vol. 22, 1987, 4281-4291.
- Ward, R., and Li, V., "Dependence of Flexural Behaviour of Fibre Reinforced Mortar on Material Fracture Resistance and Beam Size," *ACI Materials Journal*, Vol. 87, No. 6, 1990, pp. 627-637.
- Yost, J., Gross, S., and Dinehart, D., "Shear Strength of Normal Strength Concrete Beams Reinforced with Deformed GFRP Bars," *Journal of Composites for Construction*, Vol. 5, No. 4, 2001, pp. 268-275.

Appendix A

Test results of all beams

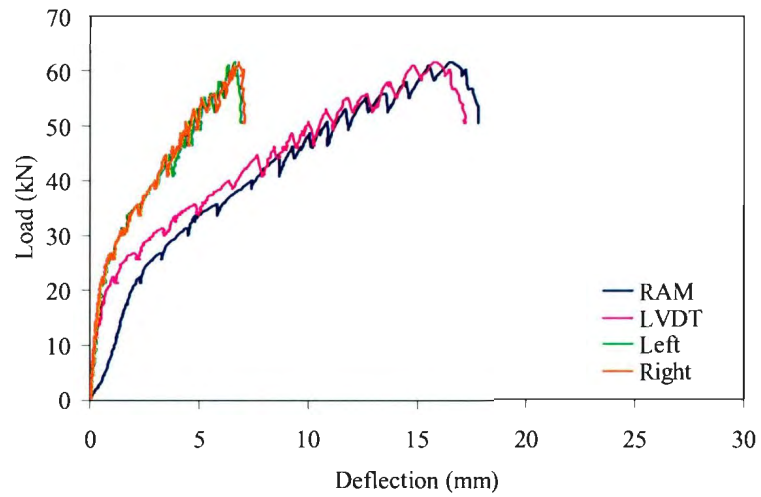


Figure A.1: Load-Deflection for beam B1

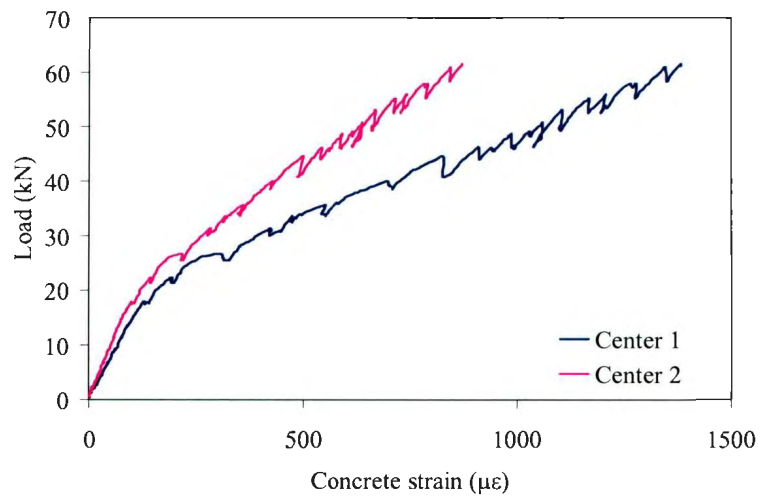


Figure A.2: Load-Concrete strain for beam B1

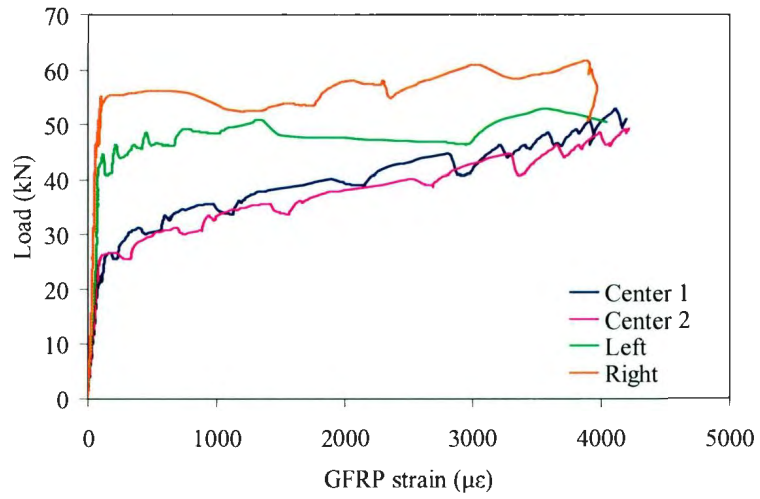


Figure A.3: Load-GFRP strain for beam B1

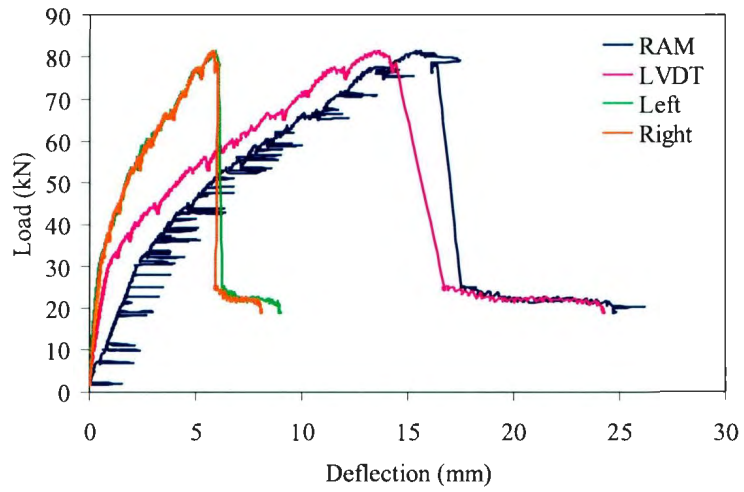


Figure A.4: Load-Deflection for beam B2

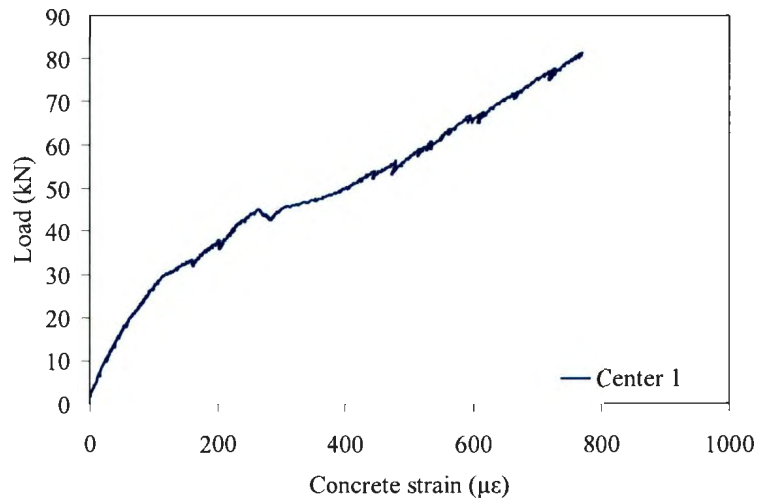


Figure A.5: Load-Concrete strain for beam B2

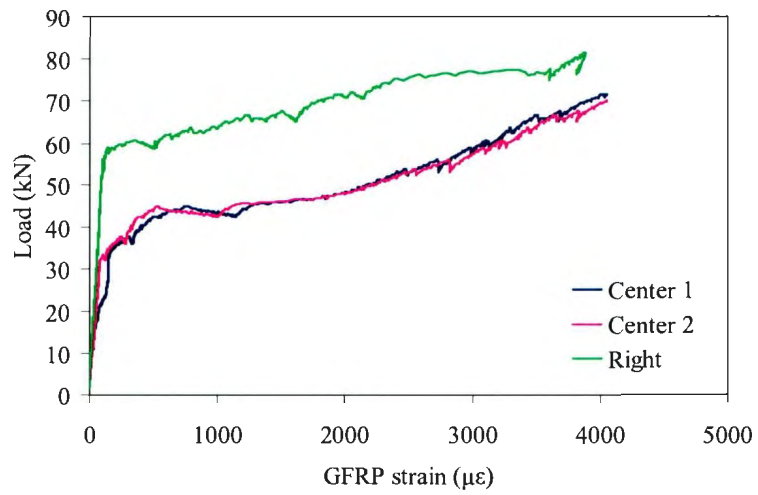


Figure A.6: Load-GFRP strain for beam B2

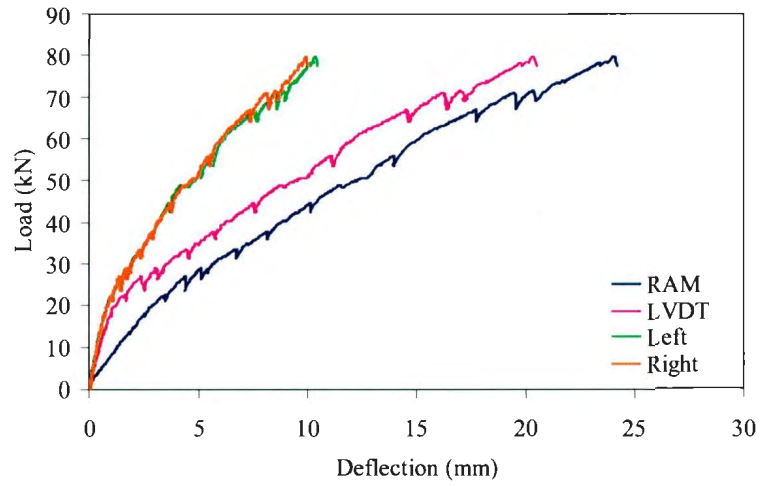


Figure A.7: Load-Deflection for beam B3

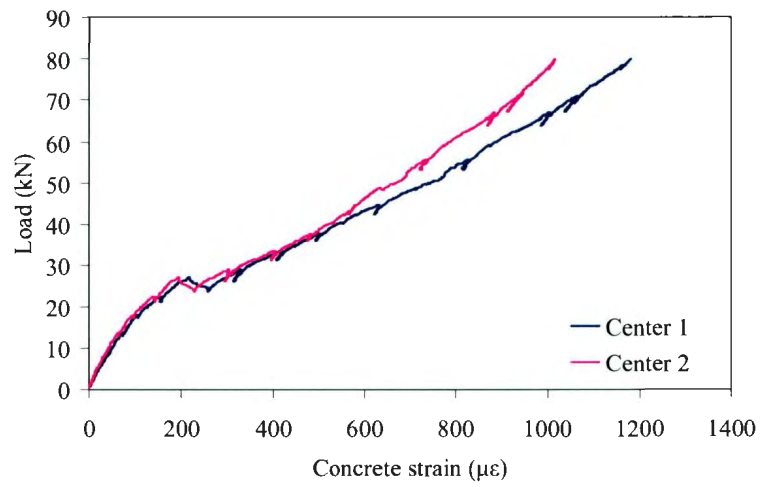


Figure A.8: Load-Concrete strain for beam B3

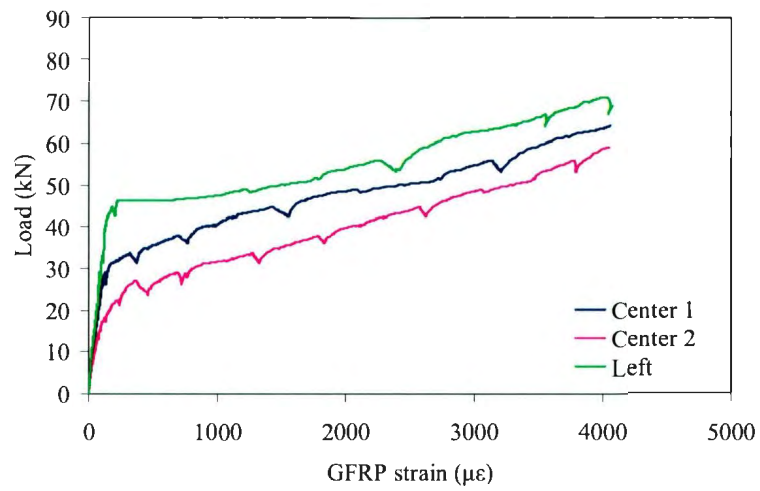


Figure A.9: Load-GFRP strain for beam B3

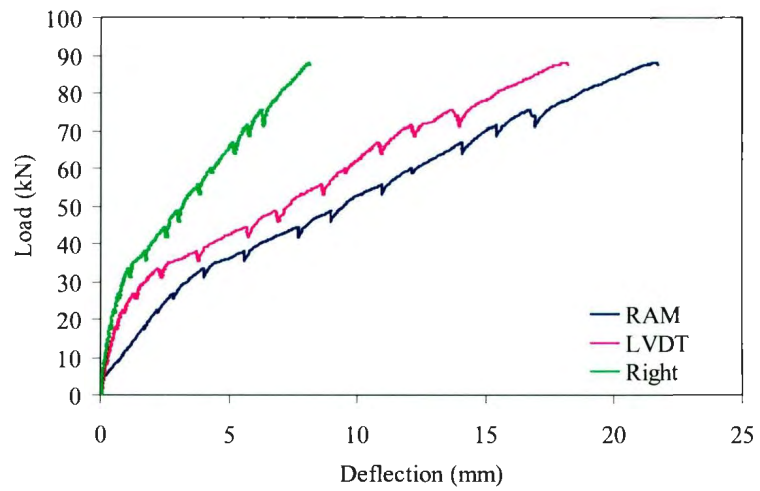


Figure A.10: Load-Deflection for beam B4

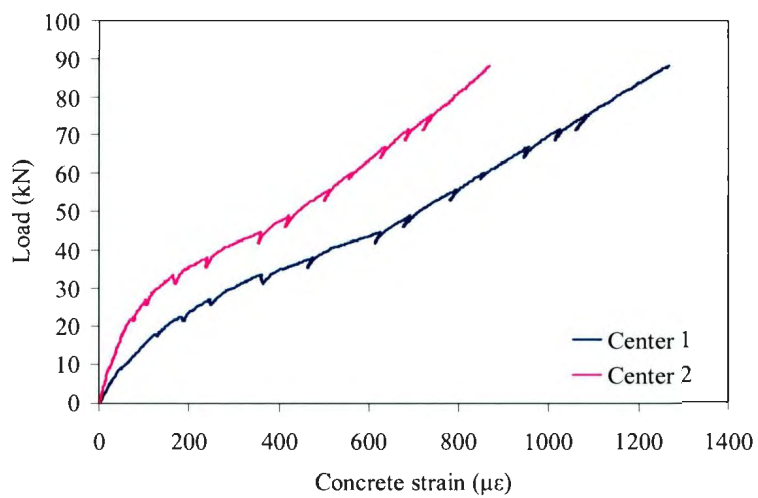


Figure A.11: Load-Concrete strain for beam B4

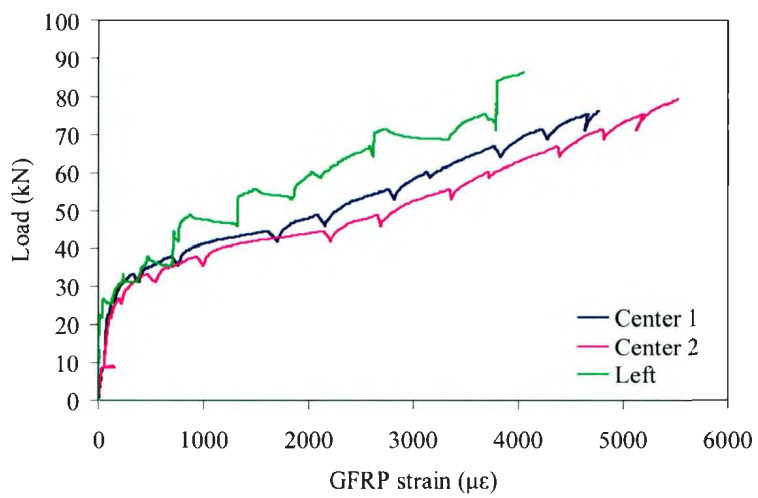


Figure A.12: Load-GFRP strain for beam B4

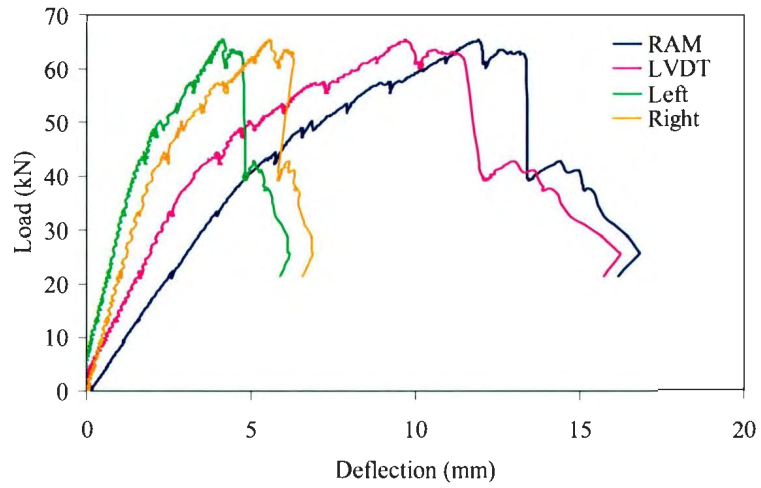


Figure A.13: Load-Deflection for beam B5

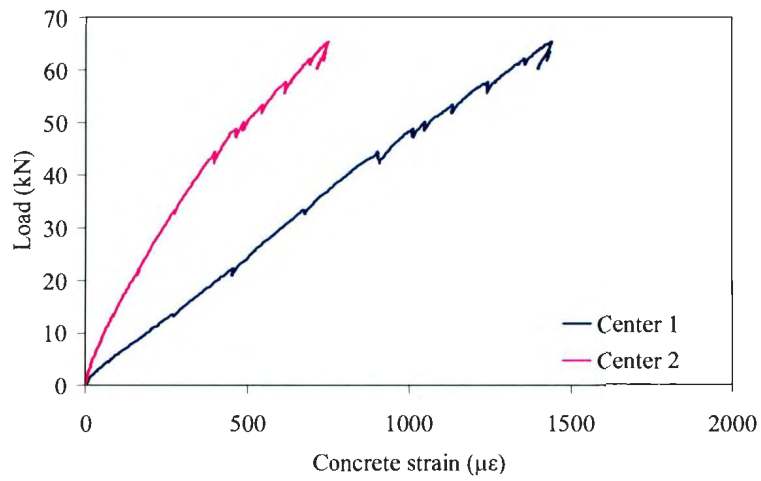


Figure A.14: Load-Concrete strain for beam B5

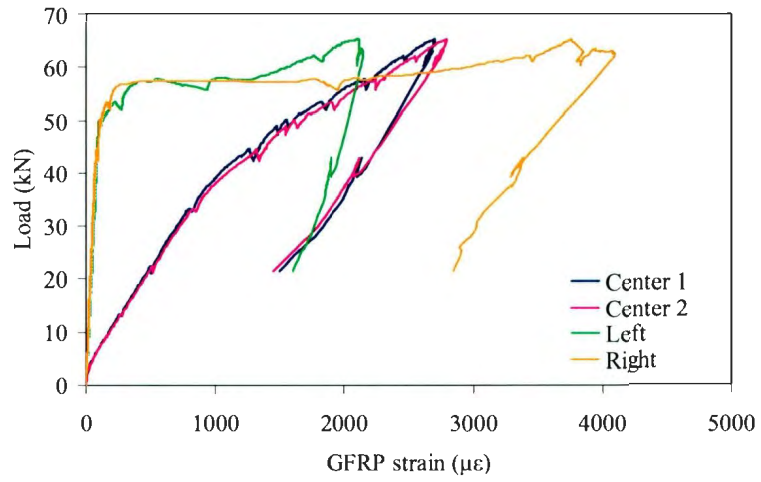


Figure A.15: Load-GFRP strain for beam B5

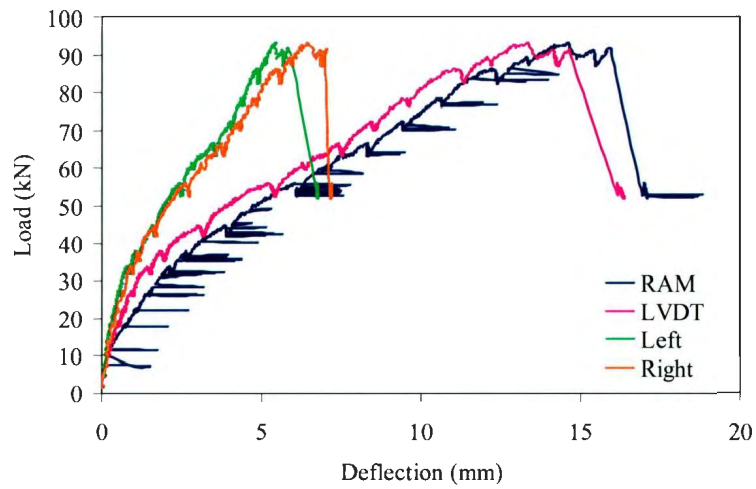


Figure A.16: Load-Deflection for beam B6

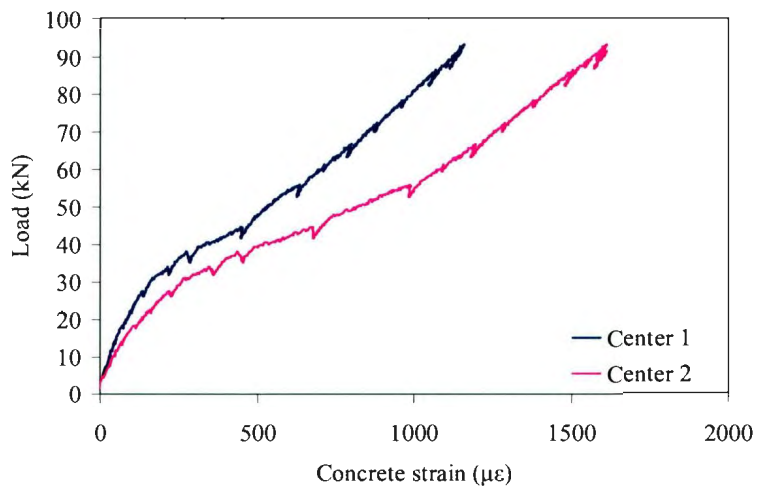


Figure A.17: Load-Concrete strain for beam B6

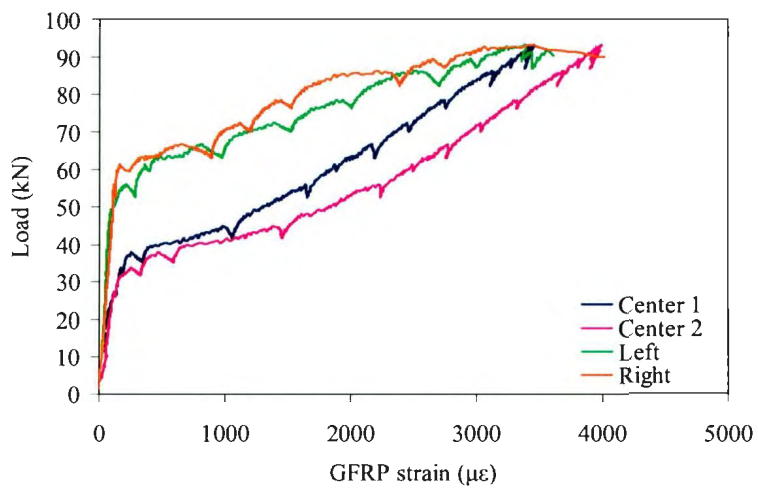


Figure A.18: Load-GFRP strain for beam B6

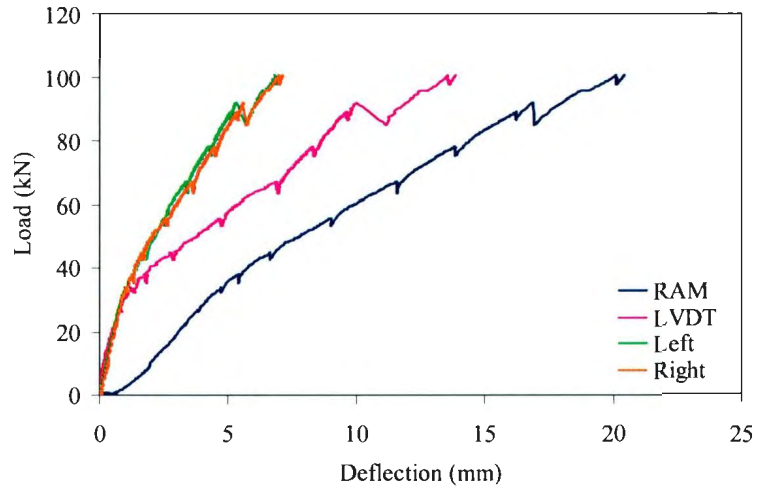


Figure A.19: Load-Deflection for beam B7

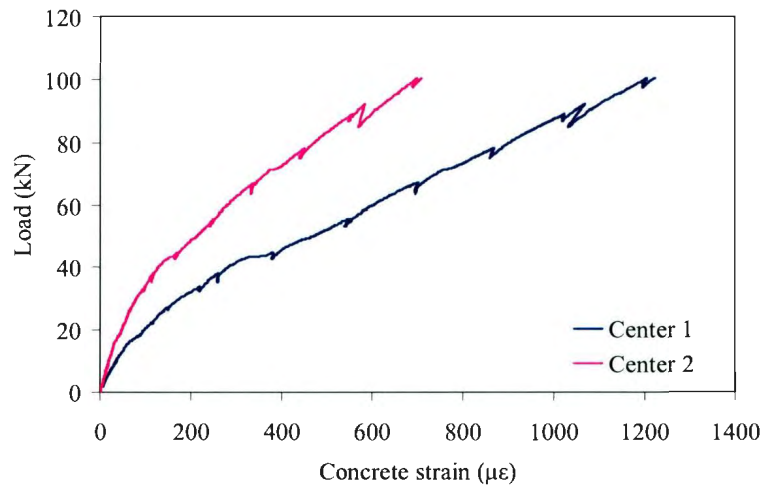


Figure A.20: Load-Concrete strain for beam B7

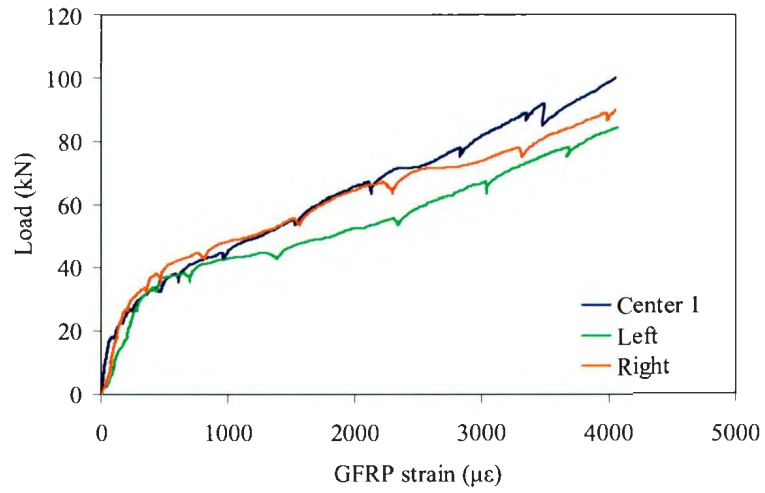


Figure A.21: Load-GFRP strain for beam B7

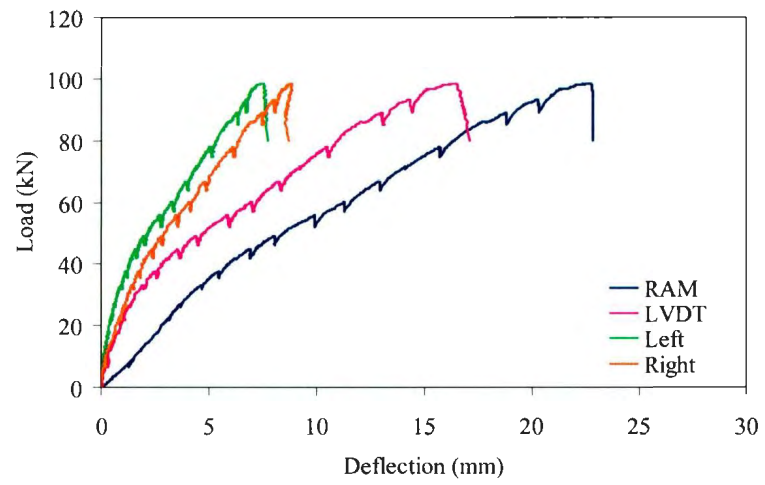


Figure A.22: Load-Deflection for beam B8

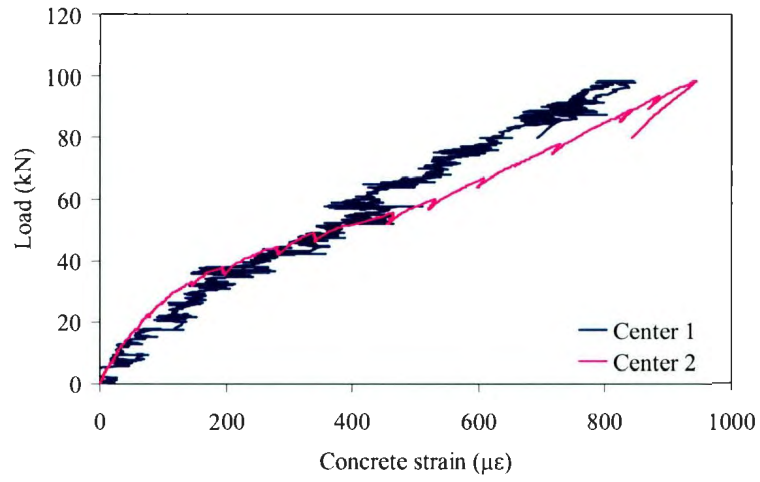


Figure A.23: Load-Concrete strain for beam B8

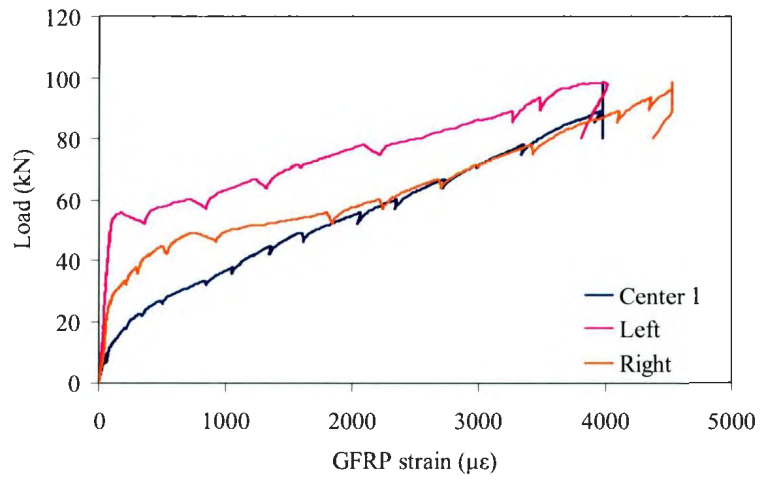


Figure A.24: Load-GFRP strain for beam B8

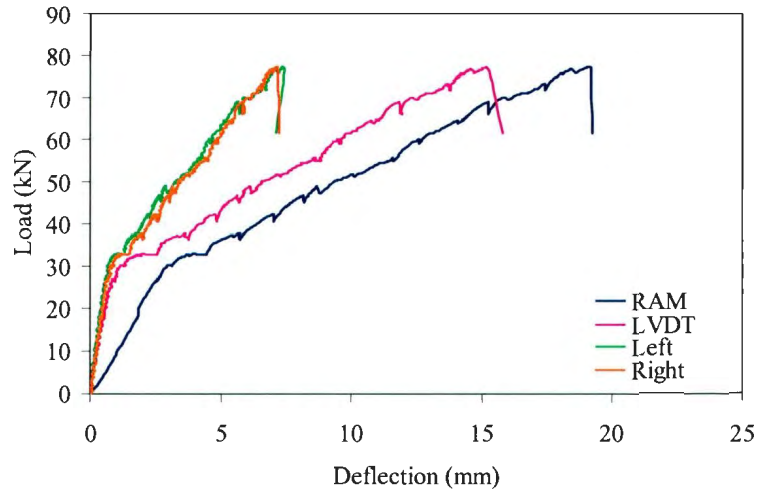


Figure A.25: Load-Deflection for beam B9

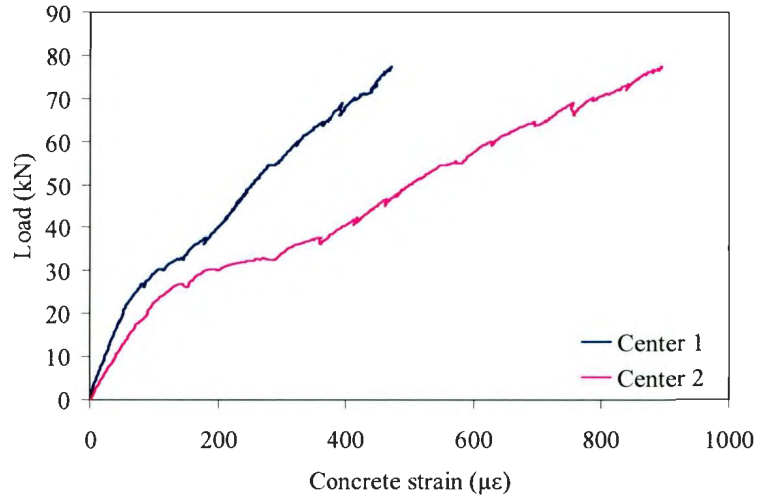


Figure A.26: Load-Concrete strain for beam B9

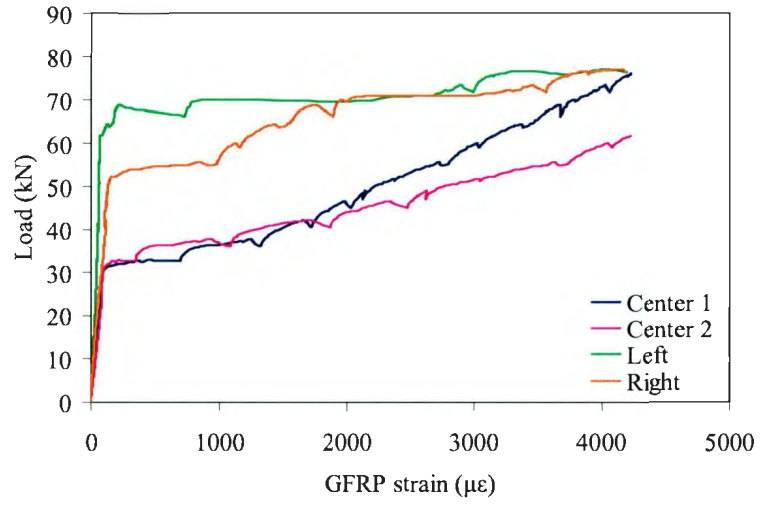


Figure A.27: Load-GFRP strain for beam B9

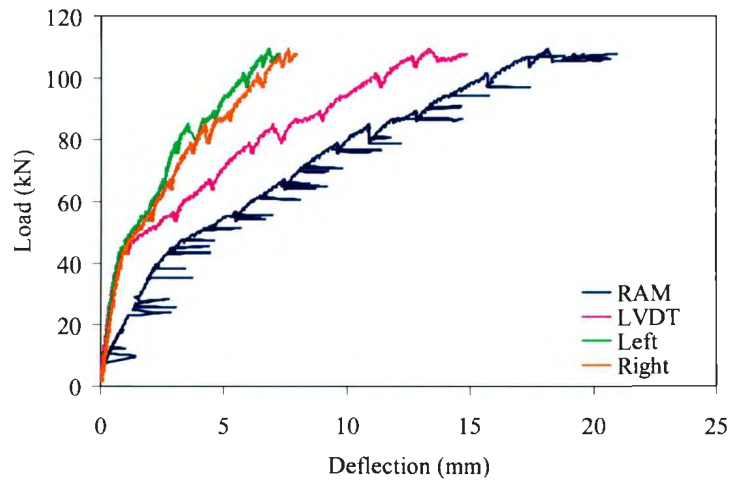


Figure A.28: Load-Deflection for beam B10

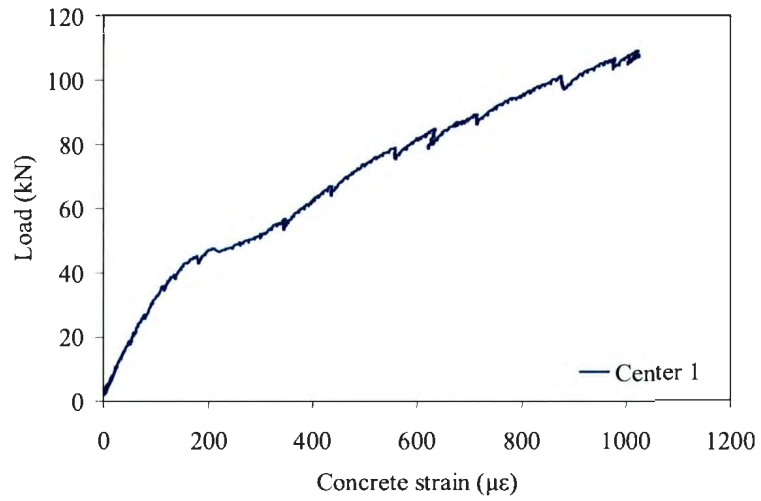


Figure A.29: Load-Concrete strain for beam B10

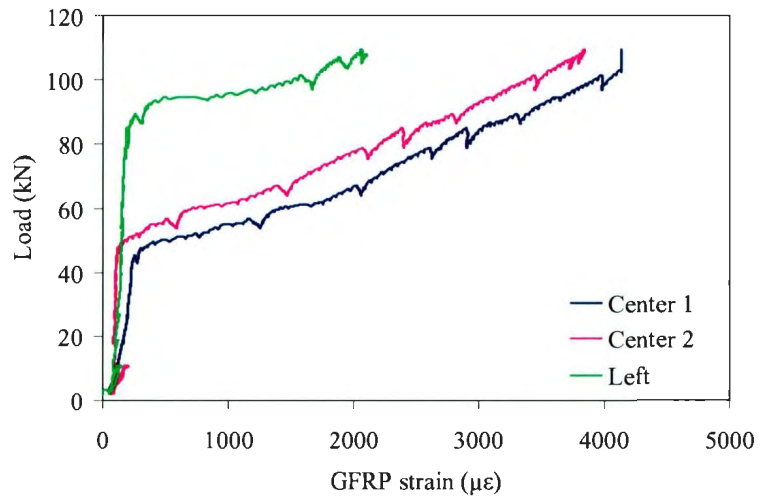


Figure A.30: Load-GFRP strain for beam B10

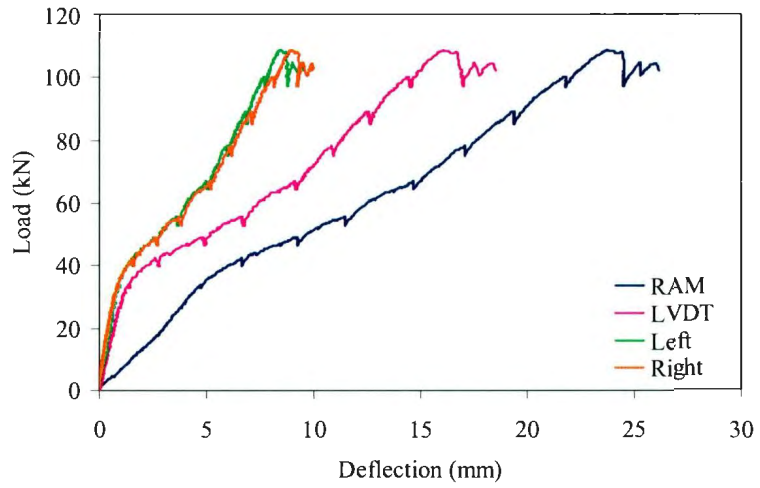


Figure A.31: Load-Deflection for beam B11

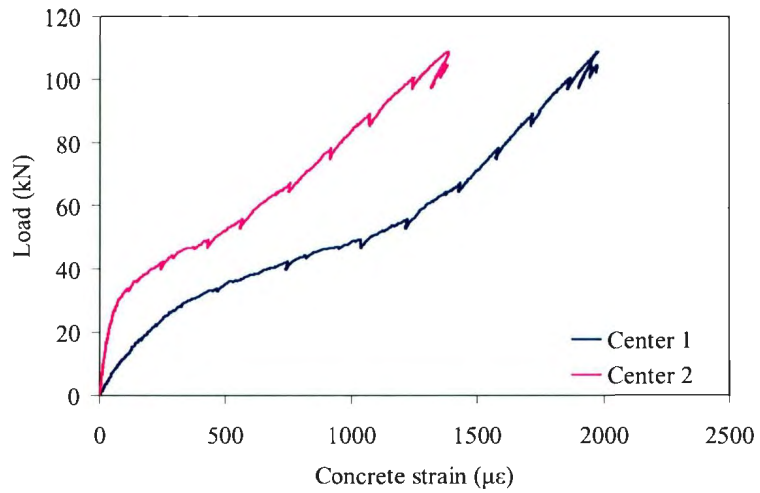


Figure A.32: Load-Concrete strain for beam B11

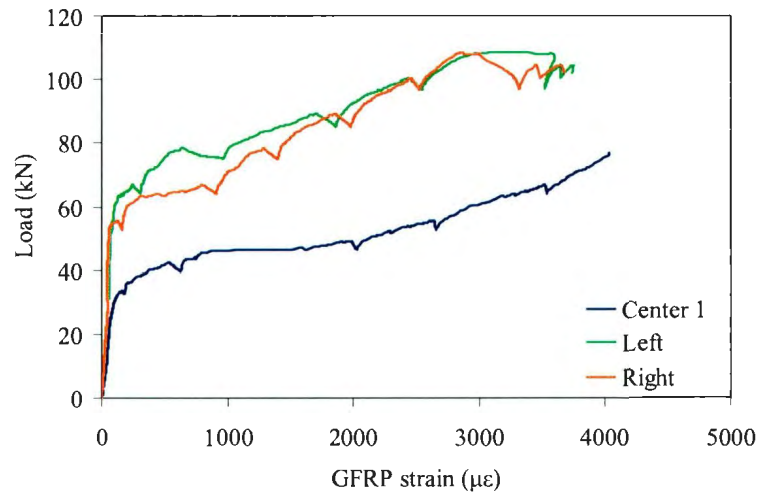


Figure A.33: Load-GFRP strain for beam B11

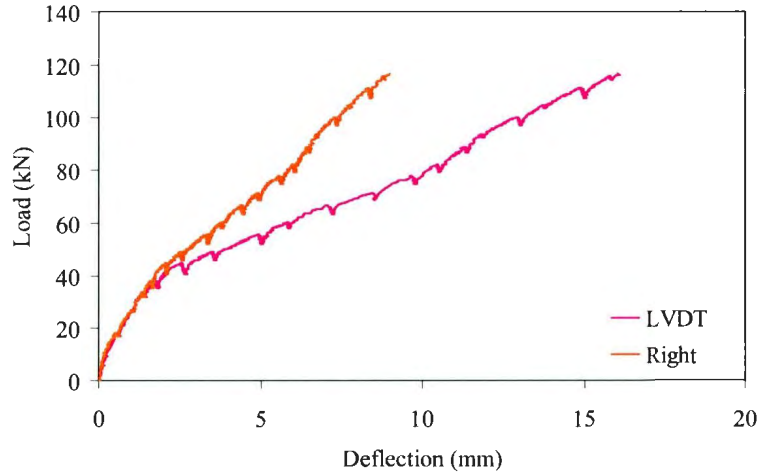


Figure A.34: Load-Deflection for beam B12

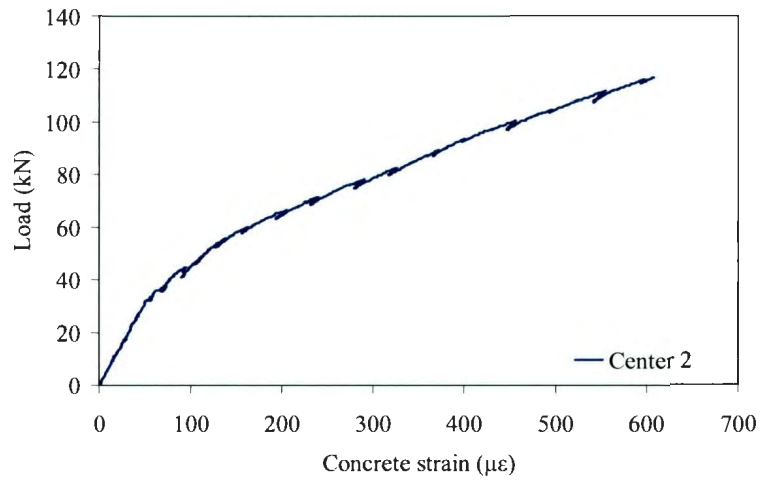


Figure A.35: Load-Concrete strain for beam B12

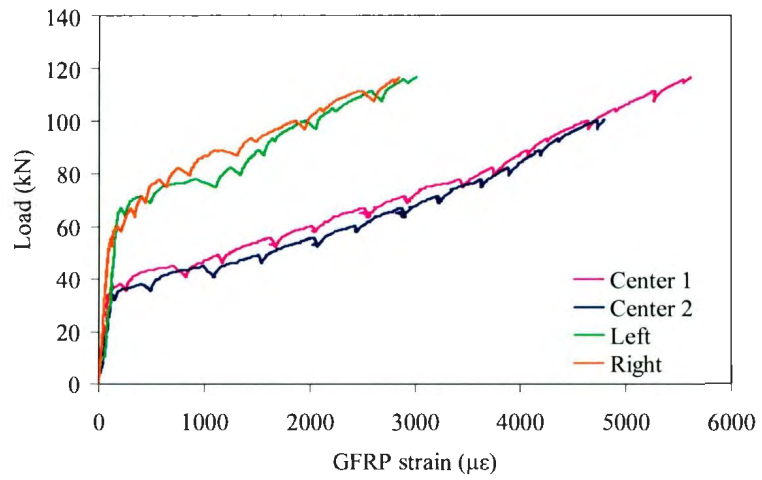


Figure A.36: Load-GFRP strain for beam B12

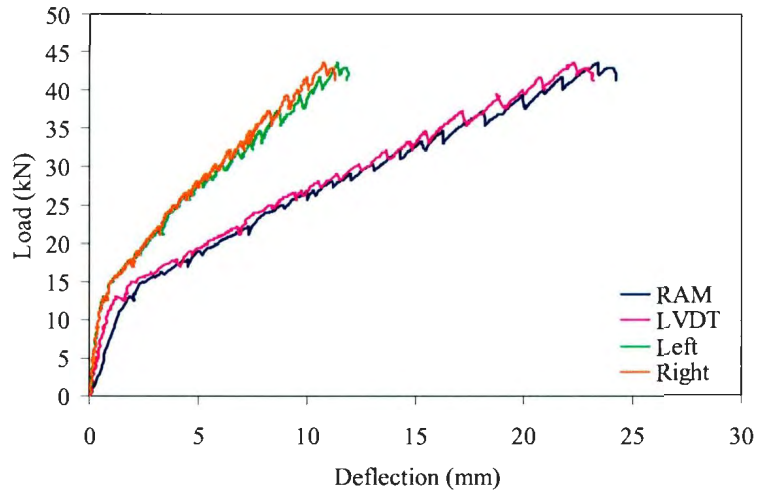


Figure A.37: Load-Deflection for beam B13

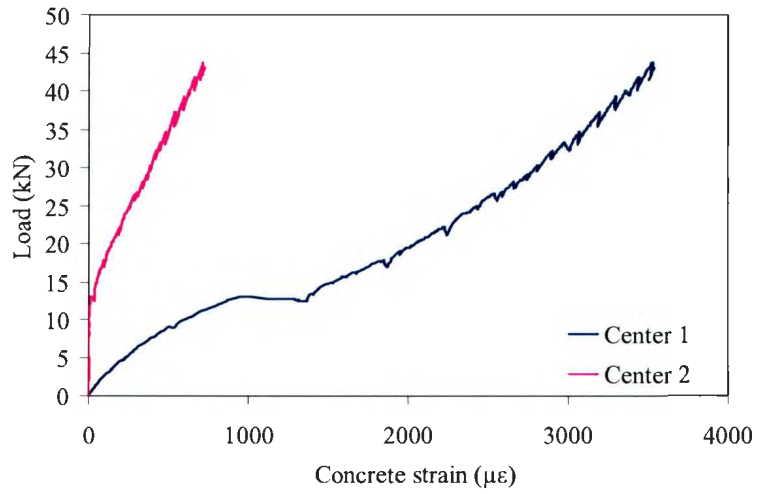


Figure A.38: Load-Concrete strain for beam B13

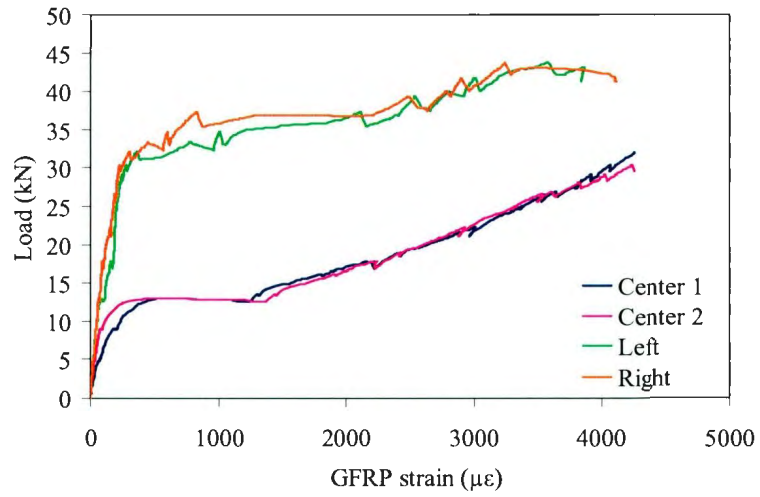


Figure A.39: Load-GFRP strain for beam B13

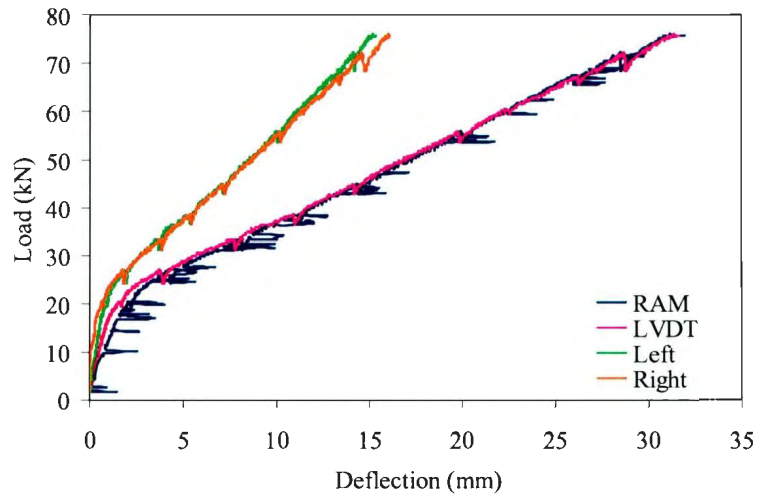


Figure A.40: Load-Deflection for beam B14

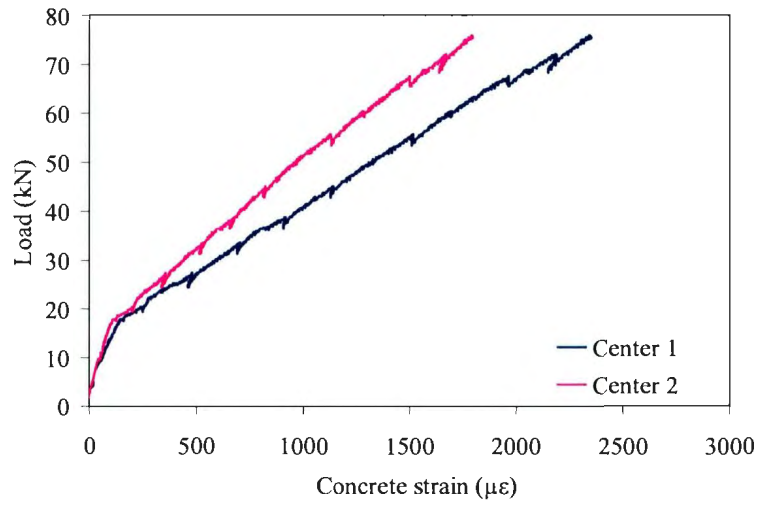


Figure A.41: Load-Concrete strain for beam B14

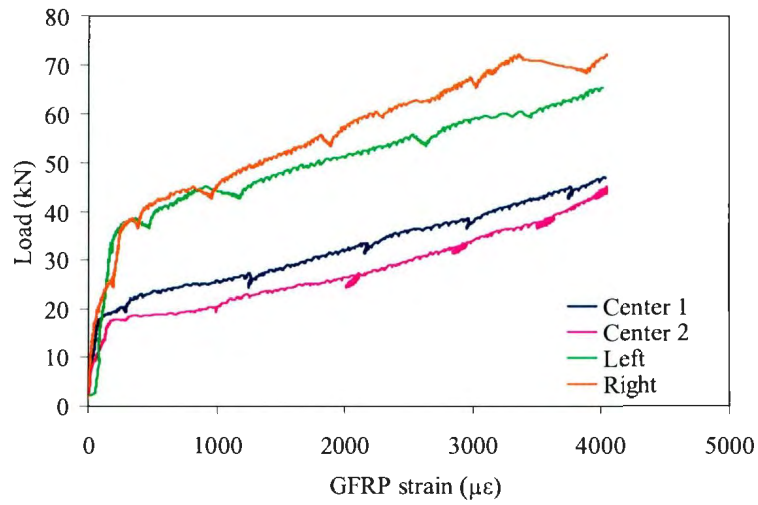


Figure A.42: Load-GFRP strain for beam B14

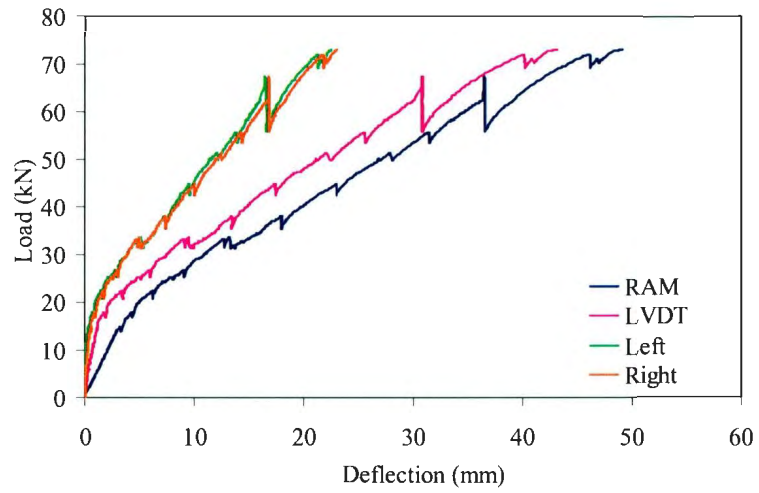


Figure A.43: Load-Deflection for beam B15

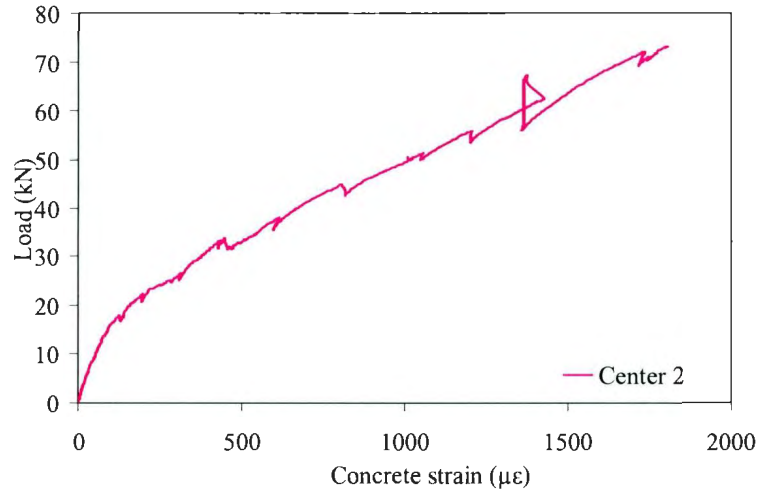


Figure A.44: Load-Concrete strain for beam B15

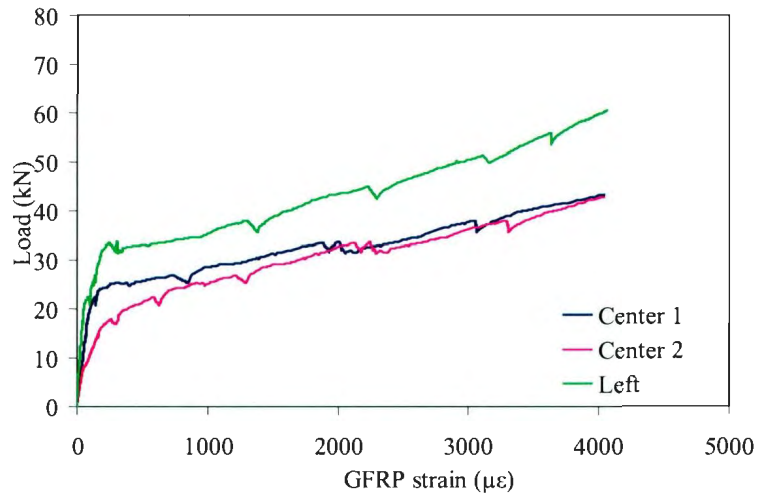


Figure A.45: Load-GFRP strain for beam B15

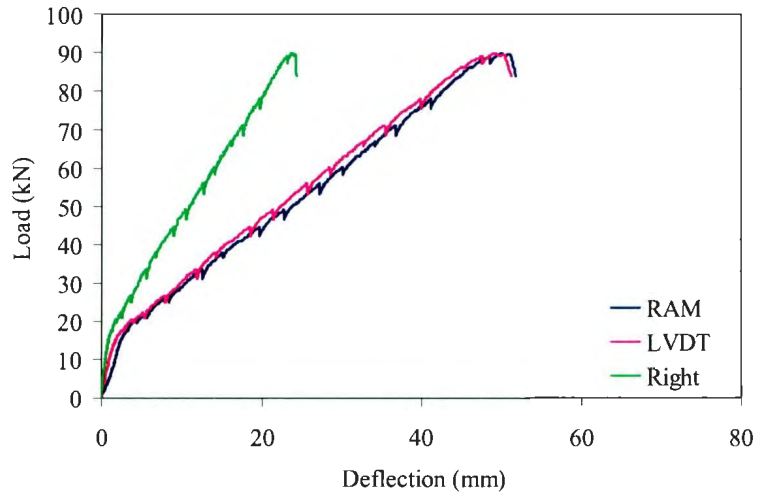


Figure A.46: Load-Deflection for beam B16

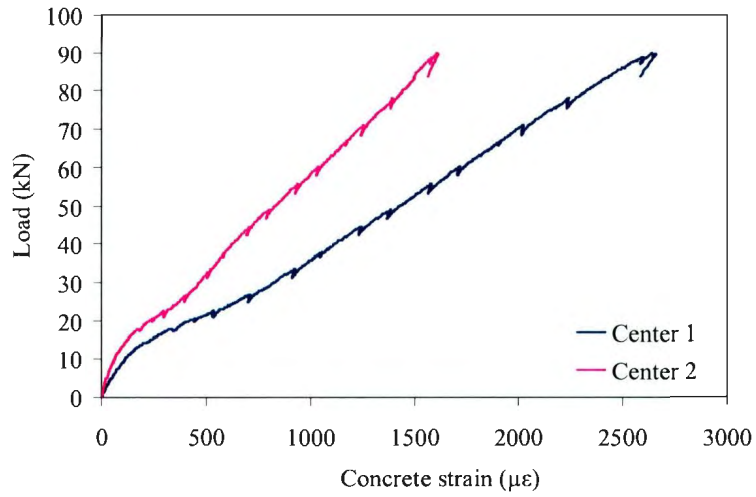


Figure A.47: Load-Concrete strain for beam B16

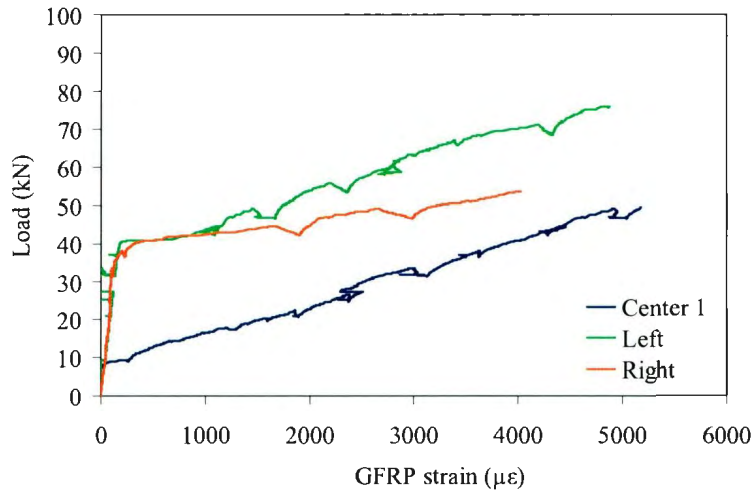


Figure A.48: Load-GFRP strain for beam B16





